University of Trento

Zhu MEI (Ph. D. Student)

STRUCTURAL HYBRID SIMULATION WITH MODEL UPDATING OF MATERIAL CONSTITUTIVE MODEL

Oreste Salvatore BURSI (Tutor)
Bin WU (Co-Tutor)

2018

UNIVERSITY OF TRENTO

Structural Hybrid Simulation with Model Updating of Material Constitutive Model

Ph. D. Head's Zhu MEI

Final Examination 18/12/2017

Board of Examiners

Prof Oreste Slavatore BURSI (University of Trento)

Prof Bin WU (Harbin Institute of Technology)

Prof Anxin Guo (Harbin Institute of Technology)

Prof Dagang LU (Harbin Institute of Technology)

Prof Zhenyu WANG (Harbin Institute of Technology)

Prof Wei WANG (Harbin Institute of Technology)

SUMMARY – SOMMARIO

When hybrid simulation (HS) with substructures is employed for assessing the seismic behavior of a large complex structure, it is unrealistic to test all the components that may exhibit strong nonlinearity. Hence, the accuracy of the numerical substructure (NS) faces an increased challenge. To this end, this paper will emphasize on improving the accuracy of the NS in hybrid simulation based on the model updating approach.

Most hybrid simulations with model updating (UHS) focus on updating the parameters of the component constitutive model (story shear model) leading to large modeling errors and the unknown detail responses. Moreover, the most extensively used component constitutive models, such as the Bouc-Wen model, are the models in a narrow sense because they are different for various RC members when the size of the component, boundary conditions, axial compression ratio, and the volumetric stirrup ratio are different from one component to the other. Thus, numerous parameters are needed to describe the displacement-force relations of different components, which leads to the huge computational burden. With this respect, this paper proposes a novel hybrid simulation approach based on identifying and updating the parameters of the material constitutive model. The main work and results are concluded as follows,

1. The unified constitutive model of unconfined and confined concrete is derived from the existing uniaxial concrete constitutive models by introducing the volumetric stirrup ratio.

2. To solve the problem that the relation of the measurements (force of the specimen of a RC member) and the identified parameters (concrete constitutive parameters) are difficult to analytical expressed, an OpenSees embedded unscented Kalman filter is proposed for parameter identification. To this end, several parts of the OpenSees source codes are developed and modified.

3. The proposed identification method and hybrid simulation based on updating the concrete constitutive parameters are respectively validated through a monotonic loading test on a RC column and a UHS on a RC frame. The results show that the convergence values of each parameter under various experimental cases are close to each other with a small variance, which indicates that the proposed identification method is robust and reliable. Comparing to the standard HS, the accuracy of the NS, hence the UHS, is significantly improved.

4. Apply the proposed UHS to a RC continuous rigid bridge with tall thin-walled piers. It concludes that the performance of the identification method is still quite good. Contrasting to the simpler structure, the improved accuracy of a large complex structure is even greater. Moreover, the accuracy of the NS can be greatly increased even though the model error is increased. By tuning the initial values of constitutive parameters, the negative influence of model error is decreased to further improve the precision of the NS. By observing the specimen, it is found that the thin-walled hollow section specimen is a bending-shear type damage mode and finally damaged due to the tensile rupture of the stirrup.

Quando la simulazione ibrida (HS) con sottostrutture viene impiegata per valutare il comportamento sismico di una grande struttura complessa, non è realistico testare tutti i componenti che possono presentare una forte non linearità. Quindi, l'accuratezza della sottostruttura numerica (NS) deve affrontare una sfida maggiore. A tal fine, questo documento enfatizzerà il miglioramento dell'accuratezza dell'NS nella simulazione ibrida basata sull'approccio di aggiornamento del modello.

La maggior parte delle simulazioni ibride con l'aggiornamento del modello (UHS) si concentrano sull'aggiornamento dei parametri del modello costitutivo del componente (modello story shear) che porta a errori di modellazione di grandi dimensioni e alle risposte di dettaglio sconosciuto. Inoltre, i modelli costitutivi del componente più ampiamente utilizzati, come il modello Bouc-Wen, sono i modelli in senso stretto perché sono diversi per i vari membri del RC quando la dimensione del componente, le condizioni al contorno, il rapporto di compressione assiale e il volumetrico il rapporto della staffa è diverso da un componente all'altro. Pertanto, sono necessari numerosi parametri per descrivere le relazioni forza-spostamento di diversi componenti, il che porta all'enorme onere computazionale. A tale riguardo, questo articolo propone un nuovo approccio di simulazione ibrido basato sull'identificazione e l'aggiornamento dei parametri del modello costitutivo del materiale. Il lavoro principale e i risultati si concludono come segue,

1. Il modello costitutivo unificato di calcestruzzo non confinato e confinato è derivato dai modelli costitutivi concreti monoassiali esistenti introducendo il rapporto tra le staffe volumetriche.
2. Per risolvere il problema che la relazione delle misure (forza del campione di un elemento RC) e i parametri identificati (parametri costitutivi concreti) sono difficili da esprimere analiticamente, per l'identificazione dei parametri viene proposto un filtro Kalman unscented incorporato di OpenSees. A tal fine, diverse parti dei codici sorgente di OpenSees sono sviluppati e modificati.
3. Il metodo di identificazione proposto e la simulazione ibrida basata sull'aggiornamento dei parametri costitutivi concreti sono rispettivamente convalidati attraverso un test di carico monotonico su una colonna RC e un UHS su un telaio RC. I risultati mostrano che i valori di convergenza di ciascun parametro in vari casi sperimentali sono vicini tra loro con una piccola varianza, il che indica che il metodo di identificazione proposto è robusto e affidabile. Paragonato allo standard HS, l'accuratezza del NS, quindi dell'UHS, è significativamente migliorata.
4. Applicare l'UHS proposto a un ponte rigido continuo RC con pilastri a parete sottile alta. Conclude che le prestazioni del metodo di identificazione sono ancora abbastanza buone. In contrasto con la struttura più semplice, la precisione migliorata di una struttura complessa di grandi dimensioni è ancora maggiore. Inoltre, la precisione del NS può essere notevolmente aumentata anche se l'errore del modello è aumentato. Sintonizzando i valori iniziali dei parametri costitutivi, l'influenza negativa dell'errore del modello viene ridotta per migliorare ulteriormente la precisione del NS. Osservando il campione, si scopre che il campione a sezione cava a parete sottile è una modalità di danneggiamento del tipo a taglio di curvatura e infine danneggiato a causa della rottura a trazione della staffa.

DEDICATION

1. **Z. MEI**, B. WU, O.S. BURSI, G. YANG, Z. WANG. Hybrid simulation of structural systems with online updating of concrete constitutive law parameters by unscented Kalman filter[J]. Structural Control and Health Monitoring, 2018, 25(2). (SCI, IF=2.355)

2. **Z. MEI**, B. WU, O.S. Bursi. Hybrid simulation with online updating: application to a reinforced concrete bridge endowed with tall piers[J]. Mechanical Systems and Signal Processing (SCI, IF=4.116, Under Review)

3. B. WU, Y. CHEN, G. XU, **Z. MEI**, T. PAN. Hybrid simulation of Frame Structures with sectional model updating[J]. Earthquake Engineering and Structural Dynamics, 2016, 45(8): 1251-1269. (SCI, IF=1.974)

4. B. WU, X. NING, G. XU, Z. WANG, **Z. MEI**, G. YANG, Online numerical simulation: A hybrid simulation method for incomplete boundary conditions, Earthquake Engineering and Structural Dynamics, 2018, 47(4): 889-905. (SCI, IF=2.355)

5. **Z. MEI**, B. WU, G. YANG. Online parameter identification of concrete constitutive model[J]. Engineering Mechanics, 2016, 33(7): 108-115. (EI, In Chinese)

ACKNOWLEDGEMENTS

In the fall of 2011, I began my Ph.D. study, and now I still remember the joy and excitement. In the six years, under the rigorous guidance of the teacher and the endless care of the family, I finally completed all the contents of doctoral studies, scientific research, and thesis writing. As time flies, I am very grateful to all those who have helped me at the end of my doctoral career.

First of all, I gratefully thank my supervisor, Professor WU Bin. During the period of the doctoral study, Prof. Wu provided me with superior research conditions and a relaxed learning environment. At the same time, he gave me enough trust and confidence, which enabled me to be firm in the face of scientific research problems.

Special thanks to Professor Oreste Salvatore Bursi, I appreciate the opportunity to study in Italy he provided me. Thank him for his rigorous and serious guidance on my thesis and research work. His humor and kindness also stayed in my wonderful study life in Italy.

Then, thanks to all the people who helped me during my doctoral study.

At last but not the least, thanks to my parents for always supporting my decision, supporting my life and supporting my ideals. I thank my husband, thank him for the company in the years of ups and downs, thank him for his care and concern, and for his tolerance, comfort and encouragement.

This subject is sponsored by the National Key Research and Development Program of the State (2016YFC0701106), the Major International Cooperation Research Project of the Natural Science Foundation of China (51161120360), the National Natural Science Foundation of China Major Research Project-Integrated Project (91315301-09), the Doctoral Program of Higher Education Institutions, and the Italian SERIES (Seismic Engineering Research Infrastructure for European Synergies) Project (FP7/2007-2013 227887).

INDICE

1. INTRODUCTION

1.1 Background and Motivation

Enormous human casualties and economic losses have been brought to human beings by earthquake disaster. China has hit many earthquakes of magnitude 7.0 and above, such as the Yushu Earthquake, the Wenchuan Earthquake, the Ya'an Earthquake, and Yutian Earthquake since 2000. Among them, the most serious is the Wenchuan earthquake which is a destructive shallow earthquake at a depth of 14 km with the magnitude of 8.0. In this disaster, 69,227 people were killed and 17,923 people were missing, with a direct economic loss of 845.2 billion yuan.

In order to alleviate the losses caused by seismic disaster, a great deal of researches have been conducted on earthquake monitoring, mechanism of earthquake formation, structure anti-seismic theory, structural post-earthquake recoverability and many earthquake-related sciences. Based on the statistics of post-earthquakes losses, we can see that the damage and collapse of buildings, bridges and other structures are the most important causes of casualties. Fig. 1-1 shows typical failure modes of reinforced concrete structure after earthquake. In order to improve the safety of structures, it is very important to study the strong non-linear behavior and seismic performance of components and structures under earthquake loading so as to master the dynamic catastrophic process of structures. Among others, structural seismic test is important means to study the seismic performance of structures, which can not only verify the theoretical results, but also find new problems so as to develop and perfect the theory.

Fig. 1-1 Typical failure mechanisms of reinforced concrete structures under earthquake

Laboratory seismic testing methods are divided into quasi-static test, pseudo-dynamic test, shaking table test (Qiu et al., 2000). The quasi-static test method is the most widely used seismic test method at present, which forces the specimen to undergo the entire process from to the final destruction through the ow-frequency cyclic loading. In this way, the carrying capacity, deformation capacity and energy dissipation capacity and damage characteristics of the specimen can be obtained. However, this method cannot provide the dynamic response of the structure under earthquake. Shaking table test is the most direct method to study the seismic performance of structures in the laboratory. It can reproduce the dynamic response and failure mode of the structure under earthquake. However, the size of the target structure tends to be severely restricted due to many factors such as laboratory space, size and bearing capacity of vibrating table, and the experimental budget. If a scaled model of the target structure is used in shaking table test, it will face the problem that the dynamic similarity cannot be satisfied. This leads to that the results of the scaled model test are difficult to extend to the prototype structure (Qiu et al., 2000; Zhang, 2010).

Pseudo dynamic test is also called the hybrid simulation, whose main idea is to solve the motion equation of the structure by computer. In the equation, the inertial force and the damping force which are easy to simulate are numerical simulated by the computer; while the restoring force of the structure which is hard to accurately simulate is experimentally simulated. In each integral step of the process, the solved displacements are static loaded on the specimen of the structure, then the restoring forces of the specimen are real measured and feedback to the equation of motion in the computer. Therefore, combing the advantages of the static loading method and the development of computer, the seismic effect can be considered through the pseudo dynamic test method. Because of this, hybrid simulation has gradually attracted the attention of engineers and scholars since it was proposed, and has been promoted and applied.

With the development of control science, computer and network technology, pseudo dynamic test method have been gradually developed such as full scale structure pseudo dynamic test, substructure pseudo dynamic test and real-time pseudo dynamic test. For large complex structures, it is not easy to implement pseudo-dynamic test on a full-scale structure due to the limitation of the capacity of loading equipment and experimental budget. Therefore, the substructure pseudo dynamic test method that can realize large-scale or even full-scale specimen is gradually developed. Substructure pseudo dynamic test separates the structure into numerical substructure (NS) and experimental/physical substructure (PS). The key components in the structure that may experience nonlinearity are isolated and loaded in the laboratory as the PS, and the remainder are analyzed by numerical simulation in a computer, i.e. the NS. As well, the motion equation of the structure is solved by the computer. In the process, the compatibility of deformation and balance of force are ensured. During the substructure pseudo dynamic test, the motion equation is solved by the coordinator /computer, the solved displacements are sent to both the NS and the PS, and then the numerically and experimentally simulated restoring forces are returned by the NS and the PS respectively to the coordinator for solving the equation at next integral step till the end of the seismic loads. The advantage of substructure pseudo dynamic test is that the testing target is only a single component or a part of the whole structure, which makes the large-scale and even full-scale specimen can be realized.

However, for large complex structures such as bridges and high-rise buildings, it is not realistic to

take out all the key components to be experimentally tested as the PS. Most of the key components that may experience nonlinearity, inevitably, need to be simulated as the NS. So, the accuracy of the NS should be pay more attention to. In order to improve the accuracy of the numerical model, scholars have been made a lot of efforts by giving more reasonable assumptions, proposing more accurate and stable numerical integration method, proposing more types of finite element (FE) units applicable to different components and structures, and proposing more accurate constitutive models to simulate the behavior of components, sections and materials. For pseudo dynamic test, the NS is built based on the existing FE principles, integration methods and constitutive models. Therefore, the emphasis of this paper is how to improve the accuracy of numerical analysis after the NS is established, and thus the reliability of the whole hybrid simulation. Model updating proposed in the 1990s to improve the simulation accuracy of numerical models of mechanical and building structures can solve this problem well (Friswell & Mottershead, 1995; Friswell & Mottershead, 2001).

The essence of model updating is to optimize the parameters in the numerical model by experimental data to reduce the errors caused by the unreasonable assumptions and errors in the numerical model and finally to minimize the specific errors between the calculated numerical model and the observed data. That is, the numerical model (which can directly the force-displacement behavior of the component or structure, or the material constitutive models used in the FE model) can be updated and improved through the experimental data. Aiming at improving the reliability of hybrid test, this paper combines the hybrid test with the model updating method, and proposes a new hybrid test method based on identifying and updating the parameters of material constitutive models. The proposed updating hybrid simulation is verified by numerical and experimental ways, and finally is applied to a thin-walled high-pier reinforced concrete continuous rigid-frame bridge to simulate the seismic behavior of the bridge. It is expected that this study will be helpful for the development of structural hybrid simulation.

1.2 State of Art for Hybrid Simulation

The hybrid simulation was first proposed by Japanese scholars in the late 1960s (Hakuno et al., 1969). The main idea of this method is to combine the computer and the actuator, where the equations of motion was solved by computer which they used was analog computer, while the actuator was employed to load on the structure to obtain the restoring force. Later in the mid-1970s, Takanashi et al. replaced the analog computer with a digital computer and adopted the central difference method instead of the linear acceleration method to solve the equations of motion (Takanashi et al., 1975). The hybrid simulation was then further developed to be used for analyzing the elastoplastic seismic behavior of structures. The early hybrid simulation is just the prototype of the now called full structure pseudo-dynamic test. Its main idea is shown in Fig. 1-2.

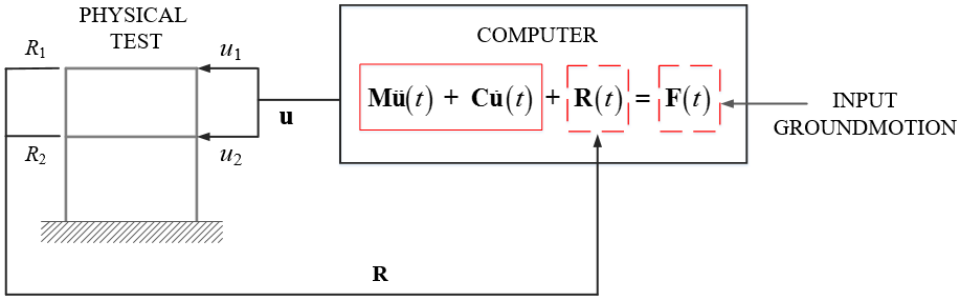

Fig. 1-2 Schematic diagram of hybrid simulation

The inertia forces and damping forces in the equation are simulated by computer, whilst the structural restoring force is obtained by experimentally loading. After receiving the feedback forces, the computer proceeds to solve the equation at the next step by a given numerical integration method and sends the solved displacements to the specimen. The cycle will go on till the end of seismic loads.

With the enlargement and complexity of civil engineering structures, the existing conditions of loading equipment and sites are difficult to meet the requirement of the hybrid simulation with large-scale specimen when the whole structure is taken to be the target structure. Therefore, the substructure pseudo dynamic test was proposed in the mid-1980s (Dermizakis & Mahin, 1985) and gradually developed. In the substructure hybrid simulation, the structure was divided into two parts: the experimental/physical substructure (PS) and the numerical substructure (NS). The solved displacements were sent to both the PS and the NS, as shown in Fig 1-3. Then, the substructures return the restoring forces $\mathbf{R}_n(t)$ (NS) and $\mathbf{R}_e(t)$ (PS) to the computer, respectively, after calculation or loading. That is, the $\mathbf{R}(t)$ is the sum of $\mathbf{R}_n(t)$ and $\mathbf{R}_e(t)$.

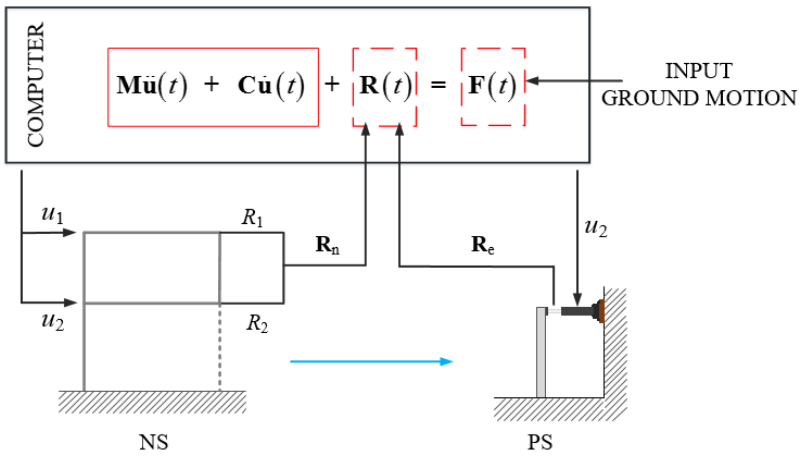

Fig. 1-3 Schematic diagram of hybrid simulation with substructures

The real-time pseudo dynamic test (Nakashima et al., 1992) is proposed to solve the problem when the effect of loading rate must be considered. Some components, such as dampers, or structures are more dependent on velocity which means the responses of these components or structures are more affected by loading rate. This leads to that the static loading of traditional

hybrid simulation cannot meet the needs.

In order to avoid the waste of existing laboratory resources and the repeat of laboratory construction, hybrid simulation are gradually expanding in the space domain. By transmitting the data through networks, several specimens can be loaded simultaneously in different laboratory located in different regions. In this way, the advantages of different laboratory resources was integrated to complete the hybrid simulation of large complex structures with multi large-scaled substructures. This is called distributed hybrid simulation, also known as international collaborative hybrid simulation (Sugiura et al., 1998; Takashi et al., 2005).

The US (NEES-Network for Earthquake Engineering Simulation) (Pauschke et al., 2003; Spencer et al., 2004), China (NetSlab-Network Structural Laboratories) (Fan, 2010) and Korea (KOCED collaboratory program) (Kim, 2014) have completed the resource integration of several local laboratories.

The following will address some key issues of hybrid simulation including the solution of motion equation, the nonlinear control, delay and compensation of actuators, and the platform for hybrid simulation.

1.2.1 Numerical integration method

In the hybrid simulation, the motion equation of the structure is discretized in time domain by numerical integral method and the displacements of the structure at each time step is obtained. Numerical integration method can be divided into explicit and implicit algorithms. If the unknown quantities (displacement, velocity acceleration) can be expressed by the known quantities at current and previous steps, then it is the explicit algorithm, otherwise it is implicit algorithm.

The advantage of explicit algorithms is that they do not require iteration, while the disadvantage is that most of them are conditionally stable and are limited by the integral step-size. Among others, the central difference method is the most classic algorithm, and is early and widely used in the field of hybrid simulation. Taniguchi et al. completed the pseudo-dynamic test of a one-bay one-story frame structure using center difference method in 1980 (Taniguchi et al., 1980). Nakashima discussed the accuracy of the central difference method and the stability margin of the method for damped and un-damped systems (Nakashima, 1985 part1 and part2). The advent of real-time hybrid testing puts forward new requirements for the central difference method. Wu et al. analyzed the accuracy and stability of the method in real-time substructure hybrid simulation (Wu et al., 2005).

In order to avoid the problem of non-convergence and over-iteration in the implicit integration methods, prediction-correction algorithm was proposed. In this method, the result of the next step are first predicted based on the previous data, and then are corrected one or more times. Both the Operating-splitting (OS) method and the Newmark-β method fall into this category of methods. However, Tada and Pan found that the stability and accuracy were poor for structures considering geometrical nonlinearity, and proposed an improved form (Tada & Pan, 2007). By combining the advantages of OS and HHT-α which is an implicit method, Combescure and Pegon proposed an α-OS method which has been applied in hybrid simulation (Combescure & Pegon, 2007). However, OS methods cannot be applied to real-time hybrid simulation, because it is only explicit for displacement, not for velocity. Wu et al. solved this problem by velocity assumption. Meanwhile, they analyzed the stability of the method and successfully applied it to a

real-time hybrid simulation (Wu et al., 2006).

For implicit methods, the advantage is that they are unconditionally stable for linear structures. The disadvantage is that there exists iterations in the process, which results in increased computational time and affects the analysis results of components with strong nonlinearity. In addition, the loading and unloading behavior caused by iterations can lead to inaccurate results. Newmark-β family and the -α family are two kinds of the most widely used implicit methods. The accuracy of the Newmark-β family is mainly controlled by the two parameters β and γ. When β = 1/4 and γ = 1/2, it is the commonly used average acceleration method; when β = 1/6 and γ = 1/2, the linear acceleration method; when β = 0 and γ = 1/2, the central difference method. Newmark (Newmark, 1959) showed that the Newmark-β family is unconditionally stable to the linear systems when $\gamma \geq 1/2$ and β = 0. Hughes (Hughes, 1977) pointed out that the average acceleration method can converge for nonlinear dynamical systems; and the convergence rate of displacement and velocity are the same. Deng (Deng, 2011) studied the stability of averaged acceleration method for nonlinear structures; and results shown that it may change to conditionally stable for dissipative structures. Though Newmark-β method can eliminate the high frequency response, it also filter out a lot of low-frequency responses of structures. This may decrease the analysis precision. Based on Newmark-β method, -α family introduced a new parameter α to filter out the high-frequency response caused by the finite element discretization, without decreasing the low-frequency response of the structure itself. If the parameter α is introduced into both the damping and stiffness terms, the method is the HHT-α method (Hilber et al., 1977); if it is only introduced into the mass term (inertial force), it is the WBZ-α method (Wood et al., 1980). Combining the HHT-α and the WBZ-α, Chung and Hulbert proposed a generalized -α method which can give the optimal combination of high-frequency and low-frequency dissipation (Chung & Hilbert, 1993).

The unconditional stability of the classical implicit integration method is limited to the linear system. When considering the nonlinearity of the structure, it may fail. Therefore, the method still possess unconditional stability for nonlinear systems is required, that is the energy method. Constraint energy momentum algorithm (Hughes et al., 1978) is a method that, based on average acceleration method, considers energy conservation through the Lagrange multiplier to correct the dynamic balance equation. In the energy-conserving integration method, the discretization is at a local level (the level of material or local coordinates) instead of the global discretization at global level used in traditional integral methods (Sim & Tarnow, 1992). However, energy-conserving integration method can only achieve energy balance when structures are elastic. The energy consistent integration method is proposed to solve the problem when structures goes into elastic-plastic phase. Crisfield and Shi proposed a uniform energy integration method based on truss elements (Crisfield & Shi, 1992). However, this method considered only the geometrical nonlinearity, not including the nonlinearity in material. Pan et al. (Wu et al., 2016; Pan, 2016) made a series study on the energy consistent integration method considering both geometrical and material nonlinearity, and applied the proposed method in hybrid simulation.

1.2.2 Loading control method and time delay compensation algorithm

Loading control method directly influences the realization of boundary conditions of specimens .It is the main part of hybrid simulation, and affects the accuracy of hybrid simulation to a large extent. Therefore, the loading control method has received a great deal of attention.

The servo -hydraulic actuator is most widely used for loading on specimens in hybrid simulations. A good strategy for actuator control will be helpful to reduce the effects of actuator delay so as to improve the accuracy and stability of hybrid simulation. Combining the PID control method and feedforward compensation method, Jung proposed a method that take into account the nonlinearity both in the oil flow of the actuator and the displacements (Jung, 2005). Wang designed an internal model control strategy and proved that this method has better robustness than PI control (Wang, 2012). Phillips and Spencer proposed a model-based approach to multi-actuator control which considered both the dynamic behavior of the actuators and the dynamic coupling between actuators (Phillips & Spencer, 2013).

According to the different control objectives, loading scheme can usually be divided into displacement control, force control and force-displacement mix control. Displacement control is a relatively mature and widely used method in hybrid simulation (Drury et al., 2002; Wagg & Stoten, 2010; Bonnet et al., 2010), because the displacement is just the solved quantity from the motion equation by computer. However, the increment of displacement for each integral step may be very small when the stiffness of specimen is large, making it difficult to guarantee the loading accuracy. At this point, force control is more applicable. In force control methods, the force command is calculated by converting the displacement command received from the computer. Sivaselvan et al. obtained a force command by introducing a flexible mechanism between the actuator and the structure to be excited (Sivaselvan et al., 2010). Kim proposed a Krylov subspace-based compatibility method to convert displacement commands to force commands and proved that the force command obtained by this method is more accurate than by traditional tangent stiffness identification (Kim, 2011). Pan et al. adopted a force-displacement mix control to complete a hybrid simulation, where the displacement control method and force control method are used to control two separate actuators connected to one specimen (Pan et al., 2010). In the meantime, the switch control strategy was adopted in the axial direction, where force control is used for pressing process, the displacement control is for pulling process. Tan et al. proposed a displacement outer loop and force inner loop control method for hybrid simulation (Tan et al., 2012). Zeng et al. developed a two loop feedback control method to keep the axial force constant and extended to multiple actuators coupled control (Zeng et al., 2014).

Time delay is the time difference between the receiving and realization of the command, which may adversely affect the accuracy and even the stability of the real-time hybrid simulation. To this end, a lot of research on delay estimation and compensation have been carried out. Darby et al. found that the change of the stiffness of the specimen will affect the magnitude of actuator delay, and provided the online estimation method of the delay (Darby et al., 2002). Wallace et al. proposed an adaptive delay compensation and improved the stability of the hybrid simulation of structures with large stiffness or small damping by overcompensation method (Wallace et al., 2010). Wang et al. used fading memory recursive least-square method to online estimate the delay. The numerical simulation of real-time pseudo dynamic test show that the accuracy, the convergence speed of the delay estimation method and the delay compensation are satisfactory (Wang et al., 2009).

Horiuchi et al. (Horiuchi et al., 1999) predicted the current step acceleration by third-order polynomial linear extrapolation by assuming linear changes in acceleration over time, and then predicted the delay compensation for the next step using the predicted acceleration and the velocity at the current step. Zhao et al. applied a first-order phase-lead network to reduce actuator delay (Zhao et al., 2003). Chen simplified the model of the servo-hydraulic system based on the first-order discrete transfer function and then compensated the actuator lag by using the inverse model (Chen, 2007). Using known structural characteristics (mass, stiffness and damping matrix) and loads, Carrion and Spencer proposed to predict actuator input displacements based on the model response to compensate the time delay (Carrion & Spencer, 2008). Phillips and Spencer developed a feedforward time-delay compensation method based on the transfer function of test structure and the model of servo-hydraulic actuator (Phillips & Spencer, 2012). Wu et al. proposed a method based on upper bound delay to compensate for the displacement and validate it with a single degree of freedom system and the five-degree-of-freedom system (Wu et al., 2012). Results shown that this method is superior to the traditional method.

1.2.3 Platform of hybrid simulation

The software platform of hybrid simulation is a necessary factor for developing real hybrid tests. In order to reduce the application threshold of hybrid simulation and further popularize the testing method, many efforts have been put into the software platform.

OpenFresco is an open source hybrid testing platform developed by Schellenberg et al. at the University of California, Berkeley (Schellenberg et al., 2006; Takahashi & Fenves, 2006). When using OpenFresco, the motion equation of structure is solved in the finite element (FE) software where the numerical substructure (NS) is established. OpenFresco is only responsible for the data transfer between the NS and the experimental/physical substructure (PS). It is note that a numerical element of the PS should be included as well in the FE model of the whole structure. Nevertheless, the restoring force of this virtual element for the PS is actually measured from the specimen, i.e. the PS. The "test cell" provided in OpenSees is precisely the element developed for this purpose. OpenFresco now offers interfaces for the FE software including OpenSees, ABAQUS, ZeusNL, and LS-Dyna, and for testing control systems including MTS, dSPACE, LabView, SCRAMNet and xPCTarget.

UI-SimCor (Kwon et al., 2006) is a platform developed by Kwon et al. at the University of Illinois at Urbana-Champaign based on the Matlab scripting language. Unlike OpenFresco, UI-SimCor is not only responsible for data transmission, but for solving the motion equation of structure with the built-in HHT-α numerical integration method. Currently UI-SimCor provides interfaces for OpenSees, Zeus-NL, ABAQUS and FedeasLab. It communicates with testing control systems through TCP/IP, LabVIEW OR NHCP (NEES Hybrid Communication Protocol).

NetSlab platform was developed by Guo et al. at Hunan University for applying the distributed hybrid simulation. This platform was later jointly improved by Hunan University and Harbin Institute of Technology. NetSlab includes the part for single degree of freedom structure (Fan et al., 2009) and as well the part for multi-degree-of-freedom structure (Guo et al., 2011).

P2P (Peer-to-Peer) is a platform for distributed hybrid simulation developed by Pan et al. (Pan et

al., 2010). On this platform, each substructure is treated equally, that is, the motion equation of each substructure is established respectively. Then the dynamic characteristics of the substructures are condensed to the boundary interface and the compatibility of the boundary conditions is responsible by the coordinator.

Hytest platform was developed by Wu et al. at Harbin Institute of Technology, which supports both standard hybrid simulation and model-updating hybrid simulation (Yang J, 2014; Yang G, 2017), and supports both local and distributed hybrid simulation. Similar to UI-SimCor, the Hytest is responsible for solving the structural motion equations as well as the data transfer between the substructures and the updating module. Currently, Hytest supports OpenSees and ABAQUS FE software and MTS control system.

1.3 State of Art for Hybrid Simulation with Model Updating

For large complex structures, such as high-rise buildings, long-span space structures, and long-span bridges, the number of key component which may exhibit strong nonlinearity under earthquakes will largely increase. When hybrid testing method is employed for investigating the seismic behavior of such structures, only one or several, but not all, of the key components can be studied experimentally as the PS due to the limit budget, laboratory sites and loading equipment. The rest key components will be numerically simulated as the NS. So, this raises the requirements for the accuracy of the numerical models of structural members with strong nonlinearity. Model updating is an effective way to improve the accuracy of numerical models, i.e. the NS in hybrid simulation. Model updating is to use the experimental data to identify/optimize the model parameters. That is the analysis results of the numerical model with these optimal parameters have a high matching with the experimental results, with a minimum error under certain criterion. By introducing the model updating into standard hybrid simulation, the parameters are optimized based on the testing data of the PS, then the optimal parameters are updated to the NS to improve the accuracy of numerical simulation, and hence the accuracy of the hybrid simulation.

The implementation of model updating mainly depends on the identification method which can be generally divided into model-based methods and non-model-based methods. Non-model based method, also known as ‘black-box’ method, such as genetic method and neural network algorithm, does not require detailed knowledge of the structure, components, or material (Nakano & Yang, 2005; Du, 2013; Hazem et al., 2014). This leads to ambiguous physical meanings of the structural or material models and their parameters. Meanwhile, taking neural network algorithm as an example, its estimating precision is related to the number of hidden layer node. As the number of hidden layer node increases, the precision increases, however, the computational efficiency decreases (Nakano & Yang, 2005). For model-based identification method, the models are usually known with the unknown parameters being identified. So, the model-based identification is also called parameter identification. In civil engineering, parameter identification focuses on identifying the parameters of constitutive models. The physical meaning

of such models and their parameters is clear and easy to understand and applied.

1.3.1 Constitutive model of beam-column element

Constitutive model (CM), also called constitutive equation, is a mathematical model that reflects the macroscopic nature of matter. In civil engineering, a CM generally reflects the stress-strain relationship of a material. In order to establish a contrast relationship with the material CM, scholars have gradually put forward the concept of section CM and component CM. The section CM reflects the relationship of the restoring force (axial force and bending moment) and the curvature in the section, whilst the component CM reflects that of the restoring forces and displacements of the structural component. Force, bending moment and stress can be collectively referred to as generalized force, while displacement, curvature and strain can be collectively referred to as generalized deformation. Therefore, the constitutive model can be understood as the relationship of the generalized force and the generalized deformation.

Over years, several methods have been developed for modelling structures and representing their nonlinear behavior under earthquake excitation. These approaches can be classified into three main categories: global model methods, structural FE model methods and continuum FE model methods (Taucer et al., 1991), as shown in Fig. 1-4. Global model method is simplest one, assuming that the material nonlinearities concentrate only at global degrees of freedom. That is to say, the force-displacement relationship at each degree of freedom is described by a nonlinear

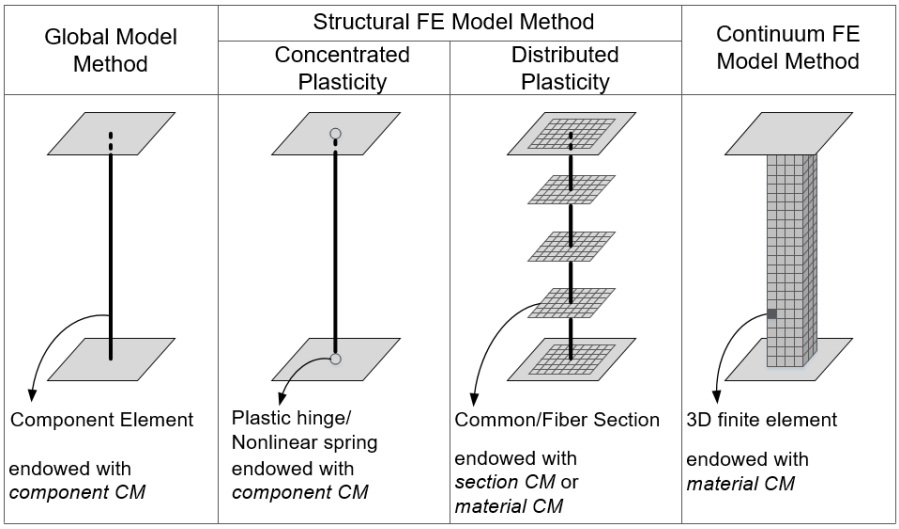

Fig. 1-4 Categories of modelling a structure

hysteresis model. However, the accuracy of the provided nonlinear responses by this method is low; and the detailed information of the section and material cannot be known. As presented in Fig. 1-4, the structural FE models take into account the material nonlinearities by two ways, concentrated plasticity and distributed plasticity. The former assumes that the material plasticity of the structural member concentrates only at the end of elements, whereas the latter assumes that plasticity distributed along the element. Continuum FE models can provide the most

accurate simulation of the nonlinear behavior, however, they are the most sophisticated and time consuming. Among the three, the structural FE models are the most widely used approach because they can meet the requirements of both the accuracy and computational efficiency. The component CMs are applicable to the global models and concentrated FE models, the section CMs are for the distributed FE models, and the material CMs are for the distributed FE models and the continuum FE models.

For the component CM, Taucer et al. summarized a number of component CMs including the models considering stiffness degradation, both the stiffness and shear degradation, the rate-based model (Taucer et al., 1991). Ibrarra et al. proposed the Ibrarra-Krawinkler model, which takes into account the stiffness and strength deterioration as well as pinching (Ibrarra et al., 2005). Ozcebe and Saatcioglu proposed a hysteretic shear model for reinforced concrete members (Ozcebe & Saatcioglu, 1989). Takizawa and Aoyama proposed a model for RC structures which contains the biaxial effects (Takizawa & Aoyama, 2010). Among others, the bilinear model and Bouc-Wen model (Bouc, 1967; Wen, 1976) are the most commonly used models in model updating of hybrid simulation.

For the section CM, there are three types of moment-curvature models that used in early study of the behavior of RC members: i) Ramberg-Osgood model (Ramberg & Osgood, 1943) came from the restoring force-displacement model of the metal; 2) the bilinear model (Gu, 2002); a bilinear-model-based section model proposed to consider both the effects of cumulative damage of concrete during reverse loading and the stiffness degradation during unloading process (Clough, 1962). To more accurately simulate the moment-curvature relation of concrete, a three-linear model and a four-linear model were proposed to represent the continually varying stiffness and energy absorbing characteristics of concrete (Takeda, 1970). Park and Young proposed a section CM that takes into the account the pinching effect generated from shear failure (Takeda & Young, 1987). Lu et al. proposed a comprehensive section CM including 10 parameters, which can be used for simulating the behavior of bending failure, shear-bending failure and shear failure (Lu et al., 2015). Wu et al. proposed a section CM considering the coupling of axial forces and bending moments, and verified the model by numerical analysis (Wu et al., 2016).

For the material CM, the most widely used in civil engineering are for steel and concrete materials. For steels, Ramberge et al. first proposed a three-parameter constitutive model in 1943, which was later called the Ramberg-Osgood model (Ramberg & Osgood, 1943). Later, Penizen proposed a bilinear model considering the effects of strain hardening of steel and the Bauschinger effect (Penizen, 1962). Menegotto et al. proposed the famous Megegotto-Pinto model (Menegoto, 1973). All these CMs for steel material above mentioned are available in the OpenSees, where the Megegotto-Pinto model is the most widely used one (Sakai & Kawashima, 2003; Bosco et al., 2016). For concrete, Sinha et al. proposed the stress-strain relationship of plain concrete under uniaxial compression (Sinha et al., 1964). Kent-Park model (Kent & Park, 1971) is the most famous and widely used CM for both the core and cover concrete by relating the parameters in core and cover concrete CM with the volumetric stirrup ratio. The model assumed that the stirrups can only enhance the ductility of concrete, but not the strength. Based on the Kent-Park model, Scott et al. proposed a CM, later called Kent-Scott-Park model (Scott et al., 1982), suitable for both the low strain rate and high strain rate concrete by adjusting

parameters to consider the influence of strain rate on confined concrete. Compared with the Kent-Park model, this model assumed that the stirrups enhanced the concrete strength and ductility to the same extent. Mander et al. proposed a new mathematic model for concrete (Mander, 1983; Mander et al., 1988), and he believed that the reinforcement of stirrup to the concrete ductility is much larger than that to the strength of concrete. Based on the Kent-Park model, Yassin [94] considered the tensile behavior of the concrete through a two-branch straight line. As the increasing of applying the FRP, the CMs of FRP confined concrete were gradually studied (Gallardo-Zafra & Kawashima, 2009; Megalooikonomou et al., 2012; Papavasileiou & Megalooikonomou, 2015). Due to the complexity of concrete material, no CM has so far been totally accepted for describing the mechanical properties of concrete material.

1.3.2 Parameter identification

System identification is to select a best model from a given set of models. This model, according a certain criteria, should be the one whose outputs can best fit the existing data. That is, if S is the system to be identified, and a model M is preset. The condition that M can be used for expressing the system S is that the error of the outputs provided by S and M satisfies the requirement according to the certain criteria. If the condition is not met, the M must be modified till the error is small enough. This optimization process is the system identification.

On the basis of the knowledge of the system to be identified, the system identification algorithm can be divided into nonparametric identification method, i.e. the 'black box' method, and parameter-based identification method, i.e. the 'gray box' method. The modern 'black box' methods, which mainly includes neural network algorithm, fuzzy logic method, genetic algorithm and particle swarm optimization, do not need to have a priori knowledge of the system S to give a preset model M. However, the physical meaning of the model of this kind of algorithm is not clear enough, which makes it difficult to be applied and promoted in the field of engineering. Moreover, the computation burden of these methods is large. In the 'gray box' methods, a relative accurate model with a certain number of parameters should be preset, and the parameters are the targets that need to be optimized according to a determined criteria.

According to the preset model, parameter identification can be divided into linear and non-linear identification methods. The preset model can be used to describe i) the relation of the parameters at the current step and those at the next step, which is called state equation/model; and ii) the relation of parameters and measurements, which is called measurement equation/model. If both the state equation and measurement equation are linear, the problem belongs to the linear estimation, otherwise, the nonlinear estimation.

Based on the process of identification, parameter identification can be divided into offline and online identification methods. The off-line algorithms, such as the deterministic least-squares method, being implemented needs that a number of data have been obtained after the test is carried out. However, in model updating hybrid simulation, the parameters need to be identified based on the data measured sequentially. This means that the number of the measurement quantity will increase, that is the dimension of the measurement will increase at each step. If a deterministic least-squares method is adopted, all the measured data obtained before the current step must be used at each step. As more observations are gathered, more computation are cost

as well as larger storage capacity is needed. With this respect, online identification algorithm is more applicable, where only the data measured at the previous step are needed. The online methods need small storage capacity providing a higher calculation efficiency.
As mentioned above, there are many different identification methods for various needs. The following contents will focus on the methods which are commonly used in the field of civil engineering.

1.3.2.1 Least square method

Least-squares estimation (LSE) is one of the most widely used methods in civil engineering. The basic principle of the method is to obtain the optimal estimation by minimizing the sum of squares of the residuals of measurements. The residual of measurement is the difference between the estimated and the measured value of the output (observation). When the credibility of each observation is different from another, a weighted least-squares estimation can be employed by weighting each measure data. The LSE belongs to offline region. In order to realize online estimation, recursive least-squares method was developed on the basis of the LSE. Later, augmented least squares, generalized least squares, and compensated least squares are gradually developed for the estimation problem with colored noise.
The LSE is widely used in civil engineering, such as the estimation of structural stiffness and damping (Caravani & Thomson, 1974; Agbabian et al., 1991; Loh & Tou, 2010), the identification of the location and level of structural damage (Chen & Bicanic, 2000; Yang et al., 2006), the identification of constant as well as time-varying parameters (Yang et al., 2006; Yang & Lin, 2004). However, the LSE can only deal with the problem belongs to linear estimation whose state equation and measurement equation are linear. It cannot be directly applied to identify the parameters of nonlinear models. For example, the identifying the parameters of a nonlinear restoring force model such as the Bouc-Wen model, the model should be linearized first. Then the LSE can be implemented. Zhang et al. successfully implemented the LSE to identify parameters of Bouc-Wen model by linearizing the equation of the restoring force and parameters using implicit integration rules (Zhang et al., 2011). Wang et al. achieved the linear measurement equation by expressing the restoration force as the combination of basic functions considering the parameters as coefficients, and identified the parameters of both the bilinear model and the Bouc-Wen model using LSE (Wang et al., 2011). However, the process of linearizing the nonlinear model is sophisticated and the precision of estimation is not good enough.

1.3.2.2 Kalman Filter

Kalman Filter (KF) (Kalman, 1960) is a linear filter proposed by mathematician Kalman in 1960, which was first implemented by Schmidt and later successfully applied to Apollo spacecraft navigation. This method belonged to LSE family solves the estimation problem of time-varying linear system. Therefore, similar with the LSE, the optimization criterion for the KF is to minimize the mean square of the output residuals. The deterministic LSE can be considered as a special case of KF. According to Bayesian theory, Doob (Doob, 1953) proves that, for parameter estimation under the cost function of minimizing the mean square of the residuals of observations, the optimal estimation is the expectation conditioned given the observation, $E(\mathbf{x}|\mathbf{y})$.

Where **x** is the state vector to be estimated, **y** is the measurements. For linear systems, the estimation provided by KF is just the optimal estimation of Bayesian, with only the need of calculating the first two moments of the variables **x** and **y**.

Fig. 1-5 shows the basic principle of KF. As shown that, a predict step was first implemented before the final correction of the variable x based on the observation residuals. The priori estimation is obtained in this predict step based on the state equation, which makes it enable to estimate the time-varying linear system. As can be seen that the predict step can be omitted when the parameters being identified are constant. The parameters can be optimized using only the observation-correct step with the measurement and its estimation. For constant parameter estimation, the KF returned to the recursive LSE.

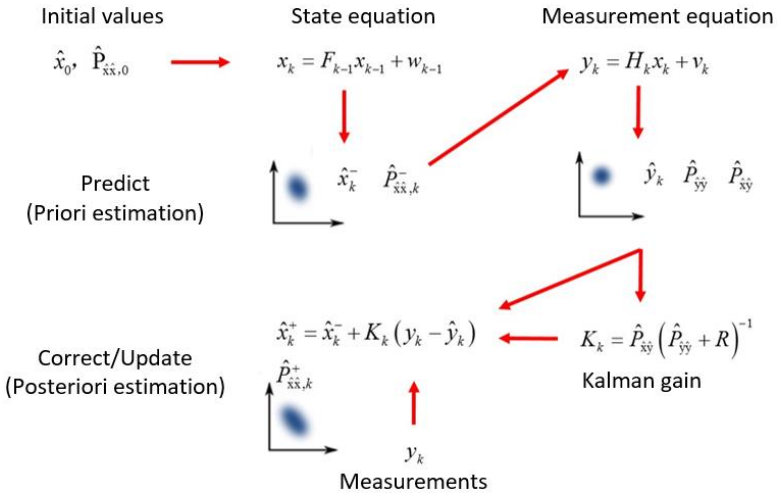

Fig. 1-5 Schematic of Kalman filter

1.3.2.3 Extended Kalman Filter

Extended Kalman Filter (EKF) is proposed to solve the problem of nonlinear estimation that KF cannot solve. The main idea of EKF is to linearize the nonlinear system in the first-order, and continue to use the linear recursive framework of KF. During the linearization process, errors were introduced, making EKF a suboptimal estimation.

The EKF was studied and applied in civil engineering began in 1980s, and was promoted and developed in the following decades. In 1980, Yun and Shinozuka applied EKF to the identification of coefficient matrices in the hydrodynamic equations of offshore structures under surges, and compared the results with the iterative linear filter-smoother (Yun & Shinozuka, 1980). The results show that both of the two methods can give relatively good estimation under the circumstance of large noise. Hoshiya and Saito applied EKF to solve the identification of structures subjected to earthquake excitation (Hoshiya & Saito, 1984). Yun et al. used the EKF method to identify the parameters of nonlinear hysteresis model used for modelling the damaged bridges (Yun et al., 1989). Ghanem et al. (Ghanem, 1995; Shinozuka & Ghanem, 1991) summarized the identification methods for anti-seismic structures and applied them to identify

the frequency and damping of structures under earthquakes. Yang et al. proposed an adaptive EKF to implement the online identification of structural parameters (Yang et al., 2006). Zhang et al. used EKF to identify the parameters of the inelastic structures that considered pinching and degradation in their hysteretic traces (Zhang et al., 2010). Li et al. proposed to combine the EKF with wavelet multiscale decomposition to identify model parameters of nonlinear structures (Li et al., 2013). Astroza et al., based on EKF, identified the parameters of the steel model used in fiber element model and achieved a good result (Astroza et al., 2015). However, EKF needs to calculate Jacobian matrices at each step, which leads to an increasing computation and even results in the system instability for a strong nonlinear problems. It is found that EKF can give a reliable estimation only when the system is linear or weak nonlinear. Furthermore, the linearization process requires the state and measurement equations to be differentiable, making the implementation of EKF difficult. In addition, the initial values of the parameters need to be identified will affect the EKF estimation. The incorrect initial values will not only lead to inaccurate estimation, but may even cause the results to divergence.

1.3.2.4 Unscented Kalman Filter

In order to better solve the problem of the identification of nonlinear systems, Julier et al. proposed the unscented Kalman filter (UKF) based on KF (Julier et al., 1995; Julier & Uhlmann, 1996). Later, other researchers (Wan & Van Der Merwe, 2000; Van Der Merwe & Wan, 2001) and Julier himself (Julier, 2002; Julier & Uhlmann, 2002) conducted an in-depth study of the UKF method to further improve the accuracy and stability of the algorithm. As the same with EKF, the UKF also built based on the linear recursive framework of KF to solve the nonlinear optimization problem. But there is no need to linearize the nonlinear systems anymore in the UKF. Instead of approximating the system by linearization, the UKF use the deterministic sampling methods and the unscented transform to approximate the first two moments, the conditional expectations and the variances of the random variables which includes both state variables need to be identified and the measurements. In the process, there are two approximations in the process of UKF (Mei et al., 2018), i) continue to use the recursive framework of KF for linear system estimation. That is, the KF can provide an optimal estimation for linear systems by using the first two moments of the state variables and the measurements. However, the first two moments are not enough to give the optimal estimation for nonlinear systems; ii) the approximations of the first two moments. Therefore, the estimation provided by UKF is not the optimal one either. However, the UKF process does not need Jacobian matrices calculation and can be used for strong nonlinear systems with a more stable and accurate estimation (Mariani & Ghisi, 2007).

The study and application of UKF in civil engineering began later than that of EKF. In 2007, Mariani and Ghisi applied UKF to the state estimation and parameter identification of SDOF structural system (Mariani & Ghisi, 2007). In the same year, Wu and Smyth used UKF to identify the parameters of a strong nonlinear model of structures and compared it with the EKF (Wu & Smyth, 2007). The results showed that the UKF is more accurate and robust to noise. In 2008, Wu et al. identified the parameters of a nonlinear hysteresis model that considered degradation and slipping of the steel bars (Wu & Smyth, 2008). In 2009, Eleni et al. used the particle filter and UKF respectively to identify the nonlinear structural system with non-collocated heterogeneous

sensors for velocity and acceleration (Eleni et al., 2009). The results shown that UKF has higher accuracy than PF as well as lower computational burden. In 2010, Chatzi et al. (Chatzi et al., 2010)] used the UKF method to identify the parameters of a nonlinear structural model based on the experimental data in provided in reference (Tasbihgoo et al., 2007). In 2013, Tao used the UKF method to online identify the shear-type nonlinear substructure and its seismic damage (Tao, 2013). Song and Dyke applied the UKF to the hybrid simulation to identify the parameters of the models of MR damper and the steel frame structure (Song & Dyke, 2013). Then the convergence value of the parameters were used to update the numerical model, which validate the effectiveness of the model updating. In 2014, Wu and Wang proposed a constrained unscented Kalman filter and applied it to identify the parameters of Bouc-Wen model (Wu & Wang, 2014).

1.3.3 Model updating hybrid test

The model updating method is an effective method to improve the accuracy of the numerical substructure (NS) in hybrid simulation by making full use of the data measured from the experimental/physical substructure (PS). According to the identification methods, the model updating of hybrid simulation can be divided into two categories, the non-model-based updating method and the model-based parameter-updating method. Due to the clear physical meaning and computational efficiency, the model-based parameter-updating methods are extensively applied. Depending on whether the parameters are being updated during the experiment, model updating can be divided into offline and online methods. Offline model updating refers to that the parameters are identified and updated after the experiment, then the model that has been updated with the identified parameters is used for numerical analysis. Hybrid simulation requires online updating where the parameters can be identified and updated at each step during the test. The schematic of the hybrid simulation with online model-based parameter updating is presented in Fig. 1-6.

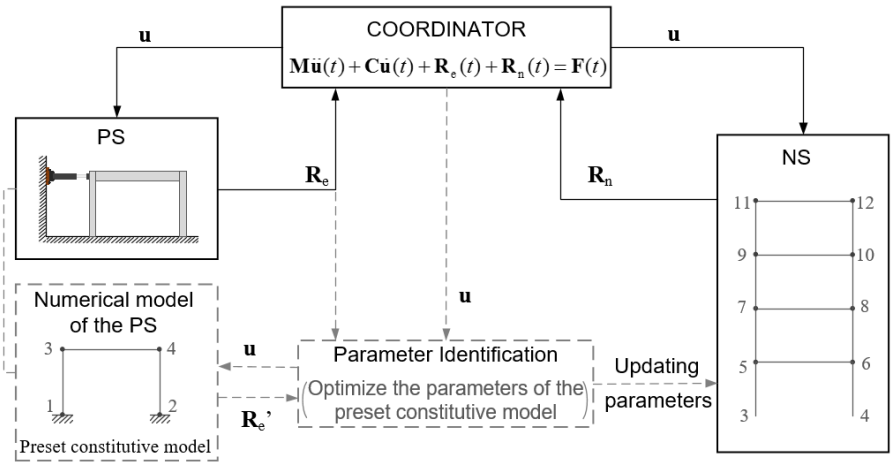

Fig. 1-6 Schematic of hybrid simulation with and without model updating

In Fig. 1-6, the standard hybrid simulation (SHS) without model updating is presented by the parts with black solid lines, in which the coordinator is responsible for solving the motion

equations of the structure and sending the calculated displacement **u** to both the PS and the NS. The PS and NS send back the measured and numerical restoring forces, $\mathbf{R}_e$ and $\mathbf{R}_n$, respectively. Then after receiving the forces, the coordinator solves the equation at next the next time step and the hybrid test goes into next step. By adding a module of model updating which is the part with gray dashed line shown in Fig. 1-6, the hybrid simulation with model updating (UHS) can be achieved. A numerical model of the PS, which includes the preset constitutive model, should be built to obtain the estimation of measurement, $\mathbf{R}_e$' in this paper, for parameter identification. According to a certain criteria, the optimal parameters which minimize the residual of measurement and its estimation, $\mathbf{R}_e$ and $\mathbf{R}_e$' in this paper, can be provided by the module of parameter identification. Then the optimal parameters will be updated to the NS with the same preset constitutive model. Note that, these optimal parameters are those for the preset constitutive model of the PS, not for the NS. So, these parameters can only be used to update the NS's components that employed the same preset constitutive model with the PS. For the preset constitutive model, it can be a hysteretic component model that directly expresses the force-displacement relationship of the structural member, a section constitutive model that describes the moment-curvature relationship of the section, or a material constitutive model that presents the stress-strain relationship. In the UHS, the coordinator is also responsible for solving the motion equations to obtain the displacement and transmitting the data. The calculated displacements are sent the PS, the NS and as well the identification module. The PS is then loaded and the measured restoring force is sent to the coordinator and the identification module. In this process, the identification module and NS are in a state of waiting. After receiving the measurement from the PS, the identification module executes the optimization process in which the NS is still in waiting state. After the optimal parameters are received from the identification module, the parameters in the preset constitutive model of the NS are firstly updated and then the computing of the NS is proceeded and the simulated restoring forces are send to the coordinator. Finally, the coordinator goes into the next step and solve the motion equation at next time step.

The UHS was first proposed by Yang WJ and Nakano, and was verified through numerical simulation and experimental way (Yang & Nakano, 2005). Using neural network algorithm, they made online predictions of the restoring force of a shear model based on the measured data from the PS. The target is a two-story frame structure, whose first story is considered as the PS, and the second story is as the NS. The experimental data of the PS is used to optimize the shear model for simulating the hysteretic behavior of the second-story frame. The accuracy of neural network algorithm depends on the number of hidden layer nodes. The increasing of the number of hidden layer nodes can improve the accuracy of the algorithm, however dramatically decrease the computational efficiency. Therefore, the application of the algorithm in hybrid simulation is limited. In 2009, Yang YS elaborated the framework of the UHS and implemented the UHS on a three-span continuous rigid frame bridge in a numerical way (Yang et al., 2009). The effectiveness of model updating to improve the accuracy of the NS, and hence the hybrid simulation, was verified by numerical simulation. In this numerical test, one of the two piers was simulated by a refined FE model to set as the PS, whist the other was simulated by a hysteretic model to taken as the NS. In the numerical simulated hybrid simulation, the conditions that influence the hysteretic behavior of the two piers are the same. So, the added hysteretic model

of the PS for parameter identification was the same as that of the NS. Therefore, the parameters optimized using the 'measured' data of PS were updated to the hysteretic model which is for the NS in the process of the hybrid simulation. In 2010, Zhang used the LSE to identify the parameters of the ideal elastic-plastic model, the bilinear model and the Bouc-Wen model, and applied them to realize the adaptive hybrid simulation (Zhang, 2010). Wang et al. applied the LSE (Wang et al., 2014) and the UKF (Wang et al., 2013) to a hybrid simulation of a two-story braced frame. The brace of the base-story frame was taken as the PS, the remainder was isolated to be the NS. The numerical model of the PS was the same as that of the brace in the secondary-story frame. During the test, the parameters of the model of the PS were identified using the restoring force of the PS, and updated to the model of the brace in the secondary-story frame. Subsequently, Wang and Wu proposed a new constrained UKF algorithm by modifying the sampling points, and applied it to a UHS (Wang & Wu, 2013). In 2013, Kwon and Kammua proposed a new idea for model updating (Kwon & Kammua, 2013). This method assumes that the model to be optimized is a weighted linear superposition of several models, and the parameters to be identified and updated are the weight coefficients for the linear superposition. The results shown that the updated model can well simulate the hysteretic behavior of PS. In 2014, Hashemi et al. carried out a UHS of one-bay one-story frame based on the OpenFresco software platform (Hashemi et al., 2013). In this test, the left column is the PS whose preset component constitutive model, the Bouc-Wen model, is the same as that for simulating the right column, i.e. the NS.

The model updating in the hybrid simulations completed in the above literature were all focused on the constitutive model at the component level. This kind of component constitutive model can satisfy the requirements that only concern the force-displacement relationship of structural members, but cannot meet the needs of those who care about the behavior of sections and even materials. Moreover, for large complex structures, the number of structural members that may experience strong nonlinearity is increasing, which may leads to that the factors that may influence the nonlinear behavior of structures, such as the dimensions of these key members, the shape of the cross-section, the volumetric stirrup ratio, the boundary conditions and the axial compression ratio, are various. However, the component constitutive models, such as the most widely used Bouc-Wen model, does not includes sufficient parameters to describe the nonlinear behavior of components or structures that cover all the above factors. Therefore, using the existing component constitutive models for model updating of hybrid simulation of a large structure needs more PSs to cover the various factors. To solve this problem, Wu et al. proposed to identify the parameters of section constitutive models (Wu et al., 2016), making model updating can be used for the structural members with the same sectional shape and materials, but with different length and sectional size. However, the model updating still cannot be used for the structural members with different sectional shape, boundary conditions, volumetric stirrup ratio for RC structures and other factors.

1.4 State of Art for RC Continuous Rigid Frame Bridges with Hollow Thin-walled Tall Piers

Bridges are great important parts of the lifeline projects. Some of them, which were built in the earthquake-prone areas, faces great potential threat. Once the bridge is destroyed, the traffic will be interrupted, which hinders the rescue work after the earthquake. Therefore, it is essential to study the seismic behavior of various types of bridges.

The RC continuous girder bridge is one of the most early and widely used bridges in the world. Due to the absence of expansion joints, such bridges have a good smoothness for driving. However, this type of bridge needs bearings whose maintenance cost is high, and the structural system needs to be converted after the bridge is closed. In the 1960s, with the improvement of construction technology, RC continuous rigid frame bridges gradually developed and applied. They not only maintains the advantage of continuous beam bridge without expansion joints for good vehicle running, but also maintains the advantage of no support and no system conversion for T-shaped rigid frame bridge.

The pier and beam of continuous rigid frame bridges are consolidation, making the integrity and seismic performance of this kind of bridge are good. Comparing to T-shaped frame bridge, the flexible/tall piers are commonly used for continuous rigid frame bridge, which may reduce the displacement at the pier top produced by shrinkage and creep of concrete as well as the temperature. A hollow cross-section is particularly common for the design of RC tall piers since it can provided provide sufficient stiffness with a reduced cross-section area which brings the benefit of cost savings, and the reduction of pier mass resulting in the attenuation of the relevant seismic responses. Therefore, the continuous ridge bridges with long span and hollow-section tall piers have been widely constructed, especially in mountainous area in southwest China due to its good spanning ability to cross deep canyons (Du et al., 2011). However, there is still no clear definition on with how much height the pier belongs to the tall pier. China Highway Bridge Seismic Design Rules (JTG / T B02-01-2008) requires that the bridge with pier height of more than 40 meters should be conducted special study. So, a bridge with a pier height greater than or equal to 40 meters is considered as a tall-pier bridge in this study. The representative tall-pier RC continuous rigid frame bridges are listed in Table 1-1.

It is seen from Table 1-1 that the flexible piers mostly adopt the hollow cross-section, and the higher the pier, the larger the section size and the smaller the thickness-width ratio. Except for Stolma Bridge, the thickness-width ratios of other piers are less than or equal to 0.1, belonging to the category of thin-wall structure. This special cross-section seriously weakens the shear capacity of the pier, which may directly change the pier into a "strong bending and weak shear" component. Research results show that many hollow thin-walled piers with shear-span ratios above 3.0 and even above 4.0 still suffer shear-bending failure or even shear failure directly (Dermizakis & Mahin, 1985). Investigations of earthquake damage show that some of the bridges, with thin-wall hollow-section piers, that built in mountainous area were seriously damaged or even collapsed though they have been seismic designed according seismic codes.

However, the study on the seismic behavior of this type of bridges is still not sufficient. The failure mechanism and the design theory for them are still inadequate. In China, the design of this type of bridges is still based on the rules for conventional bridges. In this section, the reviews are

presented from several aspects of the experimental and numerical simulation of thin-wall hollow-section tall piers, and the hybrid simulation of continuous rigid frame bridge with the type of piers.

Bridge name	Completion time	Span length (m)	Pier height (m)	Shear-span ratio	Thickness-width ratio	Shape of pier section
Gateway bridge	1985	145+260+145	48.28	4	0.1	Single-box Three-rooms
Moony bridge	1986	130+220+130	63	8.4	0.04	Single-box Single-room
Hu-Men bridge	1996	150+270+150	35	2.9	0.07	Single-box Single-room
Stolma bridge	1998	94+301+72	37	7.4	0.13	Single-box Single-room
Yuan-Jiang bridge	2003	58+182+265+194+70	123.5	8.8	0.07	Single-box Double-rooms
Niu-Lan river bridge	2007	90+170+90	126.06	10.5	0.07	Single-box Single-room
Long-Tan river bridge	2008	106+3×200+106	178	8.3	0.05	Single-box Single-room

Table1-1 Representative rigid frame bridge with hollow-section tall-piers

Notes: 1. the thickness-width ratio is defined as the ratio of the wall thickness to the smaller width of the cross-section of a rectangular section pier; 2. the shear-span ratio is defined as the ratio of pier height to the width of the cross-section.

1.4.1 Seismic performance of thin-wall hollow-section tall piers

Although there are a certain number of theoretical and experimental studies on the seismic behavior of hollow-section piers (Takahashi & Iemura, 2000; Du et al., 2011; Pinto, 2013), the research on the seismic behavior of thin-walled hollow-section pier is still limited. Sun (Sun, 2013) gave a review of 74 tests that have been implemented on hollow-section piers, among which, only the pier tested by the quasi-static method in literature (Pinto, 2013) belongs to the thin-wall hollow-section category. Li et al. analyzed the thin-wall hollow-section piers in mountainous area from the aspects of construction and mechanical properties by numerical simulation (Li et al., 2007). Liang and Li investigated the rationality of how to modeling the seismic behavior of tall piers using both the elastoplastic beam-column element and the fiber-section beam-column element (Liang & Li, 2007).

The research on the seismic behavior of thin-wall tall piers has been receiving more and more

attention since 2010. Sun et al. carried out a number of studies on the seismic behavior of thin-wall hollow section piers by numerical analysis and quasi-static tests. In 2012, using the fiber-section beam-column element, he analyzed the capacity of ductile deformation of thin-wall piers with different shaped cross-section (circular, square and rectangular section), and different pier height (Sun et al., 2012; Sun, 2012). In 2013, he studied on how to accurately modeling the hysteretic behavior of the piers considering the shear effects (Si et al., 2013). In the same year, he analyzed the shear behavior of the piers with rectangular thin-wall section by means of quasi-static tests of two specimens (Sun et al., 2013). Han et al. conducted experiments on five piers with rectangular hollow section, whose thickness-width ration were 0.128 which though is larger than 0.1 but quit close. It was found from the study that the length of the plastic hinge of the thin-wall piers are about their 1/6 height, which is much less than the recommended value of the seismic design codes of bridge (JTG / T B02-01) (Han et al., 2013). In 2014, Du et al. carried out a series of quasi-static tests on 12 RC piers with rectangular hollow section, and provided the failure modes of such piers, the cumulative probability of the width of residual crack, the distribution and cumulative probability of compressive strains when the concrete was cracking and spalling, and the relationship between compressive strains and spalling height (Du et al., 2013). On the basis of the experimental data, the force-displacement relationship of RC piers with rectangular hollow section in OpenSees were improved. In 2015, using the same designed specimens as that in the literature (Sun et al., 2013), Jiang studied damage mechanism of such piers with thin-wall section through several quasi-static tests considering constant axial force and varying axial forces (Jiang, 2015).

1.4.2 Hybrid simulation of continuous frame rigid bridges with thin-wall piers

The methods adopted in the literatures presented in section 1.4.2 were quasi-static testing method through which we cannot know the dynamic characteristic of the pier and the seismic responses of the bridge. Therefore, it is very important to learn the dynamic behavior of the bridge subjected to earthquakes. The pier height and span of the continuous rigid frame bridge are usually large. Even the specimen of the bridge structure is scaled, it still presents a high demand on the size and loading capacity of the equipment for a shaking table test. With this respect, pseudo-dynamic testing method becomes the most effective method to study the seismic performance of large bridges.

In 2010, Li Z. (Li, 2010) conducted a hybrid simulation on a 1/12 scaled model of the whole bridge is named Niulanjiang Bridge which is shown in Table 1-1. In this experiment, the bridge is simplified as a two DOFs system along the transvers direction of the bridge, as presented in Fig. 1-7(a). The lateral displacements at the top of the two piers are loaded respectively by two actuators. In 2011, Li B. (Li, 2011) used the same scaled model of Niulanjiang Bridge to study the seismic behavior of the bridge considered only one DOF in transverse direction, as shown in Fig. 1-7(b). In 2013, in exactly the same way as give in literature (Li, 2010), Shen complete the hybrid simulation of Niulanjiang Bridge and then used ABAQUS FE software to analyze the dynamic responses of the bridge subjected to El-Centro, Taft, and Wenchuan earthquake waves (Shen, 2013).

However, for large bridge structures, it is difficult to consider the influence of multiple DOFs and

high frequency through the hybrid simulation of the whole structure, due to the limitation of the number and capacity of loading equipment. While hybrid simulation with substructures, which isolates a few of key components from the target structure to be the physical substructure (PS), can consider more DOFs and the responses generated by high frequency through the numerical simulation of the remainder parts of the target structure, i.e. the numerical substructure (NS). Meanwhile, sub-structuring hybrid simulation can greatly save the costs. For building structures, especially the frame structures, the sub-structuring hybrid simulations carried out for bridge structures are inadequate (Mosqueda et al., 2008; Yang et al., 2012; Abbiati et al., 2015). The research on thin-wall tall-pier RC continuous rigid frame bridge using sub-structuring hybrid simulation is even more limited. Pinto et al. conducted a sub-structuring pseudo dynamic test to simulate the seismic behavior of the existing Talubergang Warth Bridge who has 6 piers in total (Pinto et al., 2004). The lowest pier is 16.25m, the others are all higher than 30m, among which, the highest one is 39m. The thickness-width ration is 0.08 of these piers. The experimental results shown that the seismic behavior of the bridge was poor, evidenced by irregular distribution of damage, limited deformation capacity and undesirable failure locations.

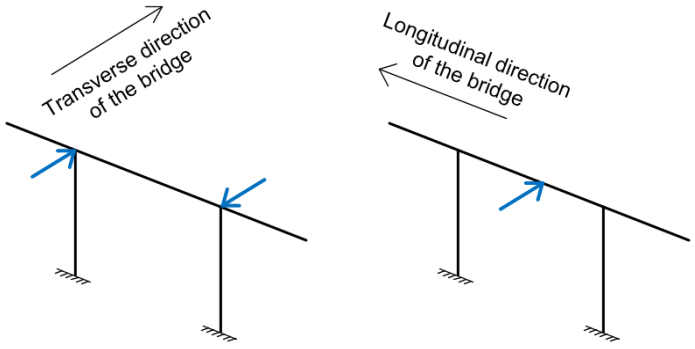

Fig. 1-7 Simplified experimental model

1.5 Main Contents

The purpose of this paper is to improve the accuracy of the numerical substructure (NS) in the hybrid simulation and hence the reliability of the hybrid simulation. The key problems to be solved in this paper are as follow:

1. The model updating in hybrid simulation mostly focuses on identifying and updating the parameters of the component constitutive model. The errors of the numerical simulation based on component constitutive model are usually large, and the knowledge of the section and material cannot be learned. Furthermore, for RC structures, there is no generalized constitutive model that can include the factors which are size of component, boundary conditions, axial compression ratio, stirrup ratio, etc. The narrow component constitutive models for different

components, such as the bilinear model and Bouc-Wen model, the identified parameters are difficult to update to the model for various components. This limits the application of model updating hybrid simulation to promote. To solve these problems, the parameters of material constitutive model were proposed to be online identified and updated in hybrid simulation.

2. The restoring force of the specimen/physical substructure (PS) was proposed to be used as the measurement in this paper as the concrete stress is difficult to accurately measure. To this end, a finite element software is needed to be the auxiliary means. The widely used software in civil engineering do not have the functions needed for the proposed parameter identification and updating. Therefore, the OpenSees whose source codes is open was employed and its codes were developed to realize the required functions.

3. The studies on the seismic performance and damage mechanism of RC continuous rigid frame bridges with thin-wall tall piers are still inadequate. Therefore, a bridge belongs to this type was taken as the target structure. A number of hybrid simulations including both the hybrid simulation with and without model updating were carried out with a view to providing reference for learning the seismic performance of such bridges to some extent.

To solve the three key issues, four main parts of contents were finished as follow and the framework of the thesis and the arrangement of chapters are shown in Fig. 1-8.

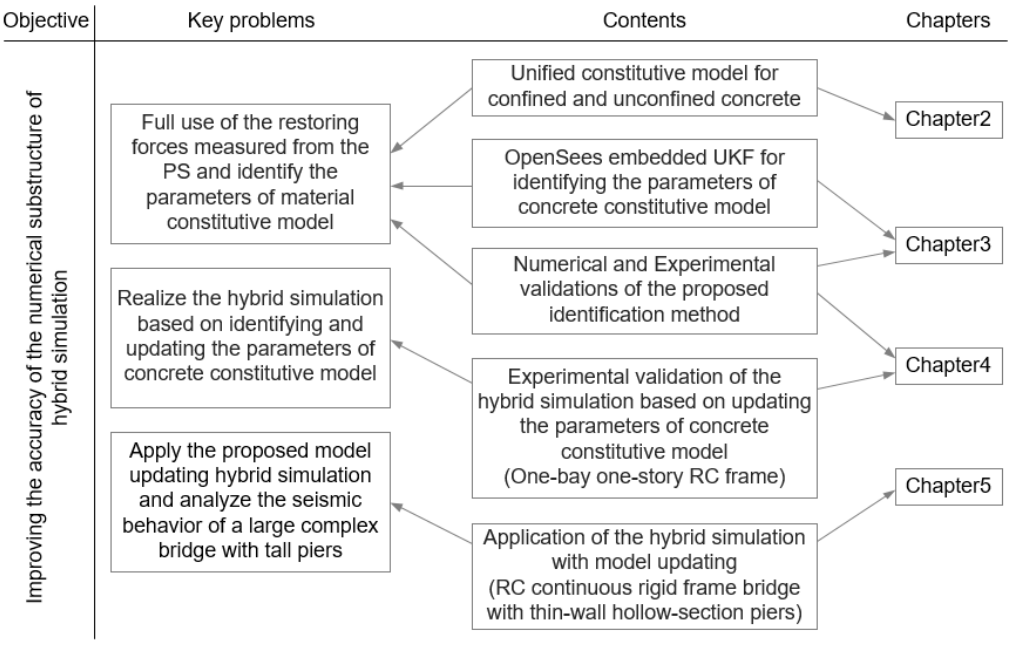

Fig. 1-8 Research strategy

1. The conditions of model updating are given; the unified constitutive model of cover/unconfined and core/confined concrete which is suitable for model updating in hybrid simulation is derived based on the existing uniaxial concrete constitutive models; the approach for determining the initial values of the parameters in this unified model is given and the sensitivity analysis of these parameters were carried out to reduce the number of the parameters being identified.

2. Analyze the estimation precision of the conditional expectation and variance provided by the

scaled symmetry sampling method adopted in the unscented transform (UT) of UKF; verify the feasibility of concrete constitutive parameter identification by numerical method with concrete stress as measurement; propose the OpenSees embedded UKF to solve the identification problem when the restoring force is taken as the measurement; verify the proposed identification method through numerical simulation and analyze the reason for the fluctuations in the process of parameter convergence.

3. Verify the identification method by experimental means; apply the identification method to the model updating hybrid simulation (UHS) of a one-bay one-story RC frame to validate the hybrid simulation based on identifying and updating the parameters of concrete constitutive model.

4. Apply the proposed hybrid simulation with updating the parameters of constitutive concrete model to a more complex RC long-span continuous rigid frame bridge with strong nonlinearity and larger model errors to validate its practicality and reliability; Analyze the seismic behavior of such irregular bridges with thin-wall hollow-section piers.

2. CONCRETE CONSTITUTIVE MODEL EMPLOYED FOR PARAMETER IDENTIFICATION AND UPDATING

2.1 Introduction

For RC structures, the component constitutive models (CMs) which were mostly used in the model updating of hybrid simulation mainly focus on Bouc-Wen model. However, the Bouc-Wen model cannot include all the factors that influence the hysteretic behavior of component, such as the area of the cross-section, axial compression ratio, reinforcement ratio, etc. Take bridge structures as an example, if only one pier can is isolated to be the PS, the other piers with different sectional areas and stirrup ratios are numerically considered, and the Bouc-Wen model is adopted to represent the behavior of the experimental/physical substructure (PS) and as well as the numerical substructure (NS), then the parameters in the Bouc-Wen model of the PS are different with those of the NS. Hence, the parameters identified for the PS cannot be updated to the NS. That is, only when the factors that influence the hysteretic behavior of the PS are the same as those of the NS, the parameters can be updated. Therefore, it is limited to use the component CM for model updating in hybrid simulation.

The idea of identifying and updating the parameters of material CM is proposed for model updating hybrid simulation. In RC structures, the behavior of concrete and its simulation have more uncertainties than those of steel bars. So, the study is focused on the CM of concrete. Due to the complexity of concrete, a lot of efforts have been done on concrete CMs since the1960s. The concrete constitutive laws can be divided into one-dimensional (uniaxial), two-dimensional and three-dimensional models (Soliman & Yu, 1967; Li & Ren, 2007; Yu & Lu, 1998). Considering that the hybrid simulation may take a long time, the uniaxial concrete constitutive model was chosen as a case study. It can not only reduce the computational cost, but also provides sufficient precision for the nonlinear analysis of bending members such as the columns in frame structures and the piers in bridge structures. There are three kinds of axial constitutive models for concrete in OpenSees (now up to nine). The concrete01 model which has a good convergence is selected for simulating the mechanical behavior of concrete, whose parameters are identified and updated.

Stirrups divide the concrete into two parts: the confined (core) and the unconfined (cover) concrete. Commonly, bases on lots of experimental results, it is assumed that the constitutive models of core and cover concrete have the same function expression but different parameter values (Kent & Park, 1971; Scott et al., 1982; Mander, 1983; Mander et al., 1988). With regard to Concrete01 model, it can be used to simulate both the core and cover concrete by using different parameter values. For cover concrete, if the concrete used in the PS is the same as that in the prototype of the NS, then the parameter values of Concrete01 used for the model of the PS are the same as those for the NS. In this case, the parameters of Concrete01 in the model of the PS, which are identified using the measured forces of the PS, can be directly updated to the Concrete01 of the cover concrete in the NS. However, for core concrete, it may occur that the factors that influence the behavior of the core concrete, such as the stirrup ratio, of the key components in the NS are different from those of the PS, when only one or two key members of a

large structure can be considered as the PS. If the Concrete01 is employed to simulate the performance of the confined concrete, the parameters for the key components in the NS are different from those in the model of the PS. In this case, the identified parameters of confined concrete in the model of the PS cannot be directly used to update the NS.
To solve this problem, using the cover concrete as a bridge, a unified constitutive law of the core and cover concrete is derived to establish the relationship between the constitutive model of the core concrete in the NS and that in the numerical model of the PS. In this way, the parameter updating in hybrid simulation can be achieved.

2.2 Conditions for Model updating

Constitutive model (CM), also called constitutive law, is a mathematical model that reflects the macroscopic nature of matter. In civil engineering, a CM generally reflects the stress-strain relationship of a material. In order to establish a contrast relationship with the material CM, scholars have gradually put forward the concept of section CM and component CM. The section CM reflects the relationship of the restoring force (axial force and bending moment) and the curvature in the section, whilst the component CM reflects that of the restoring forces and displacements of the structural component. Force, bending moment and stress can be collectively referred to as generalized force, while displacement, curvature and strain can be collectively referred to as generalized deformation. Therefore, the CM can be understood as the relationship of the generalized force and the generalized deformation.
Strictly, when we say two CMs are the same, it means both the parameters and the expressions are the same. Taking the component CM as an example,

$$F = f_1(d, \mathbf{P}_1) \qquad (2\text{-}1)$$

$$F = f_2(d, \mathbf{P}_2) \qquad (2\text{-}2)$$

where F refers to the restoring force, d the displacement, f_1, f_2 the functional expression, $\mathbf{P}_1$, $\mathbf{P}_2$ the vector of parameters. if we say the two constitutive laws, Eq. (2-1) and Eq. (2-2), are the same, that means the functional expressions are the same, i.e. $f_1 = f_2$, and the parameters are the same, i.e. $\mathbf{P}_1 = \mathbf{P}_2$. According to this, if Eq. (2-1) is for the preset constitutive law of the numerical model of the PS, Eq. (2-2) is for the NS, the condition for parameter updating is that these two CMs are the same. Then the $\mathbf{P}_1$ identified from the PS can be used to replace, i.e. update, the $\mathbf{P}_2$.
In a broad sense, the component CM should include all the factors that influence the displacement-force relationship, such as the shape of the cross section, reinforcement ratio, volumetric stirrup ratio, boundary conditions, etc. In a narrow sense, the component CM can be a force-displacement relationship for one component. The Bouc-Wen model, the ideal elastoplastic model and the bilinear model are all the models in the narrow sense. Taking the ideal elastoplastic model as an example, if this model is used for model updating, that is, this model is

employed for both the numerical model of the PS and components that need to be updated in the NS. The model is controlled by two parameters which are the stiffness and the yield strength of the component, as shown in Fig. 2-1 where F and K denote the stiffness and the yield strength of the component respectively; the subscript n refers to the NS, e the PS. If all the factors that influence the force-displacement relationship of the PS are the same as those of the NS, the component constitutive laws of the both are then exactly the same. The identified values of F_e and K_e can be updated to the NS.

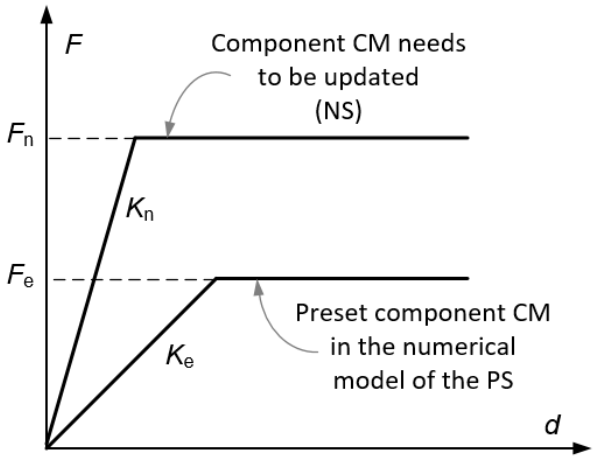

Fig. 2-1 Elastic-perfectly plastic model

However, it is unrealistic to take out all the key members as the PS. For large and complex structures such as high-rise buildings, super tall buildings and bridge structures, a large part of key components should be simulated as the NS. Among them, there are key components that possess different force-displacement relationship with the PS. That is, $F_e \neq F_n$ and $K_e \neq K_n$, making parameter updating unworkable. In this situation, if such component CM is still used for model updating, the number of the PS must be increased to satisfy various key members being updated in the NS. However, increasing the number of PS is not a good choice due to the high cost, the limitation of loading equipment in the laboratory and low computational efficiency of parameter identification.

There are basically two ways to solve this problem:

1. Derive a unified/generalized component CM including as many as the factors that influence the force-displacement of a component.

Taking the steel structure as an example, if the ideal elastoplastic model is still used to describe the force-displacement relationship of the NS to be updated and the PS. Assuming that the stiffness of the column, K, is only related to the area of the cross section. The boundary conditions, axial compression ratio, height of components and other factors of the NS and the PS are all the same. Then, we may obtain the relationship of K_n and K_e as follow,

$$K_n = \frac{A_n}{A_e} K_e \qquad (2\text{-}3)$$

where A_e is the area of the cross section of the PS; A_n the area of the cross section of the NS. It is found that the K_n can be updated through Eq. (2-3), though the two CMs are different.

From another perspective, a unified CM of the PS and the NS can be derived through the Eq. (2-3), which is,

$$F = g(d, K_e, A_e, A_n, F_e, F_n) \qquad (2\text{-}4)$$

Furthermore, if we know the relationship between F_n and F_e, such as $F_n = CF_e$, the two constitutive models can be further unified as,

$$F = g(d, K_e, F_e, A_e, A_n, C) \qquad (2\text{-}5)$$

where, A_e, A_n and C are the parameters that can be predetermined; K_e and F_e are those need to be identified and updated. This means that the component CM of the NS can be described by the parameters K_e and F_e of the CM of the PS. In this way, the parameters K_n and F_n in the component constitutive model of the NS can be updated by K_e and F_e, using the parameters A_n, A_e and C.

The parameters that directly related to the CM, like the parameters K_e and F_e in Eq. (2-5), are defined as constitutive parameters in this study, and other parameters that indirectly affects the CM through the constitutive parameters are defined as non-constitutive parameters. Therefore, from the viewpoint of model updating, the same CMs can be defined as the models have the same functional expression and the same constitutive parameters, when the non-constitutive parameters can be determined in advance. Based on this concept, the condition for model updating in hybrid simulation is that the CMs in the NS and the PS are the same.

Strictly, Eq. (2-5) is still not the essential component CM for structural components, because it does not include other factors that influence the displacement-force relationship of the components. However, it is more generalized for model updating than the CMs shown in Eq. (2-4) and Fig. 2-1. Similarly, if a more generalized component CM considering a series of factors such as the shape of the cross section, the component size, the axial compression ratio, the stirrup ratio, etc., then the component CM can be more extensively applied to model updating in hybrid simulation.

However, it is unworkable to derive a generalize component CM that includes so many factors. Even if such a CM can be obtained, the number of parameters being identified will greatly increase leading to a low computational efficiency. Meanwhile, the sectional and material information of the structural members cannot be known in detail, as well as a poor precision results using the component CM.

2. Identify and update the parameters of material CMs. When establish a finite element model of structural components, the factors containing the shape and area of the cross section, length of the component, boundary conditions, axial compressive ratio, etc. are all can be considered without affecting the material CMs. That is, as long as the prototype of the members of the NS has the same material as the PS, the same material CM can be employed for both the numerical model of the PS and the members in the NS. The optimal parameter values obtained for the numerical model of the PS can be updated to the members of the NS.

This study addresses in identifying and updating the parameters of material CMs, and applied it to model updating in hybrid simulation.

2.3 Concrete Constitutive Model

OpenSees is a widely used open source software for the seismic analysis of structures. It is used as a supplementary finite element tool to realize online identification of material constitutive parameters, due to the advantage of easy to develop.

Based on the Concrete01 model of OpenSees, a unified constitutive model (CM) of unconfined and confined concrete for model updating was derived in this section, by summarizing and deducing from the existing CMs of concrete. The unified model contains eight parameters in total, where seven of them are constitutive parameters and one is non-constitutive parameter.

2.3.1 Concrete01 model

The Concrete01 model is a uniaxial CM that provided by OpenSees, which ignores the tensile behavior of concrete. This model follows the quadratic parabola-straight line functional expression of Hognestad model to describe the compressive performance of concrete, as shown in Fig. 2-2. Segment OB is for ascending with a quadratic parabola, whilst segment BC is for descending with a straight line. In order to ensure the stability and convergence, a CD straight line is added to describe the concrete performance after failure, which the strength of the concrete remains constant and the strain increases indefinitely.

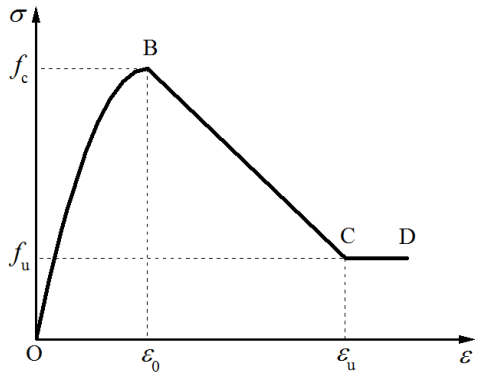

Fig. 2-2 Concrete01 model

The Concrete01 model has four controlling parameters, where f_c is the peak strength, ε_0 is the strain corresponding to f_c, ε_u is the ultimate strain, and f_u is the ultimate stress. By giving different parameter values, Concrete01 model can used for describing the mechanical behavior of concrete with different strength, and also for the behavior of core and cover concrete at the same strength level.

For different RC members A and B, their CMs of cover concrete are the same if they the same concrete material, but those for core concrete are different because their volumetric stirrup ratios

may be different. When Concret01 is employed, the functional expressions of the cover concrete A, the core concrete A, the cover concrete B, and the core concrete B are all the same. Meanwhile, the parameter values in Concrete01 of cover concrete A and cover concrete N are the same. For core concrete of A and B, the parameter values are also the same if their lateral restraint forces provided by stirrups are the same; otherwise, the values are different. However, a number of components with different lateral restraints may existing of large structures.

Taking the bridge in Fig. 2-3 as an example, the concrete material used for the three piers are usually the same. For each pier, the CMs should be distinguished by using different parameter values of Concret01, as shown by the solid and dashed lines respectively. As the concrete materials are the same from one pier to the other, the parameter values of Concrete01 for the cover concrete of the three piers should be the same for simulating the mechanical behavior. Assumed that Pier 1 is the PS, the optimal parameters of cover concrete CM for Pier #1 can be directly used to update the cover concrete CMs for Pier #2 and #3. However, it is difficult to ensure that the lateral restraints provided by stirrups are the same of the three piers. Which is, the parameter values of the confined concrete CM of the three piers are likely to be different. Let us assumed that the lateral restraint of Pier #2 is the same as Pier #1, while Pier #3 is different. Then, the optimal parameters of the confined concrete CM of the PS, i.e. Pier #1, can be directly used for updating the CM of Pier # 2, but cannot be used for Pier #3.

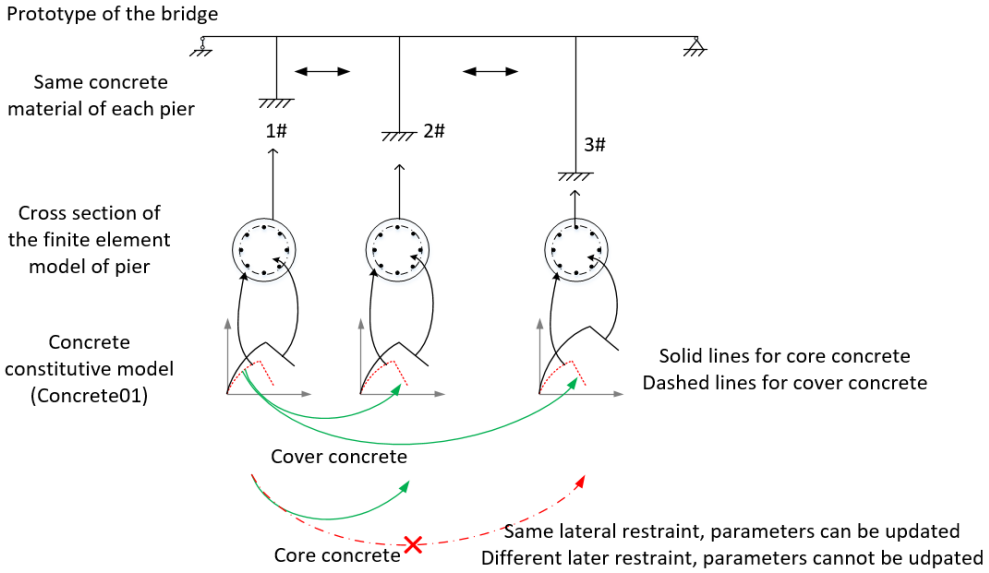

Fig. 2-3 Condition for parameter updating

This is the similar problem we confront as the above mentioned in Section 2.2 for updating the component CMs. In order to expand the range of application of updating the concrete CMs, a unified CM of involving both the confined and unconfined concrete is deduced based on the existing CMs of concrete. Then a bridge between the confined concrete CM of the PS and the NS is built through the same cover concrete CM of the PS and the NS, making the updating parameters of core concrete CM practicable.

Through the investigation on the existing CMs of concrete presented in sections 2.3.2 to 2.3.5, it

is found that the volumetric stirrup ratio is the most important factor affecting the lateral restraint force of RC members, and the relationship of parameters in core and cover concrete CM can be established through the volumetric stirrup ratio (Kent & Park, 1971; Scott et al., 1982; Mander, 1983; Mander et al., 1988; Sheikh & Uzumeri, 1983). Then, a unified CM is deduced by introducing the stirrup ratio as a non-constitutive parameter in Section 2.3.6.

2.3.2 Hognestad model and Rusch model

The Hognestad model (Hognestad, 1951) is a uniaxial CM for plain concrete, proposed by American scholar Hognestad in 1951. The model is a two-piecewise function, the ascending branch of σ-ε relation is described by a quadratic parabola and the descending branch is expressed by a straight line, as follows,

$$\begin{cases} \sigma = f_c \left[\dfrac{2\varepsilon}{\varepsilon_0} - \left(\dfrac{\varepsilon}{\varepsilon_0} \right)^2 \right] \\ \sigma = f_c + k \cdot (\varepsilon - \varepsilon_0) \end{cases} \qquad (2\text{-}6)$$

where f_c is the peak stress, which is suggested to be 0.85 times of the cylinder compressive strength of concrete; ε_0 is the corresponding strain of peak stress, whose recommended value is 0.002; ε_u is the ultimate strain, which is recommended to be 0.0038; f_u is the ultimate strength, which is suggested to be $0.85f_c$; k is the slope of the descending line, which is $(f_u - f_c) / (\varepsilon_u - \varepsilon_0)$.
The concrete CM proposed by German scholar Rusch is different from the Hognestad model only in the slope of the descending branch. The Rusch model considers the slope of the descending section as zero and ε_u as 0.0035. The difference between the two is shown in Fig. 2-4.

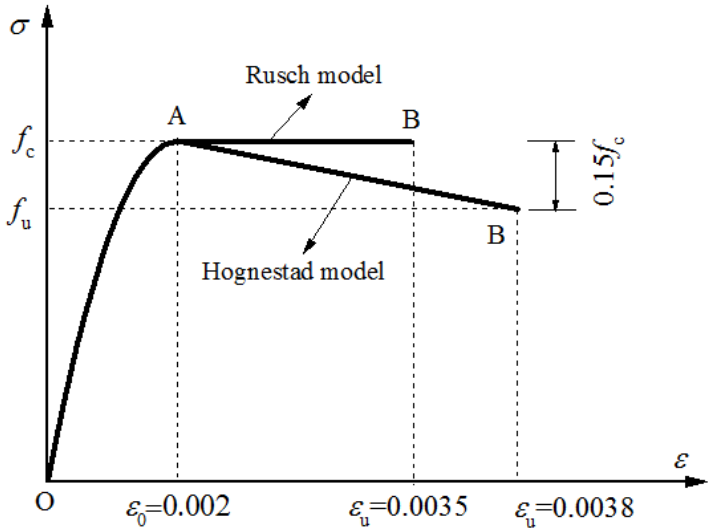

Fig. 2-4 Hognestad model and Rusch model

In order to establish the relationship between the CM of the core and cover concrete to unify the constitutive equations, the effective information is drawn from the two models as follows,

1. Functional expression: quadratic parabola-straight line function;
2. Slope of the descending branch: (f_u - f_c) / (ε_u -ε_0);
3. f_c: suggested to be the cylinder compressive strength;
4. f_u: suggested to be 0.85 f_c;
5. ε_0: recommended to be 0.002;
6. ε_u: recommended to be 0.0038 or 0.0035.

2.3.3 Kent-Park model

The Kent-Park model (Kent & Park, 1971) is a uniaxial CM for both the unconfined and confined concrete proposed by Kent and Park in 1971. It followed the Hognestad model's quadratic parabola-linear function to describe the unconfined concrete CM and extend it to the confined concrete as shown in Fig. 2-5.

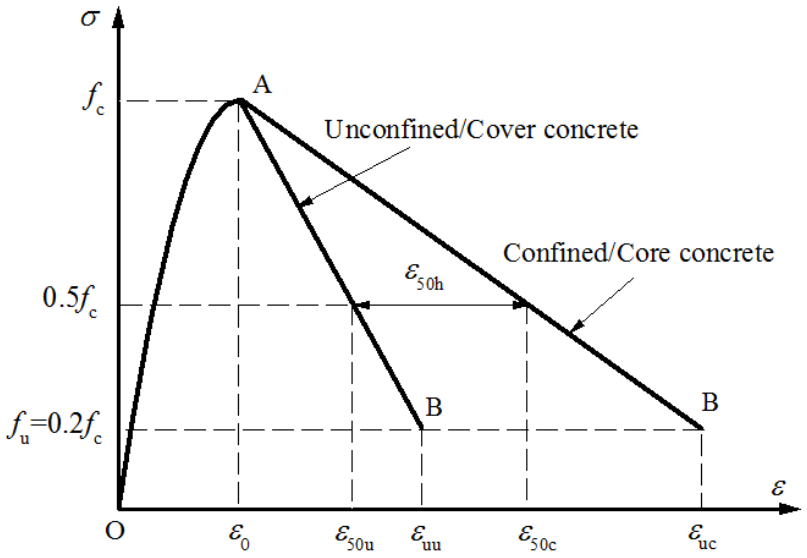

Fig. 2-5 Kent-Park model

Note: the second subscript u denotes the parameters for the unconfined concrete and c for the confined concrete.

In the Kent-Park model, the function of the core concrete is the same as that of the cover concrete, which is the quadratic parabola for the ascending branch in (2-5). It is seen that, stirrups only improve the ductility of the concrete and has no effect on the concrete strength in this model. That is, the peak stress and its corresponding strain of the confined concrete CM are the same as those of the unconfined concrete. The ultimate failure point of concrete CM is determined by the ultimate stress, i.e., f_u=0.2f_c, and the slope of the descending line. The formula of calculating the slope for core and cover concrete is,

$$k = -\frac{0.5 f_c}{\varepsilon_{50} - \varepsilon_0} \qquad (2\text{-}7)$$

where f_c is the peak stress which is, the same as that in Hognestad model, recommended to be the concrete cylinder compressive strength; ε_0 is the corresponding strain which is, also the same as Hognestad model, suggested value 0.002; ε_u is the strain corresponding to the ultimate stress ($0.2f_c$), where ε_{uu} and ε_{uc} represent the corresponding parameters of the core and cover concrete, respectively; ε_{50} is the strain corresponding to the half-peak stress ($0.5f_c$), where ε_{50u} and ε_{50c} represent the corresponding parameters of the core and cover concrete, respectively. The empirical formulas for the corresponding strain of half-peak stress are given,

$$\varepsilon_{50u} = \frac{3 + 0.29 f_c}{145 f_c - 1000} \qquad (2\text{-}8)$$

$$\varepsilon_{50c} = \varepsilon_{50u} + \varepsilon_{50h} \qquad (2\text{-}9)$$

where ε_{50h} is the difference of the strain corresponding to the half-peak stress between the core and cover concrete, as shown in Fig. 2-4. This coefficient is related to the size of the cross section and the volumetric stirrup ratio,

$$\varepsilon_{50h} = 0.75 \cdot \rho_s \sqrt{\frac{b}{s}} \qquad (2\text{-}10)$$

where ρ_s is the volumetric stirrup ratio; length of the stirrup along the direction with a shorter side of the rectangular section; s is the spacing of hoops.

Similarly, the effective information is drawn as follows to derive the unified constitutive model,

1. Functional expression: quadratic parabola-straight line function, the same as the Hognestad model;
2. Slope of the descending branch: ($0.5f_c$ - f_c) / (ε_{50} -ε_0);
3. f_c: suggested to be the cylinder compressive strength;
4. f_u: suggested to be $0.2f_c$;
5. ε_0: recommended to be 0.002;
6. ε_u: recommended to be the value corresponding to f_u;
7. Relations of the parameters in confined and unconfined concrete constitutive model,
   a) $f_{cc}=f_{cu}$;
   b) $\varepsilon_{0c}=\varepsilon_{0u}$.

2.3.4 Scott-Park model

In 1982, Scott et al. modified the Kent-Park model based on the experimental data of 27 RC specimens (Scott et al., 1982). As shown in Fig. 2-6, in this model, the stirrups not only improve the ductility of the concrete but also the strength to the same degree, namely $f_{cc} = Cf_{cu}$ and $\varepsilon_{0c}=C\varepsilon_{0u}$.

Compared with the Kent-Park model, the effective information is as follows,

Similarities:

1. Functional expression: quadratic parabola-straight line function, the same as the Hognestad model;
2. Slope of the descending branch: $(0.5f_c - f_c) / (\varepsilon_{50} - \varepsilon_0)$;
3. f_c: suggested to be the cylinder compressive strength;
4. ε_0: recommended to be 0.002;
5. The formulae for calculating the ε_{50} and ε_{50h};

Differences:

1. ε_{uu}: recommended to be the value of 0.004;
2. ε_{uc}: recommended to calculate as $\varepsilon_{uc} = \varepsilon_{uu} + 0.003 f_{yh} \cdot \rho_s$, which is $\varepsilon_{uc} = \varepsilon_{uu}(1 + 0.003 f_{yh} \cdot \rho_s / \varepsilon_{uu})$. For simplicity, the ε_{uu} that in the parentheses is set as the recommended value 0.004, then the formula can be rewritten as $\varepsilon_{uc} = \varepsilon_{uu}(1 + 0.75 f_{yh} \cdot \rho_s)$;
3. Relations of the parameters in confined and unconfined concrete constitutive model,
   a) $f_{cc} = C f_{cu}$;
   b) $\varepsilon_{0c} = C\varepsilon_{0u}$; where $C = 1 + f_{yh} \cdot \rho_s / f_{cu}$;
   c) $\varepsilon_{uc} = \varepsilon_{uu}(1 + 0.75 f_{yh} \cdot \rho_s)$;

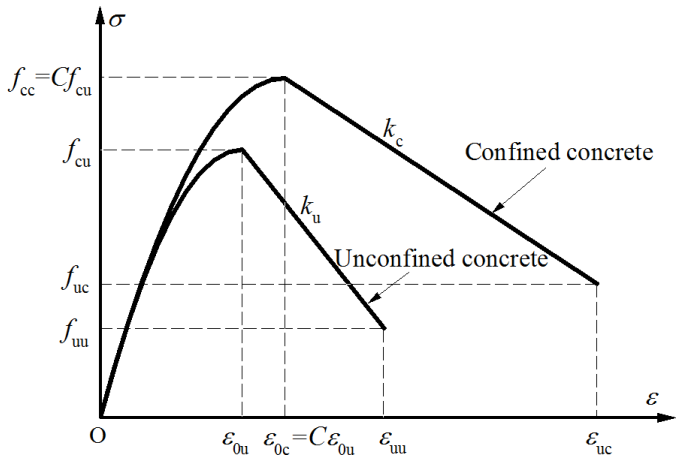

Fig. 2-6 Scott-Park model

2.3.5 Mander model

Different with the above models, the Mander model (Mander, 1983; Mander et al., 1988) uses only one curve as shown in (2-12) to describe the mechanical behavior of both the ascending and descending sections of concrete.

$$\sigma = \frac{f_c \frac{\varepsilon}{\varepsilon_0} r}{r - 1 + \left(\frac{\varepsilon}{\varepsilon_0}\right)^r} \qquad (2\text{-}12)$$

where the parameter $r = E_c / (E_c - f_c / \varepsilon_0)$; E_c is the elastic modulus of the unconfined concrete. Given the peak strength and its corresponding strain of the confined and unconfined concrete, their respective constitutive laws are obtained as shown in Fig. 2-7. For the model of cover concrete, the ultimate strain is two times of the peak strength corresponding strain, that is, $\varepsilon_{uu} = 2\varepsilon_{0u}$. For the model of confined concrete, the ultimate strain is the strain at the time of the first fracture of the stirrup which is,

$$\varepsilon_{uc} = \varepsilon_{uu} + 1.4\varepsilon_{su} \cdot \rho_s \cdot \frac{f_{yh}}{f_{cu}} \qquad (2\text{-}13)$$

where ε_{su} is the strain of the ruptured stirrup.

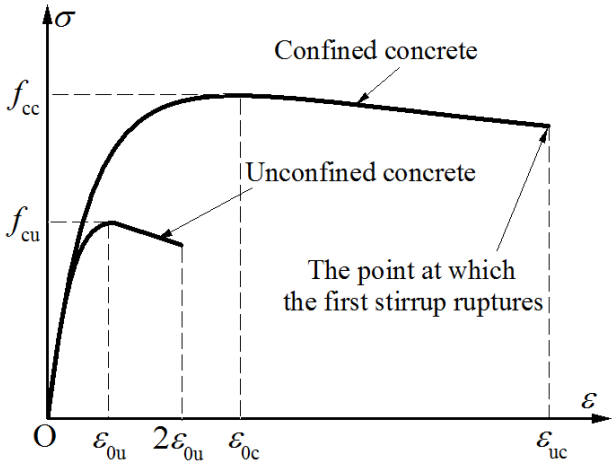

Fig. 2-7 Mander model

In the same way as the Scott-Park model, the yield strength of the stirrup and its volumetric stirrup ratio are considered to be the main factors that influence the confined concrete from both the two aspects of the strength and ductility. However, Mander model suggested that the stirrups enhance the ductility of concrete significantly more than the strength, which can be seen from the following formulae,

$$f_{cc} = f_{cu}\left(-1.254 + 2.254\sqrt{1 + \frac{7.49 f_l}{f_{cu}}} - 2\frac{f_l}{f_{cu}}\right) \qquad (2\text{-}14)$$

$$\varepsilon_{0c} = \varepsilon_{0u}\left[1 + 5\left(\frac{f_{cc}}{f_{cu}} - 1\right)\right] \qquad (2\text{-}15)$$

where, f_l is the parameters related to yield strength of the stirrup and its volumetric ratio.
As the concrete01 model in OpenSees was selected to be the target model for optimization in

this study, the functional expression of the Mander model was not to be involved in. The relations of the parameters in confined and unconfined concrete constitutive model were,

1. $f_{cc}=C_1 \cdot f_{cu}$
2. $\varepsilon_{0c}=C_2 \cdot \varepsilon_{0u}$
3. $\varepsilon_{uc}=\varepsilon_{uu}\left(1+350\varepsilon_{su}\cdot\frac{f_{yh}}{f_{cu}\cdot\varepsilon_{uu}}\cdot\rho_s\right)$

2.3.6 Unified constitutive model of confined and unconfined concrete for model updating

Effective information provided by the above mentioned constitutive models for concrete are collected and listed in Table 2-1. It is found hat the three parameters of confined concrete f_{cc}, ε_{0c}, ε_{uc} and the f_{cu}, ε_{0u}, ε_{uu} of the unfined concrete can be related by the ratio of stirrup ρ_s. The functional expressions in the latter three models for the relationships of these three parameters was employed. While, as the influences of the volumetric stirrup ratio on the three parameters were different recommended by the three models, three scale coefficients were introduced,

$$f_{cc}=\left(1+S_1\cdot\rho_s\right)f_{cu} \qquad (0\text{-}1)$$

$$\varepsilon_{0c}=\left(1+S_2\cdot\rho_s\right)\varepsilon_{0u} \qquad (0\text{-}2)$$

$$\varepsilon_{uc}=\left(1+S_3\cdot\rho_s\right)\varepsilon_{uu} \qquad (0\text{-}3)$$

And from Table 2-1, it is reasonable to assume that,

$$f_u=K\cdot f_c \qquad (0\text{-}4)$$

Substituting Eqs. (2-16) to (2-19) into Eq. (2-6), the unified constitutive law for cover and core concrete was deduced,

$$\begin{cases}\sigma=\left(1+S_1\cdot\rho_s\right)f_{cu}\left[\dfrac{2\varepsilon}{\left(1+S_2\cdot\rho_s\right)\varepsilon_0}-\left(\dfrac{\varepsilon}{\left(1+S_2\cdot\rho_s\right)\varepsilon_0}\right)^2\right] & ascent\ stage\\ \sigma=\left(1+S_1\cdot\rho_s\right)f_{cu}+k\cdot\left[\varepsilon-\left(1+S_2\cdot\rho_s\right)\varepsilon_0\right] & descent\ stage\end{cases} \qquad (0\text{-}5)$$

where the slope of the descending branch is,

$$k=\frac{\left(K-1\right)\left(1+S_1\cdot\rho_s\right)f_{cu}}{\left(\varepsilon_{uu}-\varepsilon_{0u}\right)+\left(S_3\varepsilon_{uu}-S_2\varepsilon_{0u}\right)\rho_s} \qquad (0\text{-}6)$$

For simplicity, the constitutive law can be written as,

$$\sigma=g\left(\varepsilon, f_{\mathrm{cu}}, \varepsilon_{0\mathrm{u}}, \varepsilon_{\mathrm{uu}}, K, S_1, S_2, S_3, \rho_{\mathrm{s}}\right) \qquad (0\text{-}7)$$

where, f_{cu}, ε_{0u}, ε_{uu} are the parameters of unconfined concrete; The model is for unconfined concrete when $\rho_s = 0$, confined concrete when $\rho_s \neq 0$. According to the definition given in Section 2.1.1, f_{cu}, ε_{0u}, ε_{uu}, K, S_1, S_2, S_3 are constitutive parameters, whilst ρ_s is non-constitutive parameter.

	Parameter	Hognestad model	Rusch model	Kent-Park model	Scott-Park model	Mander model
Relationship between parameters	f_{cu} and f_{cc}	-	-	$f_{cc}=f_{cu}$	$f_{cc}=(1+S_1\cdot\rho_s)\ f_{cu}$	$f_{cc}=g_2(\rho_s)\ f_{cu}$
	ε_{0u} and ε_{0c}	-	-	$\varepsilon_{0c}=\varepsilon_{0u}$	$\varepsilon_{0c}=(1+S_2\cdot\rho_s)\varepsilon_{0u}$	$\varepsilon_{0c}= 5\cdot g_2(\rho_s)\varepsilon_{0u}$
	ε_{uu} and ε_{uc}	-	-	$\varepsilon_{uc}= g_1(\rho_s)\ \varepsilon_{uu}$	$\varepsilon_{uc}= (1+S_3\cdot\rho_s)\ \varepsilon_{uu}$	$\varepsilon_{uc}= (1+S_3\cdot\rho_s)\ \varepsilon_{uu}$
Recommended value	f_{cu}	Cylinder ACS	Cylinder ACS	Cylinder ACS	Cylinder ACS	Cylinder ACS
	ε_{0u}	0.002	0.002	0.002	0.002	0.002
	f_{uu}	$0.85f_{cu}$	f_{cu}	$0.2f_{cu}$	-	-
	ε_{uu}	0.0038	0.0035	-	0.004	0.004
	S_1	-	-	-	f_{yh} / f_{cu}	-
	S_2	-	-	-	f_{yh} / f_{cu}	-
	S_3	-	-	-	$0.75f_{yh}$	（18~74）f_{yh}

Table2-1 Parameters of concrete constitutive models (ACS is for axial compressive strength.)

2.3.7 Method for determining the initial value of constitutive parameters

When using the UKF to identify parameters, the initial values of the parameters being identified should be given in advance. Therefore, the initial values of constitutive parameters f_{cu}, ε_{0u}, ε_{uu}, K, S_1, S_2, S_3 need to be predetermined. The details of the determining approach given by this study

are as follows:

1. f_{cu}: It is recommended to take the average value of cylinder axial compressive strength of concrete;
2. ε_{0u}: If no material test, it is recommended to take a large number of experimental data obtained by the empirical value of 0.002;
3. ε_{uu}: If no material test, the recommended value range from 0.0035 to 0.004 (0.0038 is chosen in this study);
4. K: Proportional coefficient of ultimate stress and peak stress of concrete, the recommended value range from 0.2 to 0.85 (0.85 is chosen in this study);
5. S_1: The recommended value f_{yh} / f_{cu};
6. S_2: Scott-Park model, recommended to take the same value as S_1;
   Mander Model, recommended the value of $5S_1$.
   The $5S_1$ is not given directly in the Mander model, but be derived by author: substituting Eq. (2-16) into Eq. (2-15), then we can obtain that,
   $\varepsilon_{0c} = \left[1+5\left(f_{cc}/f_{cu}-1\right)\right]\varepsilon_{0u} = \left[1+5\left(1+S_1\cdot\rho_s-1\right)\right]\varepsilon_{0u} = \left(1+5S_1\cdot\rho_s\right)\varepsilon_{0u}$, which is $S_2 = 5S_1$.
   ($3S_1$ is chosen in this study).
7. S_3: It is recommended to take the value of $0.75f_{yh}$.

2.4 Parameter Sensitivity Analysis

For the identification of constitutive parameters of concrete, the first choice of measurement is the concrete stress, because it is the most sensitive quantity to the material parameters. However, it is still more difficult to measure the stress accurately at present, especially when the member undergo a strong nonlinearity when wide cracks appear. Meanwhile, in the hybrid simulation, the restoring force of the specimen is relatively easy to measure with a high precision. Therefore, restoring forces of the specimen were determined to be the observation for parameter identification. In this section, the sensitivity of concrete constitutive parameters, in the unified model, to the measurement which is the restoring force was carried out. In this way, the impact of these constitutive parameters on the measurements, i.e. restoring forces, can be known, so that we can avoid to identify the non-sensitive parameters to reduce the computational burden, and hence the time of hybrid simulation.

The column, shown in Fig. 2-8 (a), was the structure for sensitivity analysis, whose cross section and the layout of the reinforcement bars are presented in Fig. 2-8 (c). Firstly, the FE model of the column was built in OpenSees by a force-based beam-column element, as shown in Fig. 2-8 (b), along which there were 5 integration points. The fiber section of the FE model of the column was shown in Fig. 2-8 (d), where the circle presents fibers of steel bars, the dark gray parts and the light gray parts are for the confined and unconfined concrete, respectively. In the FE model, the Concrete01 is employed for the fibers of both the confined and unconfined concrete, while the Steel02 is for the fibers of reinforcement bars. With the values of parameters of Steel02 were fixed, the sensitivity of the concrete parameters to restoring forces were analyzed by changing the value of one concrete parameter at a time.

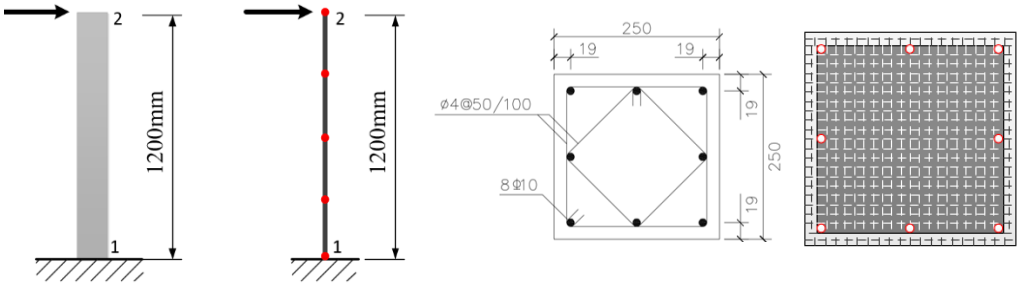

(a) Prototype of the specimen *(b) FE model of the specimen* *(c) Cross section of the specimen* *(d) Fiber section of the FE model*

Fig. 2-8 The RC column and its FE model

Each constitutive parameter of concrete is changed by ± 10%, ± 20%, ± 30% and ± 40% on the basis of the reference value. Then OpenSees FE model computed and gave the time history of the restoring force of the numerical column. Results of parametric sensitivity analysis show that f_{cu}, ε_{0u} and K are the three most sensitive parameters to the restoring force, with the relative errors up to 60%, as shown in Fig. 2-9.The parameter f_{cu} has a significant effect on the whole process of the time history; the parameter ε_{0u} mainly affects the forces before the yielding; whilst the parameter K plays a major role after yielding. The other four parameters are relatively insensitive, with the relative errors less than 2% in the whole process, as shown in Fig. 2-10. Therefore, the cases of parameter identification and update focus on only the three sensitive parameters.

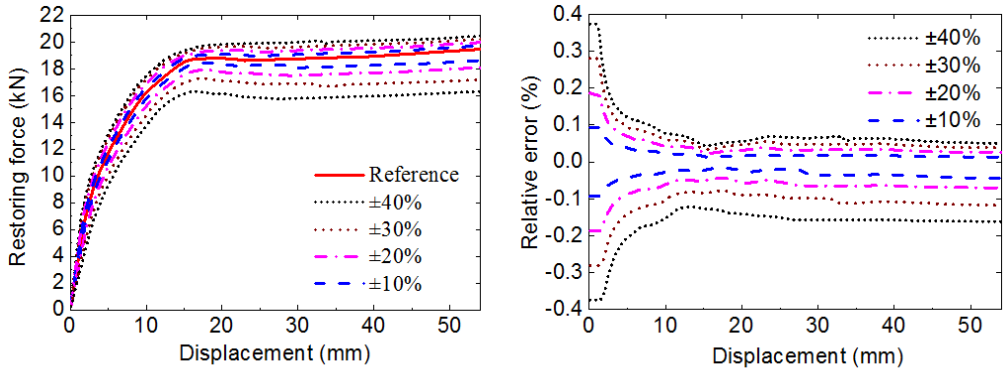

(a) f_{cu}

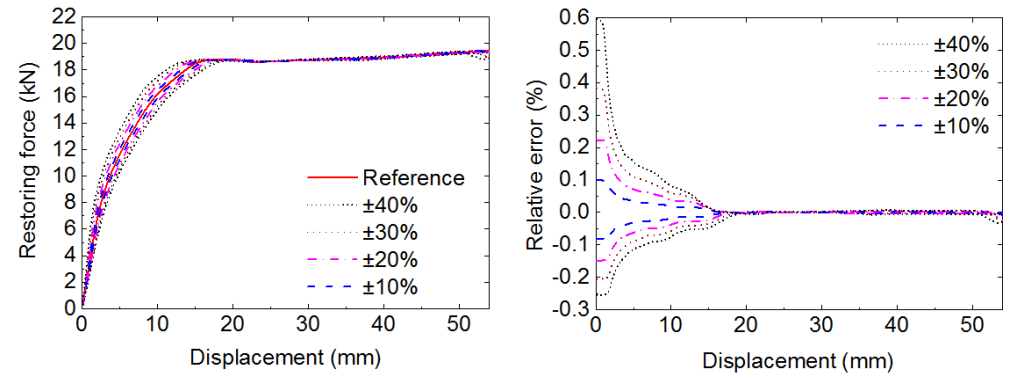

(b) ε_{0u}

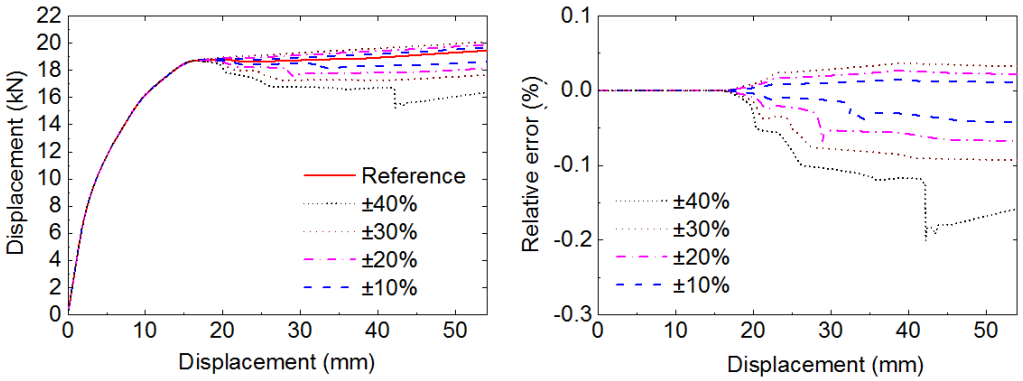

(c) K

Fig. 2-9 Results of parameter sensitivity – sensitive parameters

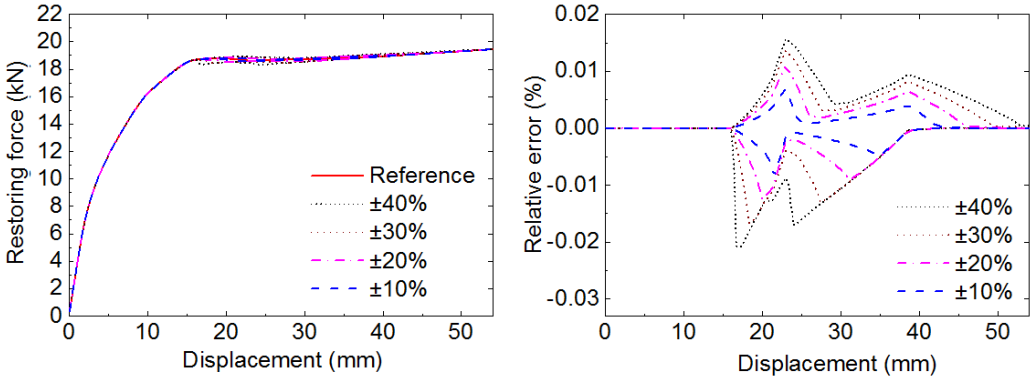

(a) ε_{uu}

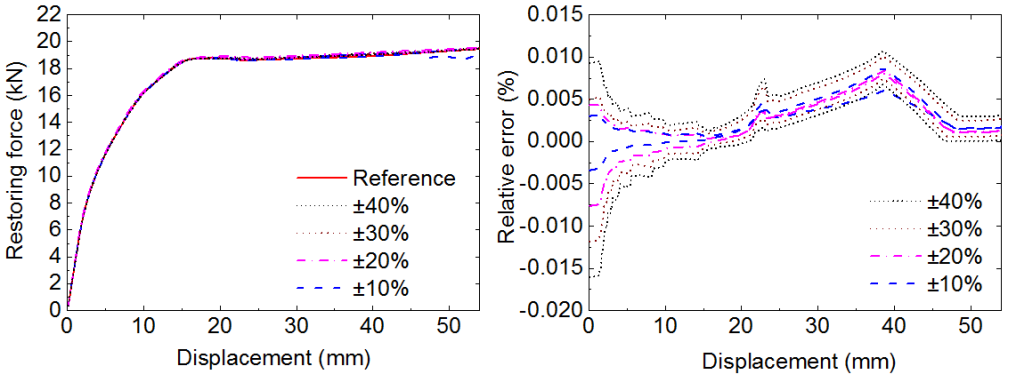

(b) S_1

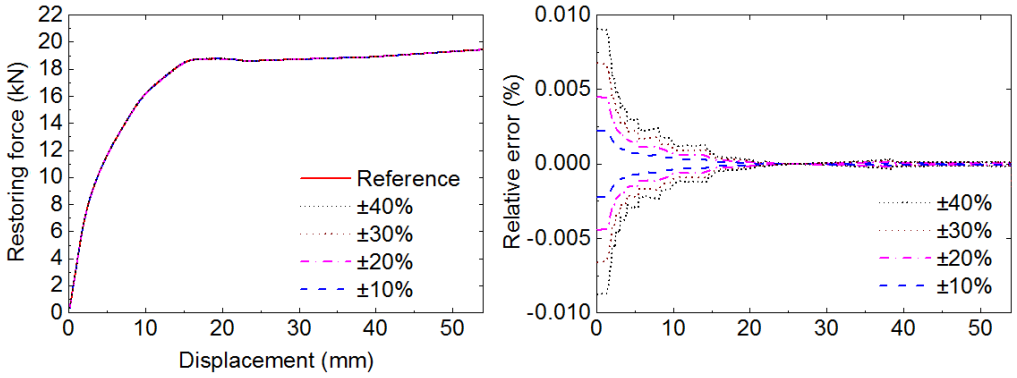

(c) S_2

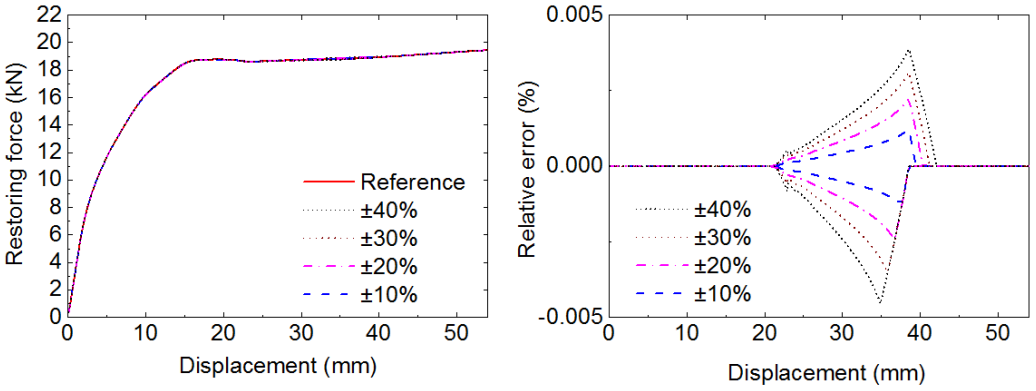

(d) S_3

Fig. 2-10 Results of parameter sensitivity – non-sensitive parameters

2.5 Summary

In order to make parameter updating of concrete constitutive model be more universality in the hybrid simulation of reinforced concrete structures, a unified model of unconfined and confined concrete was derived based on the existing concrete constitutive models. The main works were as follow,

1. The concept of the same constitutive models were clarified to illuminate the condition for model updating in hybrid simulation, by defining constitutive parameter and non-constitutive parameter.
2. Based on the existing concrete constitutive models, a unified model of unconfined and confined concrete was derived by analyzing the relationship of the parameters in both the constitutive models of core and cover concrete and introducing the volumetric parameters as a non-constitutive parameter.
3. The parameter sensitivity analysis of the constitutive parameters in the proposed unified constitutive model was carried out by using the finite element model of cantilever concrete column in OpenSees. In this way, the number of constitutive parameters that need to be identified and updated was reduced to lower the computational cost.

3. IDENTIFICATION OF CONCRETE CONSTITUTIVE MODEL PARAMETERS

3.1 Introduction

Parameter identification is an essential part of the model updating hybrid simulation. At present, the widely used online algorithms in civil engineering are recursive least squares (RLS), and the Kalman family including the Kalman filter (KF), the Extended Kalman filter (EKF) and the unscented Kalman filter (UKF). The RLS and KF are suitable for linear systems. The EKF and UKF are developed for nonlinear system identification based on KF method. A number of research shows that EKF can provide the reliable estimation only when the system is linear or very close to linear. Moreover, EKF requires that the nonlinear system must be derivable to be linearized, and during the optimizing process, Jacobian matrices need to be calculated in each recursive step. Compared to the EKF, the UKF performs well to deal with the identification of strong nonlinear systems without system linearizing and Jacobian Matrices calculating. It has the advantages of high accuracy, good robustness to noise and computational efficiency. Therefore, the identification of identifying the material constitutive parameters was implemented based on the UKF combining the OpenSees.

In this chapter, the basic principle of the UKF was elaborated starting with the KF and the estimation precision of the UKF was analyzed. Then, by means of numerical simulation, the concrete stress is taken as the observation to verify the feasibility of concrete constitutive parameter identification. With the respect of hybrid simulation, the case of taking the restoring force of the structural component as the observation was considered. To realize the parameter identification based on measuring the restoring force, the UKF embedded OpenSees was proposed and its convergence was discussed.

3.2 Principle of Unscented Kalman Flter

Both extended Kalman filter (EKF) and unscented Kalman filter (UKF) are extensions of KF in nonlinear estimation. Both of them give a suboptimal solution to the nonlinear estimation problem based on the KF recursive framework. EKF uses a way of first-order linearizing the nonlinear systems to approximate them. While, the UKF uses the Unscented Transform (UT) based on deterministic sampling method to estimate the first two-order statistics of both the state variables and measurements to estimate the state variables and measurements.

3.2.1 Fundamental of KF

Let vector **x** denote the state variables to be estimated. Assume that the state equation, also known as system equation or process equation, which is the recursion that **x** obeys, is known as,

$$\mathbf{x}_i = F\left(\mathbf{x}_{i-1}, \mathbf{u}_{i-1}, \mathbf{w}_{i-1}\right) \quad \text{(0-8)}$$

where **u** is the input vector; **w** is the vector of process noise which includes modeling uncertainty and unobservable disturbance; *i* is the time step. Let vector **y** denote the measurement, and the measurement equation which describe the relationship between the measurement and the state variables in a state-space form is known as,

$$\mathbf{y}_i = H\left(\mathbf{x}_i, \mathbf{u}_i, \mathbf{v}_i\right) \quad \text{(0-9)}$$

where **v** is the vector of observation noise. If both functions *F* and *H* are linear, the KF can be used to estimate the **x**.
The main idea of the KF is the same as that of RLS, which is, to correct **x** by **y** through

$$\hat{\mathbf{x}}_i = \hat{\mathbf{x}}_{i-1} + \mathbf{K}_i\left(\mathbf{y}_i - \hat{\mathbf{y}}_i\right) \quad \text{(0-10)}$$

where $\hat{\mathbf{y}}_i$ is the estimation of the measurement **y**, and can be obtained based on the previous estimation of **x**,

$$\hat{\mathbf{y}}_i = H\left(\hat{\mathbf{x}}_{i-1}, \mathbf{u}_i\right) \quad \text{(0-11)}$$

$\mathbf{K}_i$ is the Kalman gain,

$$\mathbf{K}_i = \mathbf{P}_{\mathbf{xy},i}\left(\mathbf{P}_{\mathbf{yy},i} + \mathbf{R}_i\right)^{-1} \quad \text{(0-12)}$$

where $\mathbf{P}_{yy}$ is the variance of **y**, $\mathbf{P}_{xy}$ is the covariance of **x** and **y**, and **R** is the variance of the measurement noise.
Unlike the RLS, the KF provides a priori estimation of **x** through the state equation,

$$\hat{\mathbf{x}}_i^- = F\left(\hat{\mathbf{x}}_{i-1}^+, \mathbf{u}_{i-1}\right) \quad \text{(0-13)}$$

Then, $\mathbf{y}_i$ is estimated using this prior estimation $\hat{\mathbf{x}}_i^-$ rather than the estimation $\hat{\mathbf{x}}_{i-1}$ at the previous step. The Eq. (3-4) can be rewritten as,

$$\hat{\mathbf{y}}_i = H\left(\hat{\mathbf{x}}_i^-, \mathbf{u}_i\right) \quad \text{(0-14)}$$

And then the estimation of **x** can be corrected, which is called the posterior estimation in the current step,

$$\hat{\mathbf{x}}_i^+ = \hat{\mathbf{x}}_i^- + \mathbf{K}_i\left(\mathbf{y}_i - \hat{\mathbf{y}}_i\right) \quad \text{(0-15)}$$

For the problem of identification of constant parameters, it can be deduced from Eq. (3-6) that,

$$\hat{\mathbf{x}}_i^- = \hat{\mathbf{x}}_{i-1}^+ \quad \text{(0-16)}$$

That is to say, the predict step from which the prior estimation of **x** is obtained can be omitted in the KF. Thus, Eqs (3-7) and (3-8) in the KF are just the same as Eqs (3-4) and (3-3) in the RLS. In other words, for constant parameter identification problem of linear system, the KF equals to the RLS.

3.2.2 Fundamental of UKF

According to Bayesian theory, Doob [107] proves that the optimal estimation of **x** is the expected value of **x** given **y**, i.e. E(**x**|**y**), with the criterion of minimizing the mean square error of the residuals of **y**. Where **x** is the variables need to be identified and **y** is the measurement as above mentioned in Section 3.2.1. For linear systems, the estimation provided by the KF by only calculating the first two moments of **x** and **y** is just the Bayesian optimal estimation. For nonlinear systems, the Bayesian method can also give the optimal estimation when the probability density function of **x** given **y** is known. However, this will result in an increase in the number of parameters, which then leads to a significant increase in computational burden. Moreover, in many cases, the required conditional probability density function cannot be known at all.

To solve the estimation problem of nonlinear systems, based on the KF, the UKF provides a suboptimal estimation for nonlinear systems. The main idea is:

1. Preserving the recursive framework of the KF for linear systems, i.e. the predict-update/correct strategy is still employed, i) Predicting step: attain the prior estimation according to Eq. (3-6); ii) Updating step: achieve the posteriori estimation, Eq. (3-8).
2. The Unscented Transform (UT) is proposed to obtain the priori estimation of **x** and the estimation of **y** under the nonlinear function *F* and *H*, the estimation of the conditional first order moment of **x** as well as **y**, and to obtain the second-order moments of **x** and **y**, $\hat{\mathbf{P}}_{xx,i}$ $\hat{\mathbf{P}}_{yy,i}$ $\hat{\mathbf{P}}_{xy,i}$.

From the main idea, it is found that there are two approximations in the UKF: i) using the recursive framework of the KF for nonlinear systems, that is, the first two moments of **x** and **y** are not sufficient for providing the optimal estimation of the parameters of nonlinear systems; ii) the approximation of the first two moments of random variables. That is the first two moments of **x** and **y** obtained by the UT are not exact values, but also estimated values.

The UT is the basis of UKF. Assume that we know the mean $\bar{\mathbf{x}}$ and variance $\mathbf{P}_{xx}$ of the state variables **x**, and the relationship between **x** and another random variable **z**, such as **z** = *g*(**x**) where *g* is a nonlinear function. Then, by using the UT with deterministic sampling method, the mean and variance of **x** after nonlinear transformation, i.e. the mean and variance of **z**, can be estimated as follows,

1. According to a certain law which is called as deterministic sampling methods, the sampling points, also known as the sigma points, of **x** can be got, which are $\chi = \left[\chi_0, \chi_1, \chi_2 \cdots \chi_{q-1}\right]$,
2. Transform each sigma points through nonlinear function *g* to attain the sigma points of **z** after nonlinear transformation, i.e. $\zeta = \left[\zeta_0, \zeta_1, \zeta_2 \ldots \zeta_{q-1}\right]$, by,

$$\zeta_i = g\left(\chi_i\right) \quad \text{(0-17)}$$

where g can be either the function *F* in the state equation or the function *H* in the measurement equation. If it is the function *F*, the sigma points for estimating the priori estimation of **x** in current step are obtained by nonlinear transform the sigma points of the posteriori estimation of **x** in the previous step. For constant parameter identification, this step can be omitted. If the function *H*, it is the sigma points for estimating **y** are obtained.

3. Calculate the first two moments of **z** and the covariance of **x** and **z**,

$$\hat{\bar{\mathbf{z}}} = \sum_{j=0}^{q-1} W_j^{\mathrm{m}} \zeta_j \tag{0-18}$$

$$\hat{\mathbf{P}}_{\mathbf{zz}} = \sum_{j=0}^{q-1} W_j^{\mathrm{c}} [\zeta_j - \hat{\bar{\mathbf{z}}}][\zeta_j - \hat{\bar{\mathbf{z}}}]^{\mathrm{T}} \tag{0-19}$$

$$\hat{\mathbf{P}}_{\mathbf{xz}} = \sum_{j=0}^{q-1} W_j^{\mathrm{c}} [\boldsymbol{\chi}_j - \bar{\mathbf{x}}][\zeta_j - \hat{\bar{\mathbf{z}}}]^{\mathrm{T}} \tag{0-20}$$

where W^{m} is weighting coefficients for average calculation; W^{c} is the weighting coefficients for variance calculation. The calculation formula of weighting coefficients varies according to different sampling method.

The UKF principle and execution are shown in Fig. 3-1. Note that, for non-constant parameter identification, the deterministic sampling and UT are executed two times in each time step, one is

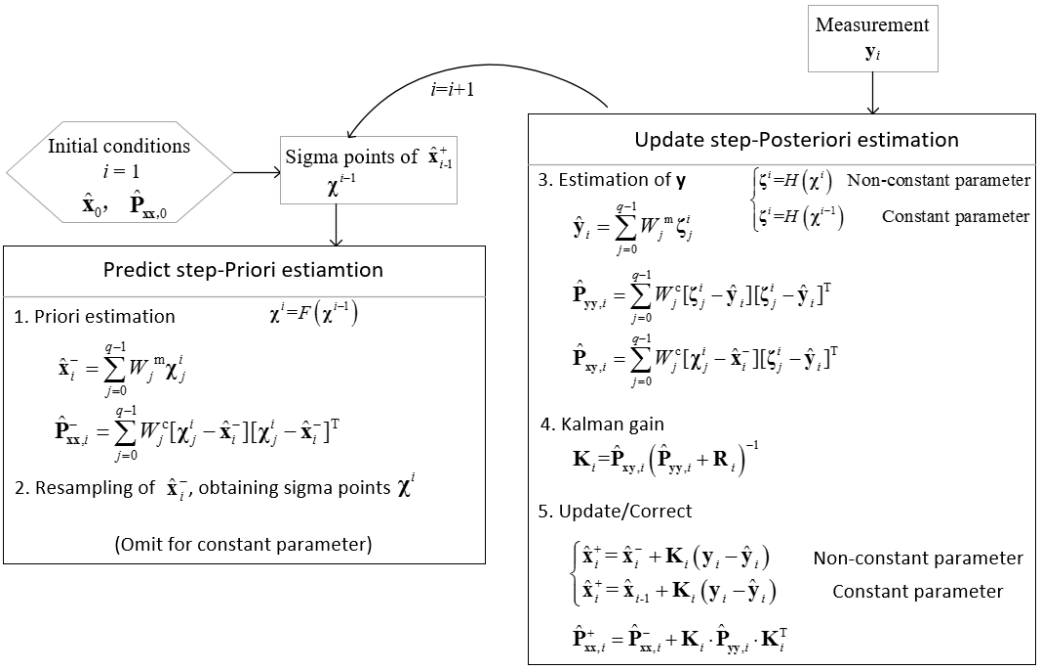

Fig. 3-1 Principle and executive process of UKF

in the predict step where the sigma points of the posteriori estimation of **x** in previous step need to be transformed, the other is in the update step where the sigma points of the priori estimation of **x** in current step need to be transformed. While for constant parameters, since the predict step can be omitted as above mentioned, the UT with deterministic sampling is executed only one time in the update step, where it is the sigma points of the posteriori estimation of **x** in previous step need to be transformed for estimating y, not the priori estimation of **x** in current step.

3.2.3 Deterministic sampling method and its precision analysis

The symmetric sampling strategy was provided in unscented transform (UT) by Julier et al. when the UKF was first proposed (Julier et al., 1995; Julier & Uhlmann, 1996). Subsequently, the simplex sampling strategies were proposed gradually, which included minimal skew simplex sampling (Julier & Uhlmann, 2002) and spherical simplex sampling (Julier, 2003). The minimal skewness sampling though reduces the number of sample points and improves the computational efficiency, it may cause the value instability with the increase of n. To solve this problem, the spherical simplex sampling was proposed. In order to obtain an estimation with higher precision, Van Der Merwe and Wan and proposed a scaled sampling strategy based on symmetric sampling by introducing coefficients α and β to adjust higher-order accuracy in Tayler expansion (Van Der Merwe & Wan, 2001). In the same way, Julier et al. improved the simplex sampling method (Julier, 2002).

The number of sample points of the simplex sampling was further reduced compared to the symmetric sampling method, which reduced to $n + 2$ from $2n + 1$. The n refers to the dimension of the state vector, here the number of parameter need to be identified. The symmetric sampling is suitable for the random variables that distributed symmetrically, such as normal distribution, while the simplex samplings are more suitable for random variables with asymmetric distribution.

3.2.3.1 Scaled symmetric sampling method

A large number of statistical results show that the strength parameter f_c of the concrete meets the normal distribution. Also, several studies show that the ultimate strain of concrete fits the Gaussian distribution. Therefore, it is more reasonable to employ the symmetric sampling method.

For the original symmetric sampling method, if the state variables that need to be identified, **x**, are Gaussian distribution, it is suggested that the tuning parameter, κ, in the sampling method be $\kappa = 3-n$, where n is the dimension of **x**. However, κ is negative when $n>3$, leading to the non-positive definite of the variance of **x** after nonlinear transformation which further results in numerical instability. The scaled symmetric sampling can solve this problem by introducing the parameters α and β. These two parameters can also tuning the estimation precision of the higher-order terms in Taylor expansion. Therefore, this sampling is one of the most widely used methods in UKF. The number of sampling points in each identification/time step is $2n+1$, and the formula of determining sampling points of the scaled symmetric method are as follows,

$$\begin{cases} \boldsymbol{\chi}_0^i = \hat{\mathbf{x}}_{i-1}, \quad j=0 \\ \boldsymbol{\chi}_{j,1}^i = \hat{\mathbf{x}}_{i-1} + \alpha\left(\sqrt{n\hat{\mathbf{P}}_{\mathbf{xx}}^i}\right)_j, \quad j=1,2,...n \\ \boldsymbol{\chi}_{j,2}^i = \hat{\mathbf{x}}_{i-1} - \alpha\left(\sqrt{n\hat{\mathbf{P}}_{\mathbf{xx}}^i}\right)_j, \quad j=1,2,...n \end{cases} \tag{0-21}$$

$$\begin{cases} W_0^{\mathrm{m}} = 1 - 1/\alpha^2 & j=0 \\ W_0^{\mathrm{c}} = W_0^{\mathrm{m}} + 1 - \alpha^2 + \beta & j=0 \\ W_j^{\mathrm{m}} = W_j^{\mathrm{c}} = 1/\left(2n\alpha^2\right) & j \neq 0 \end{cases} \tag{0-22}$$

where, $\hat{\mathbf{x}}_{i-1}$ is the estimation of **x** in the previous step, which is for the identification of constant parameters; $\left(\sqrt{n\hat{\mathbf{P}}_{\mathbf{xx}}^i}\right)_j$ is a matrix when *n*>1 and represents the -*j*th row (column) of the matrix; W_j^{m} is the weight coefficients for estimating the mean; W_j^{c} is the weight coefficients for estimating variance; α is the parameter for tuning the higher order precision of the mean and variance; β is the parameter for tuning the higher order precision of the variance.

3.2.3.2 Accuracy of UT based on scaled symmetric sampling

In this section, the accuracy of UT based on the scale symmetric sampling was analyzed by using Taylor series expansion for the case that *x* is a scalar, and the values of α and β are deduced when *x* meets the normal distribution.

Assume that the random variable $x \sim N(\bar{x}, \sigma_x^2)$, $y = f(x)$ where *f* is a nonlinear function.

1. The mean and variance of the measurement *y* are derived by using Taylor expansion as to be the reference values;

   a. Expand *y* at $\bar{x}$

$$\begin{aligned} y = f(x) &= f(\bar{x} + \delta x) \\ &= f(\bar{x}) + D_1 \cdot \delta x + \frac{1}{2} D_2 \cdot (\delta x)^2 + \frac{1}{3!} D_3 \cdot (\delta x)^3 + \frac{1}{4!} D_4 \cdot (\delta x)^4 ... \end{aligned} \tag{0-23}$$

where $\delta x = x - \bar{x}$ is a Gaussian random variable with the mean equals to zero and the variance equals to σ_x^2; $D_1 = f'(\bar{x})$, $D_2 = f''(\bar{x})$, ... $D_n = f^{(n)}(\bar{x})$.

   b. The mean of *y*

$$\begin{aligned} \bar{y} &= E(y) \\ &= f(\bar{x}) + D_1 \cdot E(\delta x) + \frac{1}{2} D_2 \cdot E\left[(\delta x)^2\right] + \frac{1}{3!} D_3 \cdot E\left[(\delta x)^3\right] + \frac{1}{4!} D_4 \cdot E\left[(\delta x)^4\right] ... \end{aligned} \tag{0-24}$$

As δx ~*N*(0, σ_x^2), it can be known that $E\left[(\delta x)^m\right]=0$ when m is a an odd number and $E\left[(\delta x)^2\right]=\sigma_x^2$, $E\left[(\delta x)^4\right]=3\sigma_x^4$ according to its moment generating function.

Submitting the moments into Eq. (3-17), the mean of *y* is attained as,

$$\bar{y}=E(y)=f(\bar{x})+\frac{1}{2}D_2\cdot\sigma_x^2+\frac{1}{8}D_4\cdot\sigma_x^4... \qquad (0\text{-}25)$$

c. The variance of *y*

$$\begin{aligned}P_{yy}&=E(y-\bar{y})^2\\&=D_1^2\cdot E\left[(\delta x)^2\right]+D_1D_2E\left[(\delta x)^3\right]-\frac{1}{6}D_2D_3E\left[(\delta x)^2\right]E\left[(\delta x)^3\right]\\&\quad+\left(\frac{1}{3}D_1D_3+\frac{1}{4}D_2^2\right)E\left[(\delta x)^4\right]-\frac{1}{36}D_3^2E\left[(\delta x)^3\right]^2-\frac{1}{4}D_2^2E\left[(\delta x)^2\right]^2+...\\&=D_1^2\sigma_x^2+\left(D_1D_3+\frac{1}{2}D_2^2\right)\sigma_x^4+...\end{aligned} \qquad (0\text{-}26)$$

2. The mean and variance of *y* by the scaled symmetrical sampling method;

a. As *x* is a scalar, *n* = 1. 2*n* + 1 sampling points and their weight factors are obtained based on Eqs. (3-14) and (3-15), respectively, as

$$\begin{cases}\chi_0=\bar{x} & j=0\\ \chi_{1,1}=\bar{x}+\alpha\sqrt{n\sigma_x^2}=\bar{x}+\alpha\sigma_x & j=1\\ \chi_{1,2}=\bar{x}-\alpha\sqrt{n\sigma_x^2}=\bar{x}-\alpha\sigma_x & j=1\end{cases} \qquad (0\text{-}27)$$

$$\begin{cases}W_0^{\mathrm{m}}=1-1/\alpha^2 & j=0\\ W_0^{\mathrm{c}}=2-1/\alpha^2-\alpha^2+\beta & j=0\\ W_j^{\mathrm{m}}=W_j^{\mathrm{c}}=1/\left(2\alpha^2\right) & j=1\end{cases} \qquad (0\text{-}28)$$

b. Nonlinear transform the sigma points,

$$\zeta_0=f(\chi_0)=f(\bar{x}) \qquad (0\text{-}29)$$

$$\begin{aligned}\zeta_{1,1}&=f(\bar{x}+\alpha\sigma_x)\\&=f(\bar{x})+D_1\alpha\sigma_x+\frac{1}{2}D_2(\alpha\sigma_x)^2+\frac{1}{3!}D_3(\alpha\sigma_x)^3+\frac{1}{4!}D_4(\alpha\sigma_x)^4...\end{aligned} \qquad (0\text{-}30)$$

$$\begin{aligned}\zeta_{1,2} &= f\left(\bar{x}+\alpha\sigma_x\right)\\ &= f\left(\bar{x}\right)-D_1\alpha\sigma_x+\frac{1}{2}D_2\left(\alpha\sigma_x\right)^2-\frac{1}{3!}D_3\left(\alpha\sigma_x\right)^3+\frac{1}{4!}D_4\left(\alpha\sigma_x\right)^4...\end{aligned} \quad (0\text{-}31)$$

c. Substituting the sigma points after nonlinear transformation, i.e. Eqs. (3-22) - (3-24), and their weight factors shown in Eq. (3-21) into Eqs. (3-11) and (3-12), the mean and variance of *y* can be obtained as,

$$\begin{aligned}\bar{y} &= W_0^{\mathrm{m}}\zeta_0+W_1^{\mathrm{m}}\zeta_{1,1}+W_1^{\mathrm{m}}\zeta_{1,2}\\ &= f\left(\bar{x}\right)+\frac{1}{2}D_2{\sigma_x}^2+\frac{1}{24}\alpha^2D_4{\sigma_x}^4...\end{aligned} \quad (0\text{-}32)$$

$$\begin{aligned}P_{yy} &= W_0^{\mathrm{c}}\left(\zeta_0-\bar{y}\right)\left(\zeta_0-\bar{y}\right)^{\mathrm{T}}+W_1^{\mathrm{c}}\left(\zeta_{1,1}-\bar{y}\right)\left(\zeta_{1,1}-\bar{y}\right)^{\mathrm{T}}+W_1^{\mathrm{c}}\left(\zeta_{1,2}-\bar{y}\right)\left(\zeta_{1,2}-\bar{y}\right)^{\mathrm{T}}\\ &= {D_1}^2{\sigma_x}^2+\frac{1}{3}\alpha^2D_1D_3{\sigma_x}^4+\left(\frac{\beta+1}{4}-\frac{1}{4\alpha^2}\right){D_2}^2{\sigma_x}^4...\end{aligned} \quad (0\text{-}33)$$

It is seen from Eqs. (3-23), (3-24), (3-25) and (3-26) that, for the symmetric sampling, the terms with the odd-numbered moments of the two sampling points $\zeta_{1,1}$ and $\zeta_{1,2}$ have the same weight factors but opposite signs, making the odd-numbered moment terms disappear in the Taylor expansion of the mean and variance.

3. Compare each terms of the mean as well as the variance in both the reference values and the calculation results of the symmetric sampling method, that is, compare the terms of Eq. (3-18) and (3-25), as well Eqs. (3-19) and (3-26).

It is found that the precision of the scaled symmetric sampling provided can at least reach to the third-order term whatever the values of parameters α and β are, where the third moments are zero. The two scaled parameters α and β are introduced to improve the precision of the estimation of the mean and variance in the fourth-order terms of the Taylor series expansion. Comparing the coefficient of the four-moment term between the reference values and those from the scaled sampling, we can obtain that

$$\frac{1}{24}\alpha^2=\frac{1}{8} \quad (0\text{-}34)$$

$$-\frac{1}{4\alpha^2}+\frac{\beta+1}{4}=\frac{1}{2} \quad (0\text{-}35)$$

Then, $\alpha^2 = 3$, $\beta = 4/3$. That is to say, when $\alpha^2 = 3$ and $\beta = 4/3$, the estimation precision of the UT transform for Gaussian distribution can be improved from the third order to the fifth order, where the fifth order of the Gaussian distribution is zero.

For multi-dimensional **x**, it can be whether the symmetric sampling or simplex sampling according to the distribution of **x** is symmetric or not. Then, the approach for determine the

values ofα and β can be used for both the two kinds of sampling. For identifying constant parameters, the $\mathbf{P}_{xx}$ (the σ_x^2 for a scalar x) will reduce to zero gradually (Wang, 2014). That is, the effect generated by higher-order moments to the precision will decrease as the time step increases. Therefore, we can give a relative small values for α andβ, and then achieve a high-precision estimation by increasing the number of identification steps.

3.3 Methodology Based on Analytical Measurement Equation

In order to verify the feasibility of identifying the parameters of concrete constitutive model (CM), a relative simple case with the concrete stress is taken as the observation. In this case, the measurement equation can be analytical expressed though it is nonlinear.

If the loading process is monotonous, that is, there is no unloading process, the measurement equation can be simple expressed as,

$$y_i = \sigma_i = g\left(\mathbf{x}_i, \varepsilon_i, \mathbf{P}_{\mathrm{nc}}\right) + v_i \qquad (0\text{-}36)$$

where y_i is the observation at ith step; σ_i is the measured concrete stress at ith step; $\mathbf{x}_i$ is the state variables need to be identified, including f_{cu}, ε_{0u}, K; $\mathbf{P}_{nc}$ is the other parameters in the concrete CM, including constitutive parameters ε_{uu}, S_1, S_2, S_3, and non-constitutive parameter ρ_s; ε_i is the concrete strain at ith step, which is taken as input; v_i is the measurement noise; g is the expression of the measurement equation. Because there is no unloading process, the measurement equation is just the skeleton curve of concrete shown in Eq. (2-20).

However, if unloading processes exist, the σ_i is no longer in a one to one correspondence with ε_i, but also related to the strain ε_{i-1} obtained in the previous step. With this respect, the Eq. (3-29) needs to be rewritten as

$$y_i = \sigma_i = g\left(\mathbf{x}_i, \varepsilon_i, r_{i-1}, \mathbf{P}_{\mathrm{nc}}\right) + v_i \qquad (0\text{-}37)$$

where r_{i-1} is defined as historical variables which related to the load path and influence the calculation results of the next step. These historical variables need to be taken as input for next calculation. Here the historical variable is the ε_{i-1} for the ith calculation.

To validate the method for identifying the concrete constitutive parameters by numerical simulation, positive problem need to be solved first to simulate the observations and inputs, σ and ε. And the parameter values used in the positive analysis are the true values for reference. As the feasibility of UKF is verified, the measurement equation shown in Eq. (3-29) is used regardless of the effect of the unloading factor. So, in the positive problem, the components are monotonically loaded to obtain the corresponding stress and strain of concrete. For inverse problem, there is no need to consider the historical variable ε_{i-1}.

The FE model of the RC cantilever column which is used for sensitivity analysis is continue to be

employed for simulating the measured stress and strain. Then by adding additive noises to the concrete stress, the observations can be simulated as,

$$y_{\mathrm{m},i} = y_{\mathrm{s},i} + E_{\mathrm{p}} \cdot y_{\max} \cdot N_{\mathrm{n}} \qquad (0\text{-}38)$$

where $y_{\mathrm{s},i}$ is the concrete stress provided by the FE model of the column; $y_{\mathrm{m},i}$ is the observations with additive noise for identification; $y_{\max}$ is the maximum value of the concrete stresses, here it is 20Mpa; N_{n} is the normalized Gaussian white noise with a maximum value of 1; E_{p} is the noise level, here the value is set to be 1%.

In the FE model, the concrete is assumed to be C20, and the stirrup is HPB235. According to Section 2.3.7, the initial values of the concrete constitutive parameters are determined and shown in the third row of Table 3-1. Where, f_{cu} is the average value of the cylinder compressive stress with a value of 19MPa; $\varepsilon_{0\mathrm{u}} = 0.002$; $\varepsilon_{\mathrm{uu}} = 0.0038$; $K = 0.85$; $S_1 = f_{\mathrm{yh}} / f_{\mathrm{cu}} = 12.4$; $S_2 = 3S_1$; $S_3 = 0.75f_{\mathrm{yh}}$. The true values of parameters with the difference more than ± 15% are listed in the second row of Table 3-1.

Parameter	f_{cu}	$\varepsilon_{0\mathrm{u}}$	K	$\varepsilon_{\mathrm{uu}}$	S_1	S_2	S_3
Truth value	23	0.003	0.75	0.005	22	15	141
Initial value	19	0.002	0.85	0.0038	12.4	37.1	176

Table 3-1 True and initial values of concrete constitutive parameters (Measurement - Stress)

The identification results are shown in Fig. 3-2 and Fig. 3-3. Fig. 3-2 shows the comparison results of the FE model using different parameter values. The curve corresponding to the initial value in the figure shows the result obtained by using the initial values of parameters in the whole process FE analysis; the curve corresponding to the identification values indicates that only the initial values of the parameter is used in the first step, then the identified parameters obtained at each step is used for analyzing at each analysis step. It is found that the F identification results are better. After the convergence of parameters, the UKF method provides a very high degree of matching between the estimated and true stresses. The maximum relative error of stress decreases from 40% to 2.1% and the maximum relative error of strain decreases from 37.0% to less than 1%.

It is seen from Fig. 3-3 that all three parameters can converge to their true values quickly and stably. The final convergence value almost coincides with the true value. The relative errors of the convergence values of the three parameters and their true values are presented in Table 3-2, which are all fall within 1%. It should be noted that, in the third figure of Fig. 3-3, the parameter K_{c} remains unchanged before 3000*με.* This because that it is only related to the descending branch of the concrete CM, and the concrete did not enter into the descending branch when the strain was less than 3000*με.*

The numerical results show that the identification of constitutive parameters of concrete based on concrete stress has higher accuracy, fast convergence rate and good robustness.

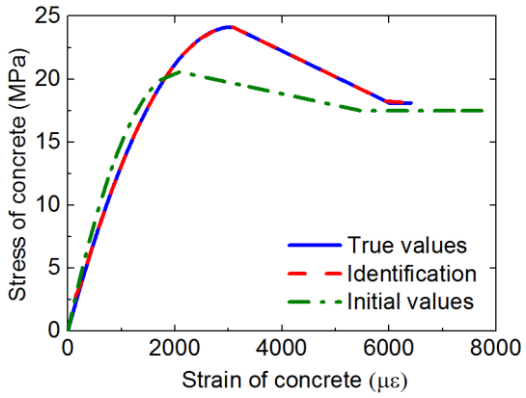

Fig. 3-2 Comparison of constitutive curve of concrete

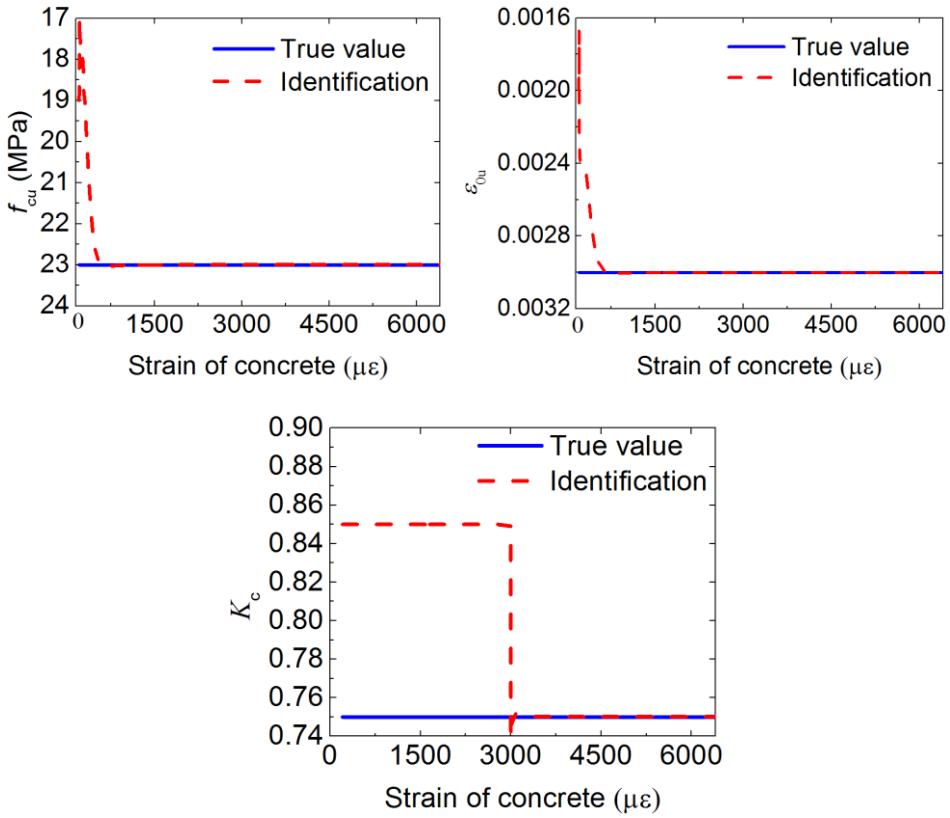

Fig. 3-3 Results of parameter identification (Measurement - Concrete stress)

Relative error（%）	f_{cu}	ε_{0u}	K
With initial value	33.3	50	63.6
With identification value	0.7	3.7	0.8

Table3-2 Relative errors of initial and identified values to the true ones (Measurement - Concrete stress)

3.4 Methodology Based on Non-analytical Measurement Equation

At present, concrete stress and strain are still difficult to be accurately measured, especially when the RC members experience strong nonlinearity and appear wide cracks. Therefore, the application of identifying the constitutive parameters based on concrete stress given in Section 3.3 is quite limited.

In hybrid simulations, displacements and restoring forces of the tested specimen are the most common observations which are with high measured precision and reliability. Therefore, taking the restoring forces of the structural members is more feasible and easy to implement and popularize. If so, however, the relationship between the observation and the constitutive parameters is hard to be analytical expressed. To solve this problem, the OpenSees-embedded UKF is proposed.

3.4.1 Principle

The measurement equation considering the restoring force as the observation can be expressed as,

$$\mathbf{y}_i = \mathbf{F}_i = G\left(\mathbf{x}_i, \mathbf{d}_i, \mathbf{P}_{\mathrm{nc}}, \mathbf{r}_{i-1}\right) + v_i \qquad (0\text{-}39)$$

where $\mathbf{y}_i$, $\mathbf{x}_i$, v_i are the same as those given in Eq. (3-29); $\mathbf{P}_{\mathrm{nc}}$ is concrete constitutive parameters that are not need to be identified; $\mathbf{F}_i$ is the restoring force measured at the *i*-th step; $\mathbf{d}_i$ is the input of displacement at the *i*-th step; *G* is the functional expression of the measurement equation; $\mathbf{r}_{i-1}$ are historical variables. Here, the historical variables may contain more the types and numbers compared with the case where stress is observed, including the restoring forces, displacements, stress, strain, etc. obtained in the previous analysis step.

Two problems need to be solved:

1. The measurement equation that describe the relationship of the concrete constitutive parameters and the restoring force of RC member is quite difficult to be analytically expressed, that is, *G* cannot be provided analytically. This leads to that the estimation value of the measurement, i.e. the force, cannot be calculated during the identification process.
2. In the hybrid test, it is very common that the structure subjects to cyclic loading including the loading and unloading process. The historical variables depended on the loading paths will have an impact on the calculation of the component restoring force in the current step. So, it is necessary to record all the historical variables generated by the previous calculation and use them as inputs for the next calculation.

With these respects, a novel method that combines the OpenSees FE software and the UKF is proposed, in which the OpenSees is embedded into the UKF to replace the nonlinear function *G*. That is the OpenSees is responsible for the nonlinear transformation of the sigma points. This can also solve the problem of historical variable. According to the fomula for nonlinear transform sigma points, Eq. (3-10), and the measurement equation expressed by Eq. (3-32), the nonlinear transformation using OpenSees can be expressed as,

$$\zeta_j^i = G\left(\chi_j^i, \mathbf{d}_i, \mathbf{r}_{i-1}\right) \qquad (0\text{-}40)$$

Where, G is the nonlinear function which expressed by the OpenSees FE model; χ_j^i are the sampling points of concrete constitutive parameters at the *i*-th step; ζ_j^i are the sampling points after nonlinear transformation, which are corresponding to the component restoring force; $\mathbf{d}_i$ is the *i*-th displacement inputs; $\mathbf{r}_{i-1}$ are the history variables generated after the analysis of step *i*-1 and saved by the FE model. Using Eq. (3-33), the sampling points of **x** and displacement inputs are sent to OpenSees, and OpenSees finish the calculation based on the previous historical variables to obtain the nonlinear transformed sampling points, ζ_j^i. Noted that all nonlinear transformation of the 2*n*+1 sampling points must be executed on the same displacement $\mathbf{d}_i$ and the same historical variable $\mathbf{r}_{i-1}$.

The main program of UKF for parameter identification is written and implemented in MATLAB. So the OpenSees FE model needs to be embeded into the MATLAB procedure. The implementation flowchart of the principle of this novel method is shown in Fig. 3-4. At each step, MATLAB sends 2*n* + 1 sampling points to OpenSees in turn, then based on the same historical variables, OpenSees calculates the *j*-th sampling points of the observation sequentially and sends the sigma points after nonlinear transformation back to MATLAB to finally obtain the estimation of the observation.

As above mentioned, the nonlinear transformation of each sigma point must be executed on the same variables, so an approach for getting unified historical variables is proposed and shown by the parts shown in the dashed box in Fig. 3-4. After all the nonlinear transformations of sampling points are finished, a new estimation of **x** at step *i*, $\hat{\mathbf{x}}_i$, can be achieved by in MATLAB. It is this new estimation that is sent to the OpenSees model again, and an additional operation is performed under the same displacement $\mathbf{d}_i$ to unify the historical variables. In this way, the unified historical variables of step *i* can be obtained for the calculation in the step *i* + 1.

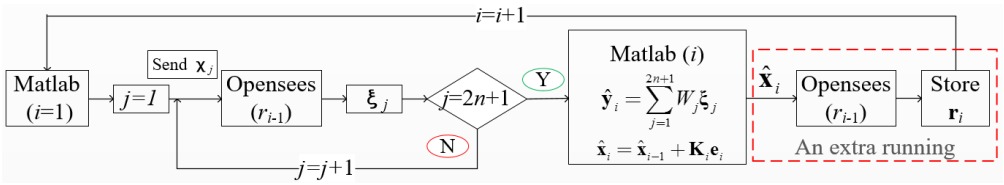

Fig. 3-4 Flowchart of parameter identification with UKF embedded with OpenSees

3.4.2 Program implementation

In order to realize the proposed identification method shown in Fig. 3-4, MATLAB and OpenSees are required to possess the following functions:

1. Data exchange between the two software. MATLAB sends the displacement command and sampling points of the parameters to OpenSees. OpenSees return the sigma points of the restoring force computing use the received data;
2. OpenSees is required to have the function of updating the parameters. OpenSees needs to calculate using each group of sampling points. That is, after receive the 2*n*+1 sampling points

in sequence, OpenSees needs to update the corresponding parameters of the concrete CM and compute in sequence 2*n*+1 times.

3. OpenSees needs to have the ability to record all the historical variables of the previous step, and restore these variables 2*n*+2 times for the 2*n*+2 computation in the current step.
4. OpenSees needs to have the ability to pause, wait, and continue computing. At each step, the main program in MATLAB is executed for estimating the parameters. During this process, OpenSees need to pause and wait for the calculation of the new parameters and displacement commands sent by MATLAB. Then, after receiving the data, the OpenSees continue to analyze with the new parameters. Then, it sends back the data and enters the waiting status again instead of terminating the analysis until receive the termination command from MATLAB.

To the first function for data exchange, the interface program for data communication is written in C++ language based on the TCP / IP protocol and embeded into Matlab by 'mex' command provided by MATLAB. In order to realize the other functions, the OpenSees source codes were developed. The modified parts of the source codes mainly include TclModelBuilder, Domain, Analysis, Element, Material and other parts, as shown in Fig. 3-5. The Domain is modified to store the received parameters or their sampling points. A New HybridStatic analysis modula for hybrid simulation has been written and added to the original Analysis module to enable functions 3 and 4.

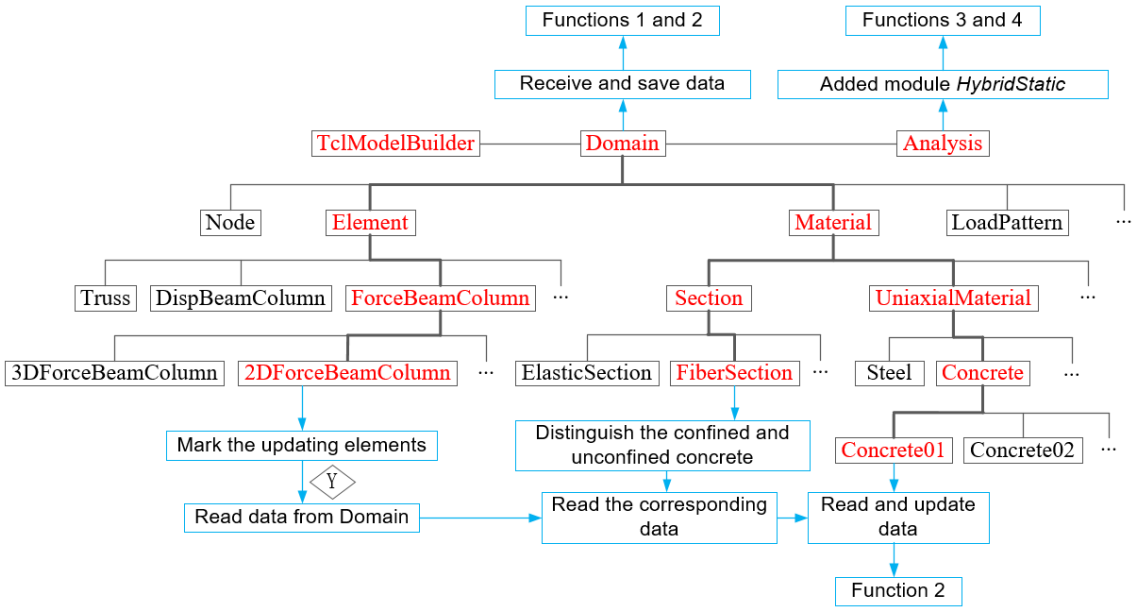

Fig. 3-5 Main parts of the modified source codes of OpenSees

The force-based beam-column element is modified to distinguished elements. That is, the elements in the numerical substructure (NS) that need to be update by new parameters are distinguished from those do not need to be updated. This allows us to mark the elements need to be updated and only updates the parameters of these marked elements.

The basic Material, and its derived class Uniaxial Material whose derived class includes

Concrete01 Material, are also modified to allow the concrete being marked. In this way, the confined concrete can be identified from the unconfined concrete, making parameters can be updated to the right material model. In addition, the modification of the material codes are for realizing the old parameters being replaced by the new parameters, i.e. updating.

The basic Material and its derived class Section and FiberSection were modified to assist in distinguishing the confined and unconfined concrete, as well the data receiving from the Domain and sending to the Uniaxial Material.

3.4.3 Numerical verification

As the same process of numerical validation with that in Section 3.3, firstly, using the same FE model of the cantilever column, carry out the forward analysis of the column subjected to monotonic loadings and obtain the corresponding restoring forces of the component; then, add noises to the structural response, i.e. the restoring forces, to simulate real observations by Eq. (3-31), where the noise level is still set to 1%, r_{max} is 24.4kN; finally, using the proposed method to identify the constitutive parameters of concrete.

The true and initial values of the concrete constitutive parameters are shown in Table 3-3. The identification results are shown in Fig. 3-6. It is seen from the figure that the proposed approach for identifying constitutive parameters of concrete has favorable accuracy, fast convergence rate

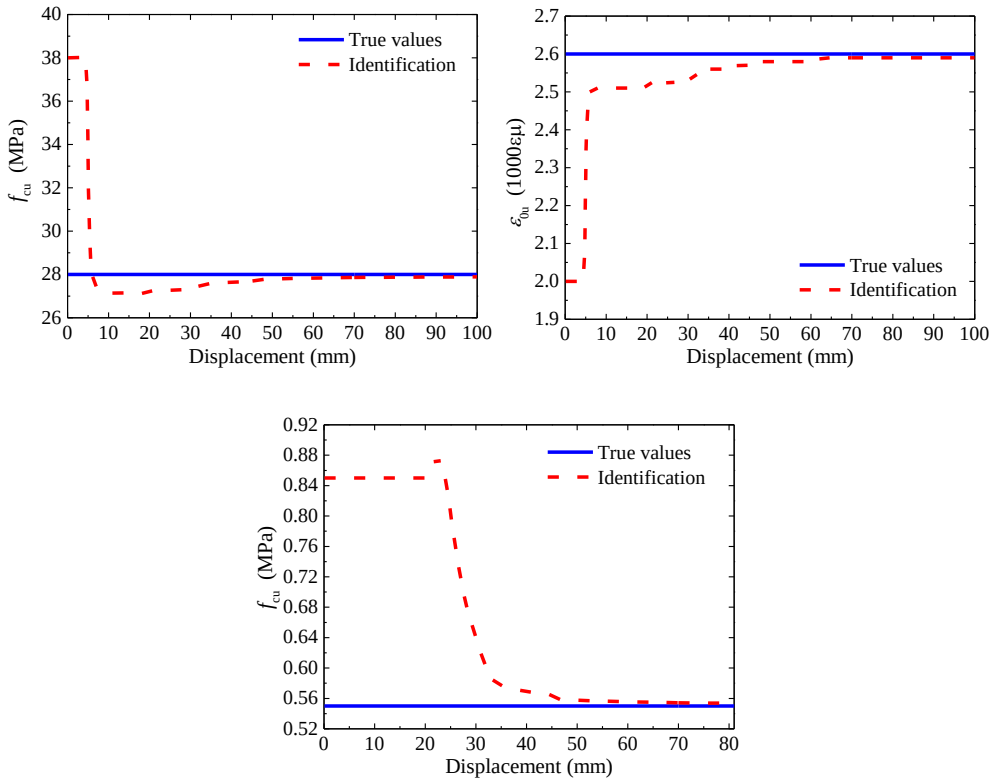

Fig. 3-6 Results of parameter identification (Restoring forces-Measurements)

and good robustness. The relative errors between the convergence values of the three parameters and their true values are listed in Table 3-4. It is seen that the relative errors of both the f_{cu} and ε_{0u} fall within 0.5%, and the relative error of the K drops to 1.5% as well. Although the relative error of the K is slightly larger than the first two parameters, the improvement is still significant compared with the initial error of 110%.

Though the convergence speed is a little lower than the case based on the stress of concrete, the parameters can convergence to the true value finally with a relative good speed and stability. This reason of the lower rate is that the calculation of the restoring forces is also affected by the constitutive models of reinforced bars, as well as other factors such as element type and integral method. In other words, the correlation between the concrete constitutive parameters and the restoring force of the members is not as strong as that between parameters and the concrete stress.

Parameter	f_{cu}	ε_{0u}	K	ε_{uu}	S_1	S_2	S_3
Truth value	28	0.0026	15.4	0.0045	8	24	157
Initial value	38	0.002	32.3	0.0045	8	24	157

Table3-3 True values and initial values of the constitutive parameters of concrete (Restoring forces-Measurements)

Fig. 3-7 shows the comparison of force-displacement curves of the column. It can be seen that the restoring forces provide by the FE model with the identified parameters have a relative large errors from those with true parameter values when the displacement is less than 8mm. As shown in Fig.3-6, we can see that during this period, the improvement brought by the parameter identification cannot be enough to make up for the influence of the error generated by the initial values of parameters as well as the model errors. With the gradual convergence of the parameters, the coincidence between the estimation and true values of the restoring forces is obviously improved.

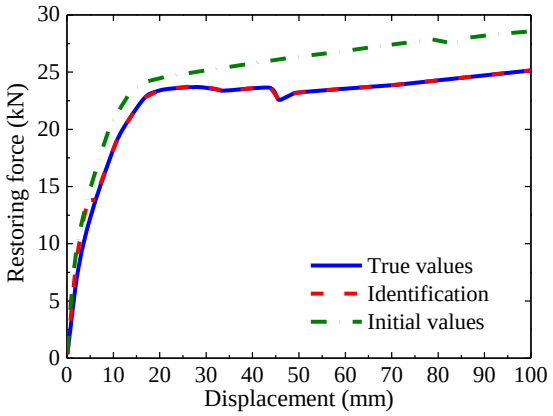

Fig. 3-7 Comparison of force-displacement curve

Relative error（%）	f_{cu}	ε_{0u}	K
Initial value	35.7	23.1	110
Identified value	0.4	0.3	1.5

Table3-4 Relative errors of initial and identified values to the true ones (Restoring forces-Measurements)

3.5 Convergence Analysis of UKF Method

From Fig. 3-3 and Fig. 3-6, we can see that the parameters are not monotonically convergent, but with fluctuation, either the stress or restoring force is taken to be the measurement. In this section, the case with only one parameter f_{cu} being identified is investigated firstly. The characteristic of monotonic convergence of the time-varying linear system with one parameter identified is proved theoretically, and verified by the numerical simulation. Then the identification case of two parameters f_{cu} and ε_{0u} being identified is numerical simulated. Finally, the reason of fluctuation of parameters during the convergence process is discussed from the perspectives of parameter sensitivity and the identification method.

3.5.1 Relationship of parameter f_{cu} *and component restoring force*

When the constitutive parameter f_{cu} is the only one to be identified, the relationship of the f_{cu} and concrete stress can be simply expressed as in Eq. (3-34), according to the Eq. (2-20).

$$\sigma_i = h(\varepsilon_i) \cdot f_{cu} = h_i \cdot f_{cu} \tag{3-34}$$

in which, h_i is a nonlinear function with ε as independent variable.

For a beam-column element, the base shear can be expressed as in Eq. (3-35) when there is no external force along the length of the element.

$$F = (M_1 + M_2)/2 \tag{3-35}$$

where, M_1 and M_2 represent the bending moment at each end of the element respectively, which are calculated as follows,

$$M_j = \int_l (a_j N + b_j M) ds \quad j = 1, 2 \tag{3-36}$$

where a_j as well as b_j is the coefficient associated with the shape function; l is the length of element; N and M are the axial forces and moments on the cross section, respectively, which are calculated as follows,

$$N = \int_A \sigma_i dA + N_s \qquad (3\text{-}37)$$

$$M = \int_A z\sigma_i dA + M_s \qquad (3\text{-}38)$$

in which σ_i is concrete stress, given by Equation (3-34); z is the distance to neutral axis; N_s and M_s are the axial force and moment on the cross section, provided by the reinforced bars.
By substituting Eq. (3-34) into Eq. (3-37) and Eq. (3-38), respectively, the axial force and bending moment on the cross section can be obtained. Then the bending moment at the end of the element can be attained according to Eq. (3-36) ; Finally, submitting Eq. (3-36) into Eq. (3-35), the restoring force of the element can be described as

$$F = H_i \cdot f_{cu} + R_{s,i} \qquad (3\text{-}39)$$

with the f_{cu} as the independent variable. Where, $R_{s,i}$ is the restoring force provided by all the reinforced bars, and can be regarded as a constant in each integration step i; H_i is also can be calculated as a constant in each step by $H_i = (a_1 + a_2 + b_1 z + b_2 z) A \cdot l \cdot h_i / 2$.
So far, we can find a linear relationship of F and f_{cu} in each integration step from Eq. (3-39). That is, *a* time-varying linear system.

3.5.2 Proof of monotonic convergence of UKF for single parameter

3.5.2.1 Theoretical proof

For identification of linear systems, the UKF is the same as the KF. That is, the UKF gives exactly the same estimation results as the KF gives. Therefore, if the monotonic convergence of the KF for one parameter of a time-varying linear system can be proved, the same conclusion can be drawn for the UKF.
A more general form of time-varying linear system for Eq. (3-39) is presented as,

$$y_i = H_i \cdot x_i + C_i + v_i \qquad (3\text{-}40)$$

where, C_i is a constant for each time step i; x is the parameter to be estimated; y is the observation; v is the measurement noise. Then the estimation of measurement can be obtained by Eq. (3-40) as,

$$\hat{y}_i = H_i \cdot \hat{x}_i + C_i \qquad (3\text{-}41)$$

Then, according to the KF, i.e. Eq. (3-3), the estimation of x is,

$$\hat{x}_i = \hat{x}_{i-1} + K_i \left(y_i - \hat{y}_i \right) \qquad (3\text{-}42)$$

where, K_i is the Kalman gain,

$$K_i = \frac{H_i P_{i-1}}{H_i^2 P_{i-1} + R} \quad (3\text{-}43)$$

in which, P_i is the variance of x; R is the variance of measurement noise. Substituting Eqs. (3-40), (3-41) and (3-43) into Eq. (3-42), we can obtain that

$$e_i = a e_{i-1} \quad (3\text{-}44)$$

in which,

$$e_i = \hat{x}_i - x \quad (3\text{-}45)$$

$$e_{i-1} = \hat{x}_{i-1} - x \quad (3\text{-}46)$$

$$a = \frac{R}{H_i^2 P_{i-1} + R} \quad (3\text{-}47)$$

From Eq. (3-47), we can draw that a <1, because $H_i^2 P_{i\text{-}1}$> 0 and R>0. Therefore, we can conclude from Eq. (3-44) that e_i is monotonic convergence, and hence monotonic convergence for x is obtained.

3.5.2.2 Numerical verification

Using the same numerical cantilever column and parameter identification method as in Section 3.4.2, but, in this case, only parameter f_{cu} is identified and all other constitutive parameters of concrete are set to true values. Fig. 3-8 shows the identification result. It can be seen from the figure that the numerical simulation gives the same conclusion as the theoretical proof. The f_{cu} converges to the true value monotonically without fluctuations.

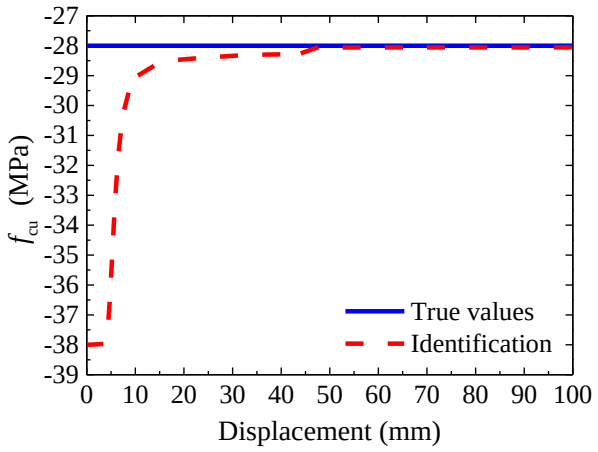

Fig. 3-8 Single parameter identification - f_{cu}

3.5.3 *Analysis of convergence fluctuations*

In the same way as single parameter identification, the numerical simulation of identifying two parameters f_{cu} and ε_{0u} are carried out. The results are shown in Fig. 3-9, from which we can see that the convergence process of the parameter f_{cu} is disturbed when the parameter ε_{0u} is added. Fluctuations are appeared of the f_{cu} with the process that the identified values are firstly larger than the true value, then less than the true value, and finally converged.

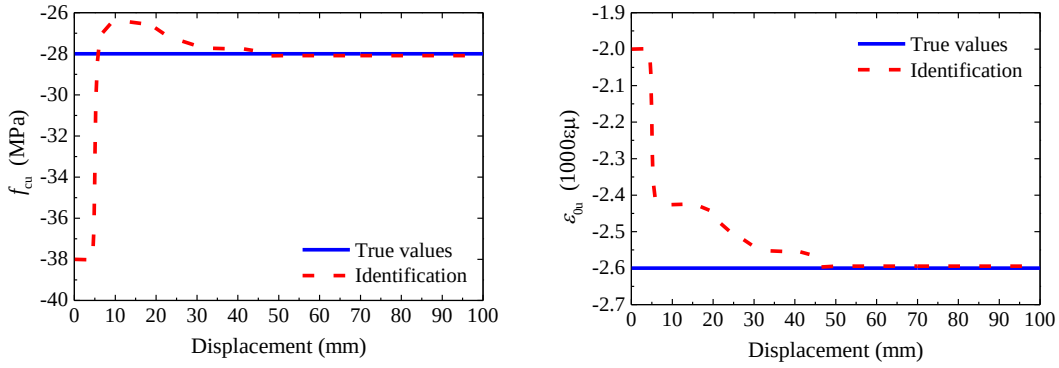

(a) Parameter f_{cu} (b) Parameter ε_{0u}

Fig. 3-9 Two parameters identification - f_{cu}, ε_{0u}

From the sensitive analysis of parameters, it is evident that different parameters have different sensitivities to the component restoring forces. This phenomenon could lead to various convergence rates for each parameter, thus further cause fluctuations in the estimation process, as illustrated in Fig 3-10.

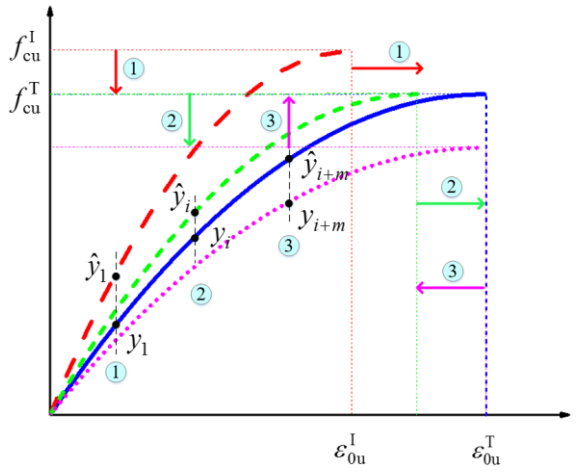

Fig. 3-10 Reason for fluctuations

In particular, the solid blue curve represents a stress-strain relation determined by the reference values f_{cu}^{T} and ε_{0u}^{T}; whilst the red long-dashed curve was determined with the initial

values $f_{\mathrm{cu}}^{\mathrm{I}}$ and $\varepsilon_{0\mathrm{u}}^{\mathrm{I}}$. In this case, the estimated values of the measurement at the initial step is greater than the real measured one, i.e. $\hat{y}_i > y_i$. Then, in subsequent steps, the identified f_{cu} has to decrease and $\varepsilon_{0\mathrm{u}}$ must increase towards the true value to allow the estimated force to approach the measured one. As a result, f_{cu} and $\varepsilon_{0\mathrm{u}}$ may exhibit different convergence rates. Let's assume that the former one converges to the true value faster than the latter, which results in the green mid-dashed curve of shown in Fig.3-10. As the estimated force denoted by the green curve is still greater than the measured value, f_{cu} should further decrease and $\varepsilon_{0\mathrm{u}}$ further increase to pull down the estimated force towards it's the real measured one, which results in the pink short-dashed curve in Fig. 3-10. Due to error correction property of Kalman-family filter, the estimated forces should gradually in accordance with the real measured ones, which will thus drive the estimated parameters to converge; as a result, f_{cu} will go back to and toward to the true value. Therefore, the fluctuation of f_{cu} arises in the identification process, as shown by the vertical arrows numbered ①, ② and ③.

According to the analysis, we can know that the fluctuation may not appear only once, it could emerged a few times during the convergence process. This is proved by the cases presented in the following chapters.

3.6 Summary

Based on UKF, this chapter presents a method to identify the parameters of concrete constitutive model. The feasibility of identifying these constitutive parameters is verified by the case that concrete stresses are taken as the measurements. Subsequently, in order to make the method be more versatile in hybrid simulation, method of OpenSees-embedded UKF was proposed for identifying the constitutive parameters, and verified by numerical simulations. Finally, the reason of fluctuations existing in the convergence process is discussed. The main conclusions are as follows,

1. Starting from the Kalman Filter, the principle of the UKF and its relationship with recursive least square method are expounded. The accuracy of the unscented transform with the scaled symmetric sampling method is analyzed. Effects of the scalded coefficients of sampling on estimating the mean and variance is discussed, and the optimal values of the sampling coefficients are obtained for the case when the estimation of a Gaussian random variable reaches to the fourth-order precision of Taylor expansion.
2. Taking concrete stresses as the observations, the parameters of concrete constitutive model are identified by using UKF realized in Matlab to verify the feasibility of identifying the concrete constitutive parameters. Numerical simulation results show that the UKF has favorable accuracy, convergence rate and robustness in the case of choosing concrete stress as the measurement.
3. A more complicated nonlinear problem that the measurement equation is hardly to be analytical expressed is solved by proposing the method of OpenSees-embedded UKF. This make the identification method be more universal for hybrid simulations with model updating. Numerical simulations are carried out to verify the proposed methods, and the results show

the parameters converge quickly with a high precision and stability.

4. Both the theoretical proof and numerical validation are presented to illustrate the characteristic of monotonic convergence of the UKF for single parameter identification of time-varying linear systems. The different sensitivities of concrete constitutive parameters leading to the different convergence rate causes the fluctuation during the convergence process.

4. HYBRID SIMULATION WITH UPDATING THE CONCRETE CONSTITUTIVE PARAMETERS

4.1 Introduction

The model updating method is an effective method to reduce the numerical sub-structure error in the hybrid simulation. The key of the model updating is the parameter identification method. The accurate and effective identification of model parameters is one of the key factors in the model updating hybrid test. Because only when the parameter identification is completed efficiently and accurately, the optimized parameters can be used to update the numerical substructure, and then the simulation results provided by numerical substructure will be more accurate and, hence, the hybrid simulation can be more accuracy.

At present, the model updating hybrid experiments completed by domestic and foreign scholars are mostly based on the component constitutive model (Hazem H. et al., 2014; Wang T. et al., 2013; Hashemi M.J. et al., 2014; Shao X. et al., 2015), which limits the popularization and application of model updating. To solve this problem, Wu et al. [85] proposed a model updating hybrid experiment based on the cross-sectional constitutive model. However, this only solves this problem to some extent, so that the model updating can be extended to members with the same section but different heights. Therefore, based on the most basic material level, this paper proposes a new hybrid test based on constitutive model of material. This makes the model updating hybrid test can be applied to the mixed experimental research of complex structures such as high-rise buildings and long-span bridges with fewer test sub-structures.

In this chapter, the OpenSees-embedded method of identifying constitutive parameters of concrete proposed in Chapter 3 is verified through the monotonic static loading test of reinforced concrete columns. The recognition method was applied to the model updating hybrid test and verified by the model updating hybrid test of single-story single-span RC frame. Finally, the results of the model-updating hybrid simulation are given.

4.2 Verification of Concrete Constitutive Parameters Identification

The same procedure as presented in Chapter 3 was applied to the numerical validation, where the observations used in the identification of this chapter originate from monotonic loading static tests of reinforced concrete cantilever columns, rather than from numerical simulations.

4.2.1 Test arrangement

The prototype of the cantilever reinforced concrete column used in this section is shown in Fig. 2-7 (a) and its cross-section design is shown in Fig. 2-7 (b). The experiment is completed in the structure and seismic laboratory of Harbin Institute of Technology. According to the loading frame

of the laboratory, the specific design of the specimen is shown in Fig. 4-1.

The effective height of the column (column bottom to the action of the actuator position) is 1200mm, the cross-sectional size of 250mm × 250mm. The section is equipped with 8 longitudinal bars of HRB335 bars with a diameter of 10 mm and the stirrup bars are made of HPB235 bars with a diameter of 4 mm. At the bottom of the column with a height of 500mm, the spacing of 50mm. In order to avoid the abnormal cracking between the column bottom and the foundation, the reinforced bars are extended to the bottom of the foundation and anchored. The foundation is designed to fix the specimen to the loading frame as shown in Fig. 4-2. As seen that the foundation is anchored to the load frame by a total of 8 bolts with 4 bolts on each side. The height of the fixing beam is designed to be 434 mm, taking into account both the moment of section and the loading location of the actuator.

In the monotonic static test, the axial force of the specimen is not taken into consideration, and the specimen is loaded by a horizontal actuator which is displacement controlled. It is seen from Fig. 4-2 that the specimen was not directly connected with the actuator but was connected with the actuator by external steel plates. Two steel plates are fix to the top of the specimen by four bolts through the two plates, and then connected to the actuator.

Two Linear Variable Differential Transformers (LVDTs) are laid out along the horizontal direction as shown in Fig. 2 to measure the displacement of the foundation as well as the column top.

In order to ensure that the specimen can fully realize the received displacement command, the difference between two LVDTs is used as the target of outer-loop control. In other words, the difference between the two LVDTs is the actual displacement of the specimen. From the final testing data, we see that the displacement of the foundation is less than 0.2mm.

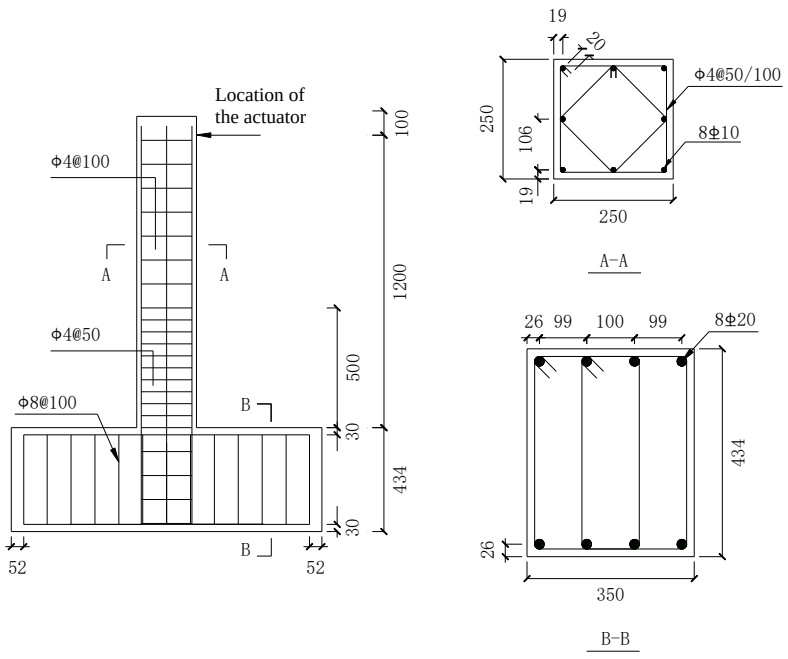

Fig. 4-1 Design of the reinforced concrete column

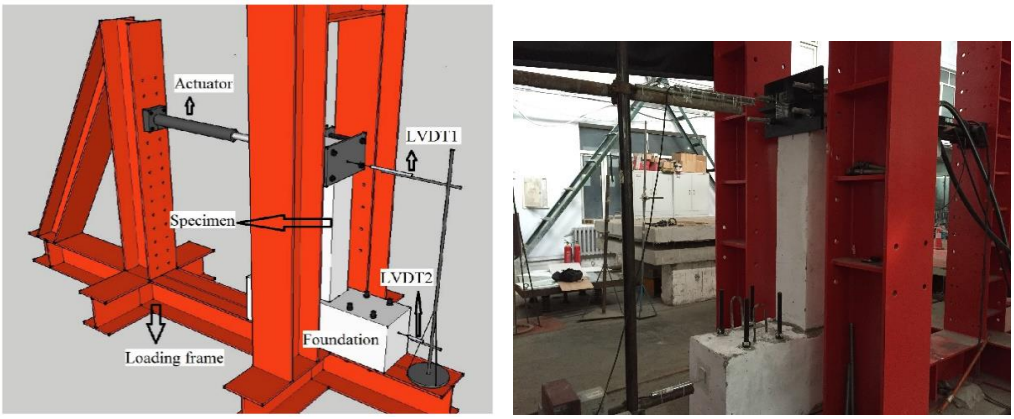

Fig. 4-2 Loading frame of the column and arrangement of the LVDTs
LVDT = Linear Variable Differential Transformer

4.2.2 Concrete constitutive parameters identification

As mentioned earlier, in order to obtain an estimate of the observation, here the base shear of RC columns, a finite element model of the specimen in Section 4.2.1 is to be established in OpenSees. Since the prototype of the finite element model used in the previous analysis for parameter sensitivity and numerical verification is exactly the specimen shown in 4.2.1, this section can be used directly in this section. The model information is shown in Fig. 2-1. In the finite element model, the steel reinforced constitutive model adopts Steel02, and the preset concrete constitutive model used for parameter identification is the Concrete01 model.

For determining the parameter of yield strength in Steel02, three tensile tests were carried out with the loading speed of 4800N / min. The test results are shown in Fig.4-3. After calculation, the mean of yield strength of the reinforcement was calculated to be 354MPa, which was used for the value of the yield strength parameter in the constitutive model of reinforced bars. The elastic modulus of the steel was also measured, which was E_s = 1.96 × 105MPa.

Through the material tests, the average cubic compressive strength of concrete was obtained, which is μ^s_{f150} = 56.2MPa, so as to obtain the average value of the cylinder axial compressive strength of concrete is

$$\mu_{fc} = 0.88\alpha \times \mu^s_{f150} = 42.712\text{MPa} \qquad (4\text{-}1)$$

where, α is related to the strength of concrete. When the strength is less than 50MPa, α = 0.76. Stirrups used in the specimen are high-strength plain steel with a diameter of 4mm, whose tensile tests were carried out with a loading speed of 1000N/min. The results which are presented in Fig. 4-4 show that the stirrup has no obvious yielding platform. The maximum tensile forces obtained from the three tests were 8550.62N, 8611.25N and 8558.10N, respectively. Taking 85% of the average value of the three forces to be the yielding strength, the yield stress are then attained as f_{yh} = 579.9MPa. Finally, the initial values of the constitutive parameters of concrete are calculated and shown in Table 4-1.

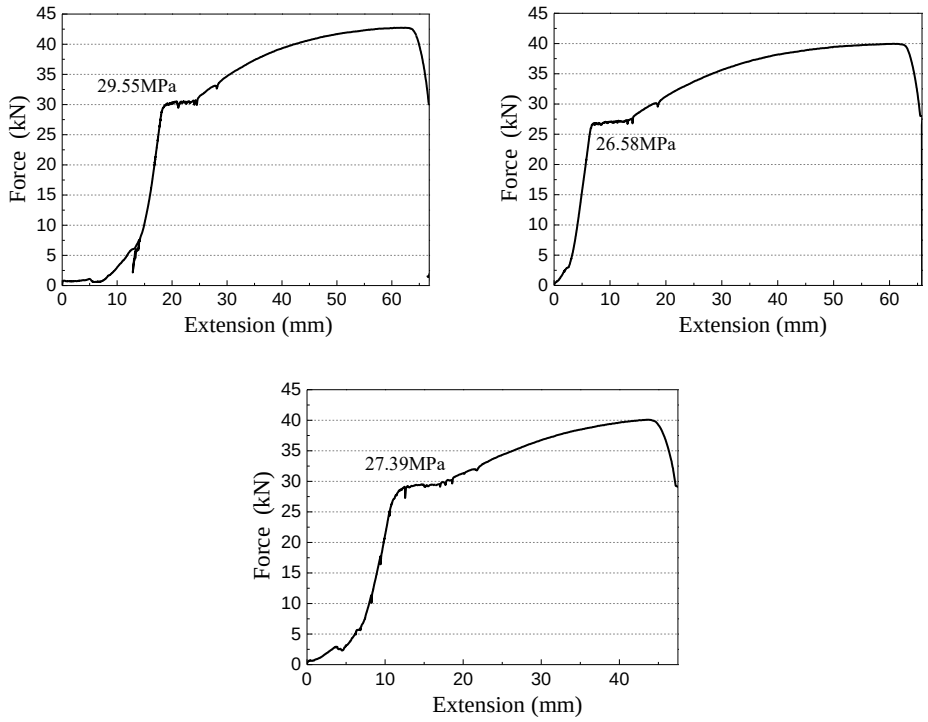

Fig. 4-3 Tensile tests of reinforced bars

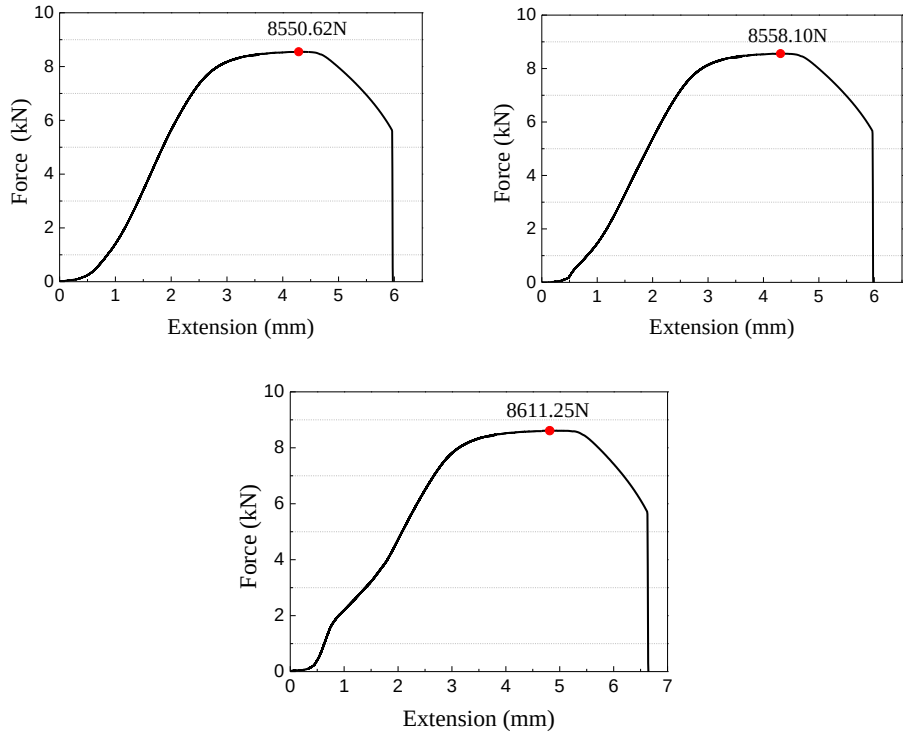

Fig. 4-4 Tensile tests of stirrups

Parameter	f_{cu}	ε_{0u}	K	ε_{uu}	S_1	S_2	S_3
Initial values	43	0.002	0.85	0.0038	13.5	40.5	458

Table4-1 Initial values of the constitutive parameters of concrete

After obtaining the restoring force of the RC column from the static test, the parameter identification is carried out and the results are shown in Fig. 4-5. As can be seen from Fig. 4-5 (a) to (c), the proposed method for identifying the parameters of concrete constitutive model still has good convergence rate and robustness using the experimental data. As previously discussed in Section 3.5.3, the parameter fluctuates multiple times in the process of convergence. The parameters f_{cu} and K fluctuates two times, and the parameter ε_{0u} fluctuates three times.

Fig. 4-5 (d) shows a comparative analysis of the displacement-force relationship of the column. The 'Material test' in the legend which is drawn by the green dash-dotted line shows the simulation results given by the finite element model with the initial values of the parameters are using in the entire computing, where the initial value of the parameters f_{cu} and f_{yh} are those obtained from the material test. The 'Identification' drawn by the red dashed line presents the results with the identified values at each step. From the comparison we can see that the displacement-force curve with reference to 'Identification' is in good agreement with the measured one, especially when the column appears strong nonlinearity.

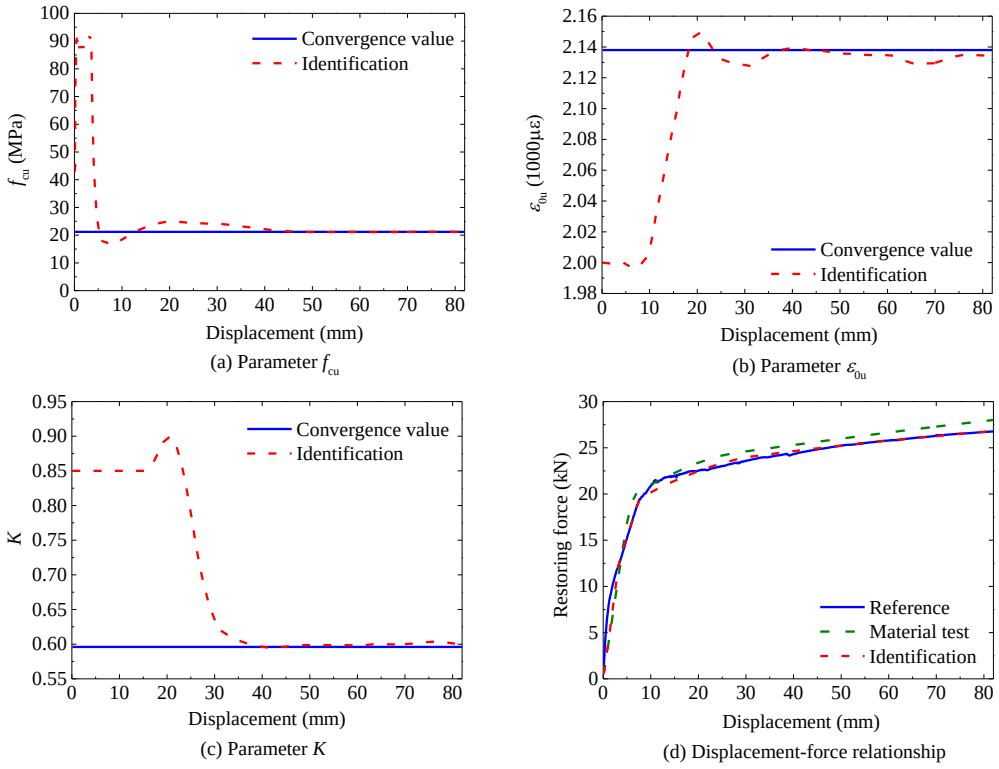

Fig. 4-5 Results of parameter identification

It is noteworthy that, in Fig. 4-5 (a), the identified value of the parameter fcu jumped from an initial value of 43MPa to 90MPa in the first few steps. This is because the default constitutive model, i.e. the Kent-Scott-Park model, ignores the tensile strength of concrete. In fact, the tensile strength plays a significant role in the restoring force of a flexural member when the loading is very limited; if it is ignored, the UKF method will force the compression strength to significantly increase to compensate for the loss of tensile strength. The error introduced by the default model itself in describing the behavior of the material is called model error.

At the end of the test, the concrete were severely cracked at the tensile side, and crushed at the bottom of the compressive side. The test is stopped at a lateral displacement of 82mm, because the actuator is approaching its maximum movements. The specimen is not completely destroyed, as shown in Fig. 4-6 and Fig. 4-7, with three main cracks generated in the tensile side and one main crack in the bottom of the compressive side as well as the spalling. The maximum width of cracks in the tensile side is 6mm, as shown in Fig. 4-6(b). And from Fig.4-6(c), it is observed that the crack caused by tension almost run through the specimen along the loading direction.

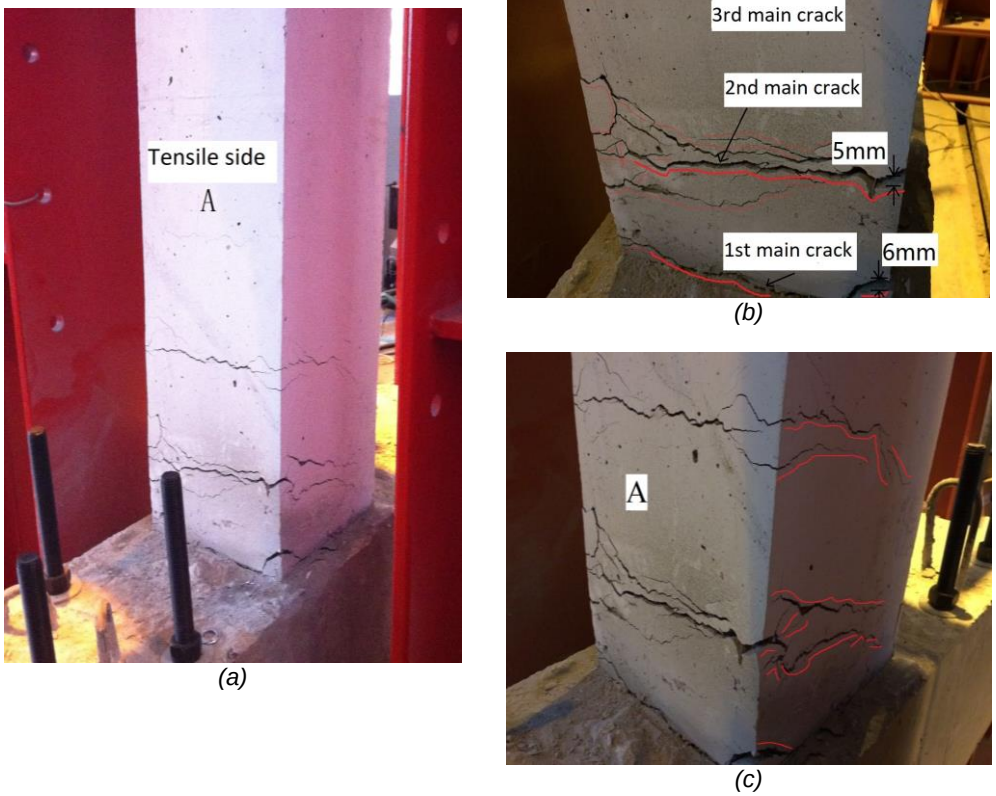

(a)

(b)

(c)

Fig. 4-6 Photos of the specimen after testing-View of tensile side

Fig. 4-7 Photos of the specimen after testing-View of compressive side

4.3 Experimental verification of hybrid simulation with model updating

Both the numerical and experimental verification show that the proposed identification method which considers the restoring force as measurement has high convergence speed and reliability. Therefore, in this section, the identification method was applied to a hybrid simulation of a one-bay one-story RC frame to verify the hybrid simulation method based on identifying and updating of the parameters of concrete constitutive model.

4.3.1 Test system

The standard hybrid simulation without model updating (SHS) divides the structure into two main parts, one is the experimental/physical substructure, i.e. the PS, and the numerical substructure, i.e. the NS, as shown in the solid line in Fig. 1-6. The system for hybrid simulation includes the coordinator which is for solving the motion equation of the structure, the MTS controller responsible for the PS, and a piece of FE software for the NS. Then the model-updating hybrid simulation (UHS) comes out by adding a model updating module including parameter identification, as shown in Fig. 1-6.

The UHS optimizes (identifies) the parameters of the model of the PS by full using of the experimental data of the PS, and then updates the model of the NS with these optimal parameters. With respect to the hybrid simulation with concrete constitutive parameters updating proposed in this study, the main flowchart is shown in Fig. 4-8. Hytest is the platform used in this paper, whose coordinator is responsible for the control of the whole test, the data transmission and the solution of the structural equations of motion. Matlab is responsible for parameter identification with UKF. OpenSees is responsible for numerical modeling which can be divided into two parts:

1. Same as the SHS, OpenSees is responsible for the modeling of the NS;
2. An extra task of OpenSees is to build a FE model of the PS to meet the sampling requirement to assist in the parameter identification.

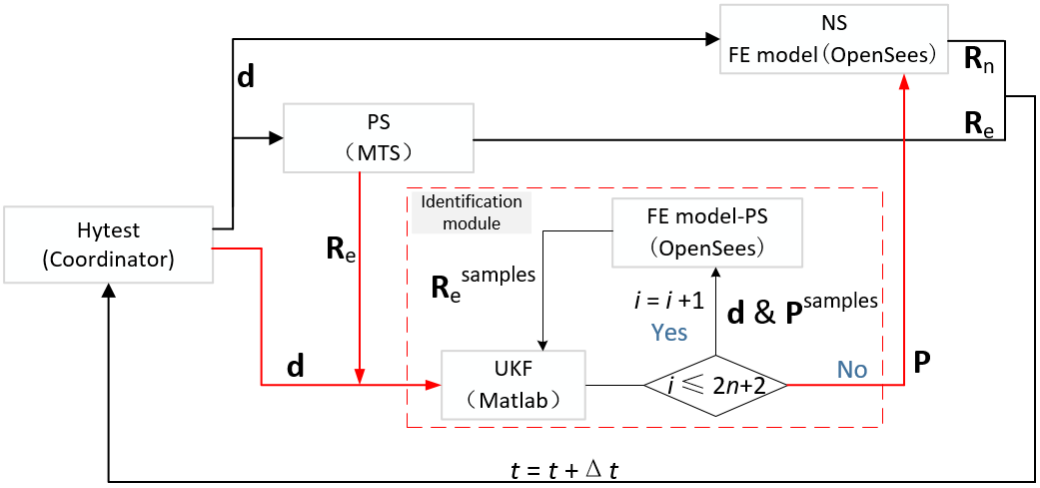

Fig. 4-8 Flowchart of the hybrid simulation with model updating

In order to ensure the validity of the model updating, it is first necessary to ensure that the concrete constitutive model used in the NS components to be updating is the same as that used in the FE model of the PS. Then, by identification method, the parameters in CCM of the FE model of the PS are optimized and the updated to CCM of the NS components. As described in Chapter 3, for the OpenSees-embedded UKF, the OpenSees FE model of the PS will be used to calculate the $2n+1$ samples of restoring force ($R_e^{samples}$ in Fig. 4-8) by using the $2n+1$ samples of the parameters ($P^{samples}$ in Fig. 4-8) given by Matlab; and then Matlab will estimate the restoring force based on these $R_e^{samples}$; Finally, the parameters are estimated in the Matlab and used to update the CCM of the certain components of the NS.

The flowchart of the UHS is as follows:

1. The coordinator sends the displacement to both the NS and the PS;
2. The NS continues to wait for the optimal parameters calculated by the identification module; the PS loads after receiving the displacement and sends back the measured restoring force to the identification module and the coordinator, respectively;
3. Identification module (Matlab) executes after receiving the measured forces to optimize the parameters and send them to the NS;
4. The NS receives the optimal parameters, updates them to the CCM, and then feedback the restoring force under the displacement command *d* to the coordinator;
5. The coordinator solves the structural equation of motion for the next time step. The loops of the above steps from step 1 to 5 proceeds until the seismic load ends.

4.3.2 Test Layout

In this section, a one-bay one-story RC frame is used as a target structure for experimental verification of the hybrid simulation with identifying and updating the concrete constitutive

parameters, as shown in Fig. 4-9. The left column is isolated from the structure to be the PS and the 1/2 scaled specimen of the parts below the inflection point of the left column is constructed in the laboratory. The remainder of the structure is full-size simulated as the NS. For the scaled specimen, its dimensions are exactly the same as the RC column used in the experimental validation in Section 4.1, as shown in Fig. 4-1. Since the top of the specimen is just the point of contra-flexure of the left column, there is no bending moment to load. So, the loading is also the same as that shown in Fig. 4-2.

Assuming that both the axial and the bending stiffness of the beam are infinite, the NS can be further simplified to a RC column with only the horizontal freedom, as shown in Fig. 4-10. The NS is simulated by force-based beam-column elements in the OpenSees with five integration points are evenly distributed along the column height. The constraint command at the top of the right column is (0, 1, 1) to simulate the only existing horizontal freedom.

As the NS is a full-scale model, its cross-section form should the same as that shown in Fig. 2-8(d). However, the length of the cross section and the diameter of the rebars should be increased by two times.

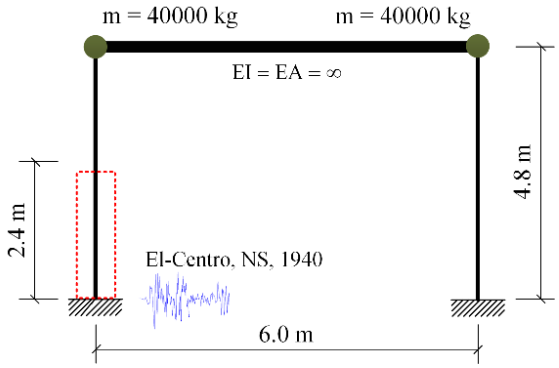

Fig. 4-9 Prototype of reinforced concrete frame

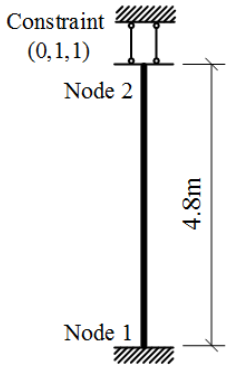

Fig. 4-10 Numerical substructure modelling in OpenSees

For the scaled specimen of the PS, according to the known similarity of length units,

$$l_{\mathrm{m}} = S \cdot l_{\mathrm{p}} \qquad (4\text{-}2)$$

the similarity of the units of angle, force and bending moment are as follows,

$$\theta_{\mathrm{m}} = \theta_{\mathrm{p}} \qquad (4\text{-}3)$$

$$F_{\mathrm{m}} = S^2 \cdot F_{\mathrm{p}} \qquad (4\text{-}4)$$

$$M_{\mathrm{m}} = S^3 \cdot M_{\mathrm{p}} \qquad (4\text{-}5)$$

where *l* represents length unit; *θ* the angle unit; *F* the force unit; *M* the moment unit. The subscript m for the scaled specimen; p the prototype of structures; *S* the similarity factor, *S* = 1/2 in this paper. As a result, the scaled relation of displacements as well as forces transmitted between the coordinator and the two substructures can be obtained considering the proportional factor caused by the inflection point, as listed in Table 4-2.

Transferred data	PS		NS	
	Displacement	Force	Displacement	Force
similar ratio	1/2	1/4	1	1
ratio associate with inflection point	1/2	1	1	1
Displacement sent by Coordinator	*d*/4	--	*d*	
Force received by Coordinator	-	$4R_e$	--	R_n

Table4-2 Scaled factor for data transferred between coordinator and substructures

Note: *d* is the displacement obtained by the coordinator for solving the differential equation of full-scale structure motion; R_e is the measured restoring force of the PS; R_n is the calculated restoring force of the NS.

The hardware of the hybrid simulation mainly consists of three computers, one computer is responsible for the Hytest software platform, the computation of the NS (OpenSees) and the execution of the identification module (Matlab + OpenSees); the second computer is the platform of MTS controlling and loading system; the third computer is MTS controller. Fig. 4-11 shows the operation process during the hybrid simulation.

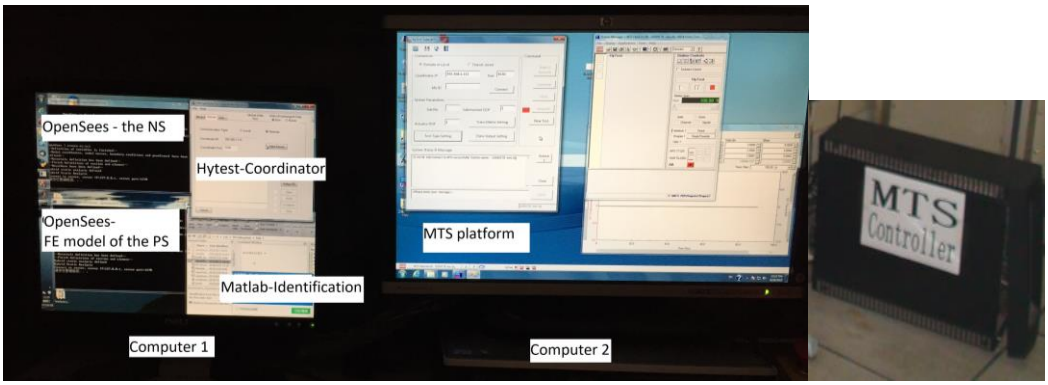

Fig. 4-11 Hardwares of model-updating hybrid simulation

4.3.3 Results of hybrid simulation

Six cases of hybrid simulation are carried out of two specimens of a one-bay one-story RC frame subjects to the El-Centro (NS, 1940) earthquake loads, which are shown in Table 4-3. The reference case refers to the numerical simulation of the pseudo-dynamic test of the RC frame. In this case, the PS and the NS are all numerically modeled by OpenSees. In both the FE models of the PS and the NS, the values of the parameters of the concrete constitutive model (CCM) are those convergence values obtained from case II. The initial values of the parameters are the same as those using for the identification of the static test in section 4.2.

Case	I	II	III
PGA=0.4g	Standard hybrid simulation without model updating (SHS)	Hybrid simulation with model updating (UHS)	Reference case
PGA=1.0g	SHS	UHS	Reference case

Table4-3 Cases for hybrid simulation of reinforced concrete frame

Fig. 4-12 and Fig. 4-13 show the results of the case PGA = 0.4g, whilst Fig. 4-14 and Fig. 4-15 show the results of the case PGA = 1.0g. Results show that the parameters can converge instantly and stably. This can further indicate that the proposed identification method performs well in the hybrid simulation and has high robustness to measurement noise.

In the case of PGA = 0.4g, the parameter *K*, which is only related to the descending branch of the constitutive law of concrete, does not contribute to the component restoring force because that the earthquake loads are not strong enough to promote the concrete enters into the range of descending behavior. As a result, there is no change in the identification process of *K*. So, the unchanged *K* is not presented in Fig.4-2.

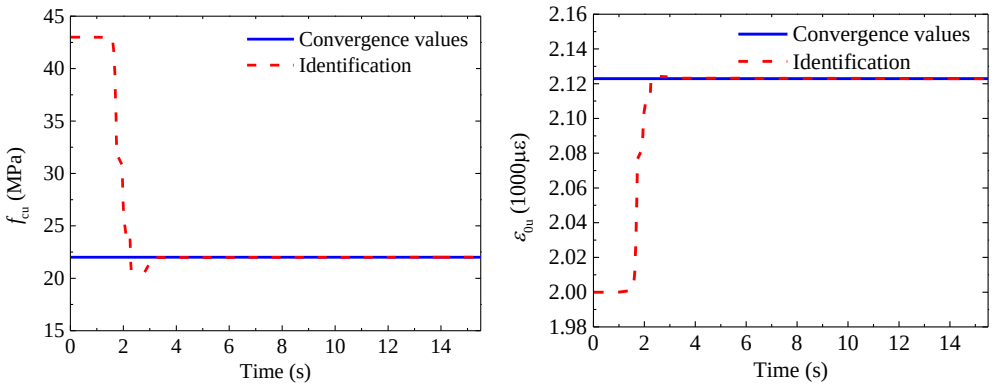

Fig. 4-12 Results of parameter identification (PGA=0.4g)

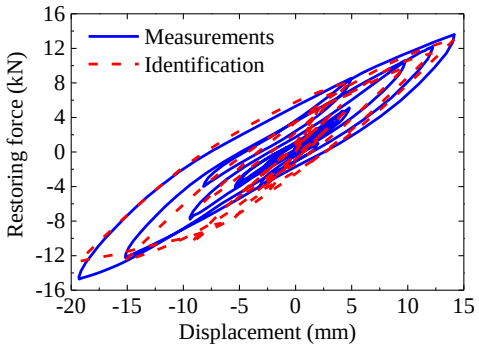

(a) Force-displacement curves – Comparison of real measurements and identification results

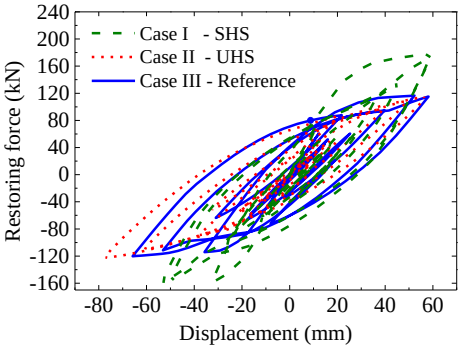

(b) Comparison of force-displacement curves at top of the frame

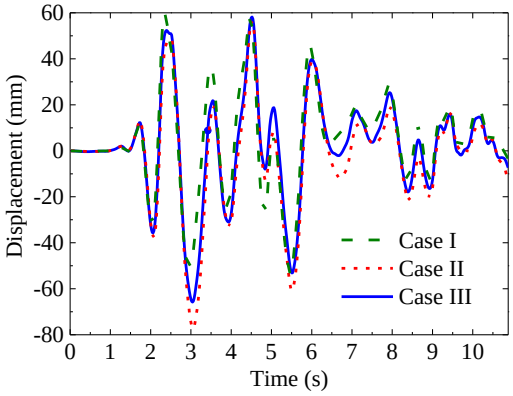

(c) Comparison of the displacement histories at the top of the frame

Fig. 4-13 Responses of the reinforced concrete frame (PGA=0.4g)

It is found from Fig. 4-13 (a) and Fig. 4-15 (a) that the force-displacement curve provided by the FE model using the identified parameters is in good agreement with the measured one. From Fig. 4-13 (b) and Fig. 4-15 (b), it is seen that there is a big difference between the force-displacement curve at the frame top given by the SHS and by UHS. As the identified results matches the reference measured results better, we can conclude that model updating of the concrete constitutive parameters has greatly improved the accuracy of hybrid simulation. The same conclusion can be drawn from the comparison of the displacement histories of the three cases, as shown in Fig. 4-13 (c) and Fig. 4-15 (c).

Since the reinforced bars and the concrete of the columns are the same in the above three cases, including the monotonic static test, the RC frame hybrid simulation with PGA = 0.4g, the frame hybrid simulation with PGA = 1.0g, we can assume that the CCMs and their parameters are the same for both the concrete and rebars. In order to better demonstrate the reliability of the proposed method, the convergence values of the three cases and their mean and standard deviation are listed in Table 4-4. The results show that, for each parameter, the convergence values in the three cases are very close with a quite small standard deviation. Among them, the standard deviation of strength parameter f_{cu} is less than the statistical standard deviation of C40 concrete with the value of 5.98. Then, we can conclude that the proposed identification method has good stability and reliability.

Case	f_{cu} (MPa)	ε_{0u}	f_{ru} (MPa)
(I) Monotonic loading test	21.21	0.002138	12.69
(II) PGA=0.4g RC frame hybrid simulation	22.01	0.002123	--
(III) PGA=1.0g RC frame hybrid simulation	23.35	0.002116	14.76
Mean	22.19	0.002125	13.73
Standard deviation	1.53	1.59×10^{-5}	1.46

Table4-4 Comparison of the convergence value of concrete constitutive parameters

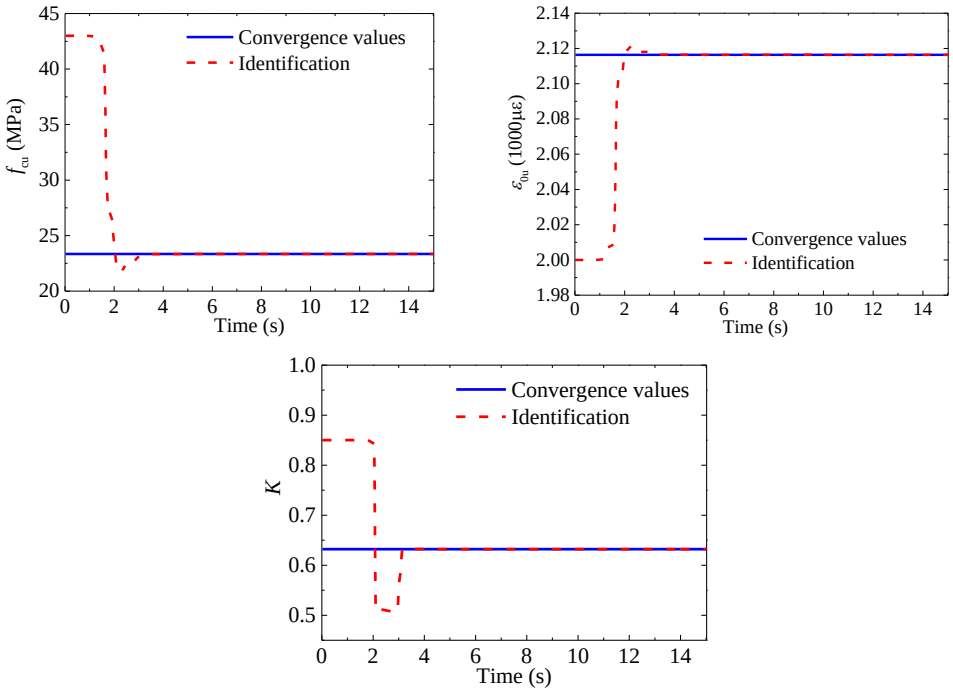

Fig. 4-14 Results of parameter identification (PGA=1.0g)

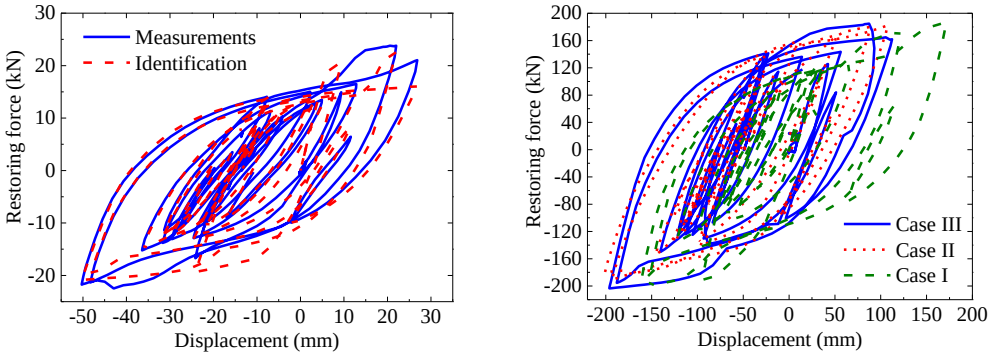

(a) Force-displacement curves – Comparison of real measurements and identification results

(b) Comparison of force-displacement curves at top of the frame

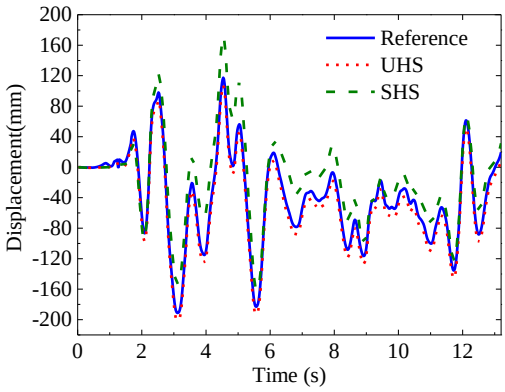

(c) Comparison of the displacement histories at top of the frame

Fig. 4-15 Responses of the reinforced concrete frame (PGA=1.0g)

By comparing the failure of the specimens of UHS and SHS, it is found that the inaccuracy of the NS leads to the inaccuracy of the results of the whole hybrid simulation, which leads to different location and order of the occurrence of cracks, and different damage level. Fig. 4-16 and Fig. 4-17 respectively show the damage of on both tensile and compressive sides of specimens. From Fig. 4-13 (b) and Fig. 4-15 (b), it can be found that the stiffness of the RC frame obtained by the SHS is larger and the displacement is smaller than the UHS when the level of seismic load is low. While the stiffness is less estimated following with a twice larger deformation when the level of seismic load is high. This can also be seen from the damage of the specimens: i) PGA=0.4g, there are only two narrow cracks generated by the SHS, while one main a wider crack by the UHS; ii) PGA=1.0g, however, more severe damage occurs in the case of SHS than

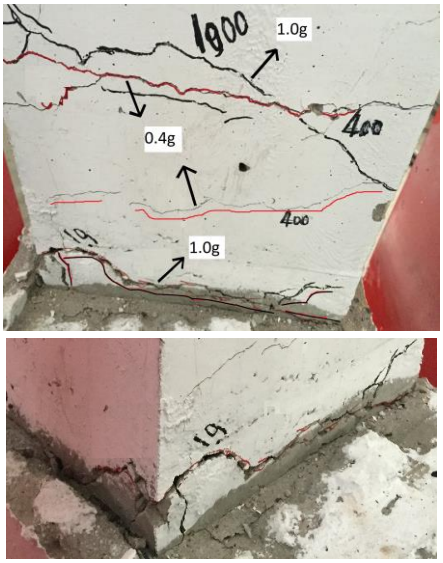

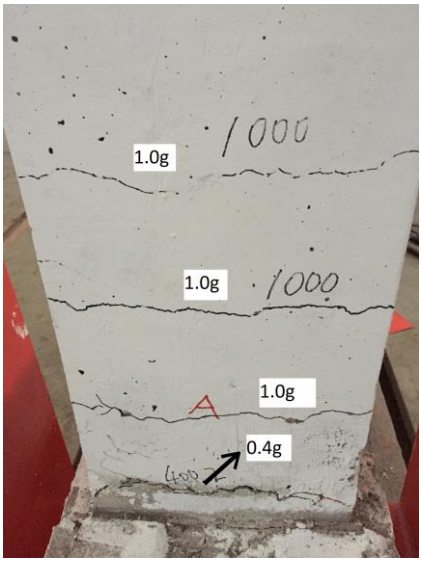

(a) SHS *(b) UHS*

Fig. 4-16 Damage of the specimen – View of tensile side

the UHS. Where the bond between concrete and rebars is lost in the tensile side of the column, and crushing appears in the compressive side; while the damage level in the case of the UHS is much lower. This indicates that the SHS over estimates the seismic performance of RC frame under the low-level seismic loads; while underestimate the seismic performance of structures under the high-level seismic loads, which leads to a wasted performance. In comparison, the UHS gives more accurate estimates.

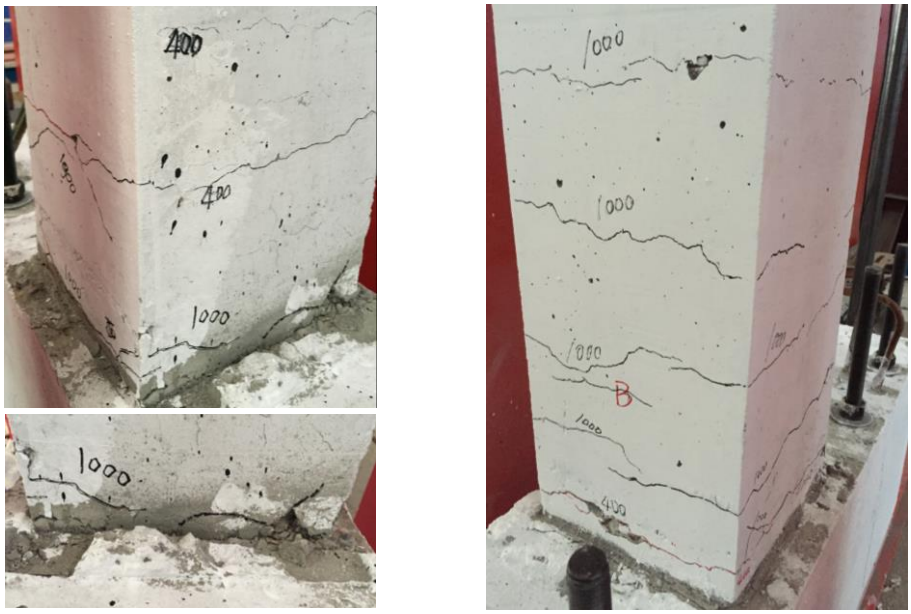

(a) SHS *(b) UHS*

Fig. 4-17 Damage of the specimen – View of compressive side

4.4 Summary

In this chapter, both the hybrid simulation with updating the concrete constitutive parameters and the OpenSees-embedded UKF method for parameter identification are experimentally validated. A monotonic static test of a RC column is carried out for verifying the identification method, and six cases of hybrid simulations are implemented on two specimens of a one-bay one-story RC frame to verify the model-updating hybrid simulation. Conclusions are as follows:

1. The OpenSees-embedded UKF for identifying the concrete constitutive parameters has high robustness and reliability, and the convergence rate of parameter is fast. It can be applied to model-updating hybrid simulation.
2. The accuracy of the hybrid simulation with updating the concrete constitutive parameters is greatly improved compared with the standard hybrid simulation. The novel method can be further extended to large and complex structures.
3. The location, the order of crack occurrence and the damage intensity of the specimen are different for the the SHS and the UHS. Under low-level seismic load, the SHS overestimated

the seismic performance of the RC frame. However, underestimate the seismic performance under the high-level seismic loads, which may cause the waste of structural capacity.

5. HYBRID SIMULATION WITH MODEL UPDAITN ON A REINFORCED CONCRETE RIGID FRAME BRIDGE WITH TALL PIERS

5.1 Introduction

In the 1960s, with the improvement of construction technology, T-type rigid-frame bridges was developed rapidly. Subsequently, the continuous rigid frame bridge with T-shaped rigid-frame was gradually developed and widely applied, because that this kind of bridge is good for smoothly driving and with no need of setting support, making system conversion. As reinforced concrete continuous rigid frame bridges adopt the form of pier girder consolidation, they have good integrity and seismic performance, and becomes one of the most popular alternative bridge types in long-span bridges.

Continuous rigid frame bridges are often endowed with flexible piers to reduce the displacement at the pier top caused by shrinkage and creep of concrete and temperature. Flexible pier is usually tall pier following the thin-walled hollow section. Because of its good ability to cross the valley, this type of bridge is widely used for the highway and railway bridges in the western mountainous areas of China. In this region, the earthquakes are frequent with high seismic intensity. As a result, the bridge structure in this area faces a more severe earthquake test. According to the survey results of seismic damage, the damage of irregular bridges such as curvilinear bridges, overpasses and high-piers bridges in mountainous areas are more serious, and some of the bridges are even directly collapsed under the strong earthquakes. At present, the research results show that shear resistance of the special structure with hollow thin-walled section were weakened to a great extent, and the failure mode of components changes from bending failure to bending-shear failure or even to shear failure directly. However, the research on the seismic behavior, failure mechanism and seismic design method of these irregular bridges is still not insufficient. At present in China, the seismic design of bridge with high pier is still based on the common bridge seismic design rules. Highway Bridge Seismic Design Rules (JTG / T B02-01-2008) of China clearly points out that the bridge with pier height more than 40 meters need to be devoted to the study.

The main work of this chapter is to study the continuous rigid frame bridge with hollow thin-walled high piers, the standard hybrid simulation (SHS) without model updating and the hybrid simulation with online updating (UHS) the parameters of concrete constitutive model (CCM) were carried out. The main purpose are as follows:

1) To further experimentally validate the OpenSees embedded identification method for identifying the parameters of CCM on a large-size component with stronger nonlinearity.

2) To analyze and reduce the negative influence of model error on parameter identification. The thin-walled hollow section members are greatly affected by the shear deformation. Using the uniaxial-concrete constitutive model to simulate the mechanical properties of such piers will result in larger initial model errors.

3) To investigate the feasibility, stability and reliability of the proposed hybrid simulation based on online updating the parameters of CCM on large and complex structures.

4) To analyze the failure mechanism, ultimate failure mode and seismic performance of the RC rigid frame bridge with thin-walled hollow piers based on the testing results.

5.2 Background of the Bridge

Niulanjiang Bridge is located in Yunnan-Guizhou Plateau where the terrain is steep with lots of mountainous and canyons. The Niulanjiang Bridge connects the two cities, Qujing and Zhaotong, in Yunnan Province and belongs to the section of Zhaodai Expressway K260 + 297 ~ K260 + 897. The bridge is 600m long and 12m wide with a design speed of 80 km / h. The bridge is about 70.1km from Huize County and about 22.5km from Ludian County. According to the Code for Seismic Design of Buildings of China, Qujing City is in the area of seismic fortification intensity of 7 degrees, while the seismic fortification intensity of Huize County is 8 degrees. According to the design specification, we can see that the 7-degree fortification of Niulanjiang Bridge is adopted. The design seismic acceleration is 0.1g and the characteristic period of response spectrum is 0.3s.

The main bridge is a three-span reinforced concrete continuous rigid frame bridge with a span of 90m + 170m + 90m. The approach bridge is partial prestressed concrete continuous beam bridge. The layout of the entire bridge is shown in Figure 5-1.

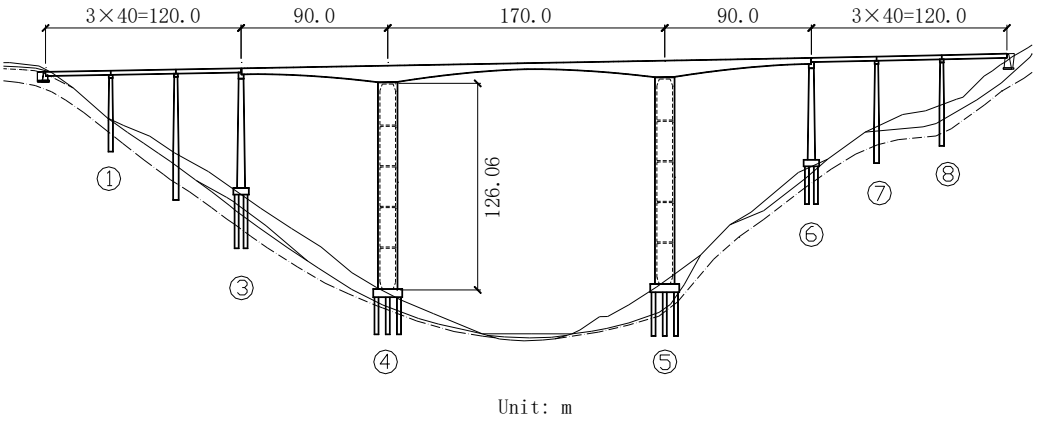

Fig. 5-1 Layout of the bridge

The super structure of the main bridge adopts a variable section box girder. The beam height at the root of the main pier is 10.0 meters and the beam height of the mid-span and end of the bridge span is 3.7 meters. The height of beam between the pier root and the mid-span used 1.75 parabolic curves. The two piers of the main bridge are exactly the same with a pier height of 126.06 meters and a thin-walled hollow rectangular cross section. The size of the cross-section along the longitudinal direction of bridge is a constant with a value of 12m, while that along the transvers direction is a variable from 6.7m at the pier top to 10.7m at the bottom of the pier. The thickness of the thin-wall is unchanged of 80m along the height of pier, which is shown in Figure

5-2. The concrete strength level of the pier is C50 concrete, while that of the beam is C40.

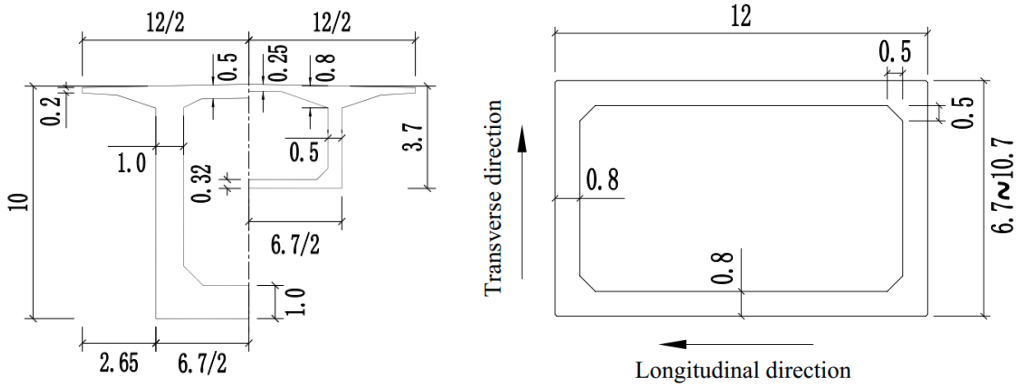

(a) Cross-section of the box girder *(b) Cross-section of the main piers*

Figure 5-2 Cross-section for the box girder and hollow pier of Niulanjiang bridge

5.3 OpenSees Finite Element Model of the Main Bridge

In order to ensure that the modelling of the numerical substructure (NS) in hybrid simulation is correct, a refined finite element model of the main bridge was established first, and verified by the field measured data of the bridge. After confirming that the refinement model of the main bridge was correct, the refined model was simplified and its correctness was verified according to the calculation results of the refined model. Then, the corresponding part of the simplified model was taken out as a NS to increase the computational efficiency of the NS. In this way, the time of hybrid simulation can be reduced as a result.

5.3.1 Refined model

As shown in Figure 5-1, the dimensions of the two main piers of Niulanjiang Bridge are exactly the same. Along the pier height, the pier was divided into five hollow sections by four diaphragms. The height of the first four hollow sections from the bottom to the top is 25 meters and the height of the hollow section connected to the box girder in the last section is 26.06 meters. The two-dimensional model of the main bridge is established in OpenSees. The two directions in the plane are the longitudinal direction and the vertical direction (the pier height direction). The out-plane is the transverse direction of the bridge. Each hollow section is modeled using three force-based elements. Box girders can be divided into four sections, each using eight force-based elements. The specific layout of nodes and elements is shown in Figure 5-3.

As mentioned in Section 5.2, the cross section of both the main pier and the box girder is variable, while the dimensions of the cross section of each element in OpenSees are fixed. In order to solve this problem, the continuous variable section of the main pier and box girder is approximated by the subsections. The principle is shown in Figure 5-4 (a). Taking the element

1-101 in Figure 5-3 as an example, the cross-section size of along the transverse direction of the prototype pier varies continuously along the pier height. In this paper, the cross-section size of element is approximated with the mean of the cross-section size at Node 1 and Node 101. Similarly, the cross-sectional dimensions of elements can be determined in turn. Fig. 5-4 (b) and (c) show the approximate elevation of the pier and the super structure.

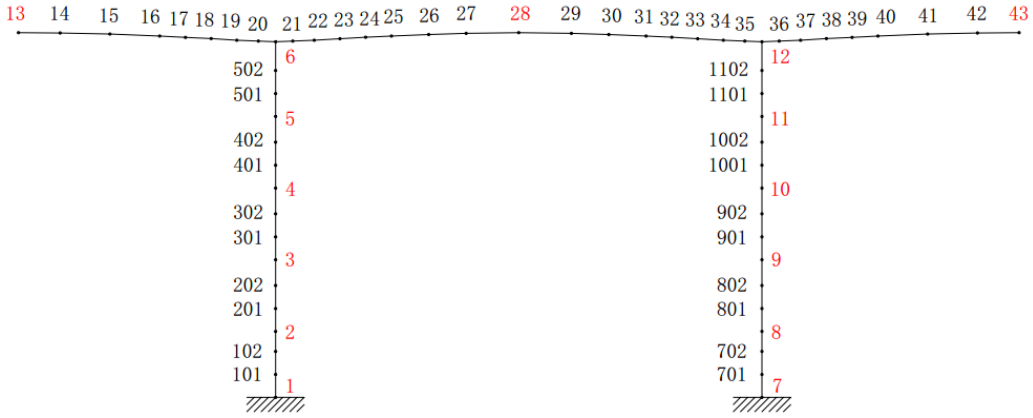

Fig. 5-3 Nodes and elements of the refined finite element model for Niulanjiang bridge

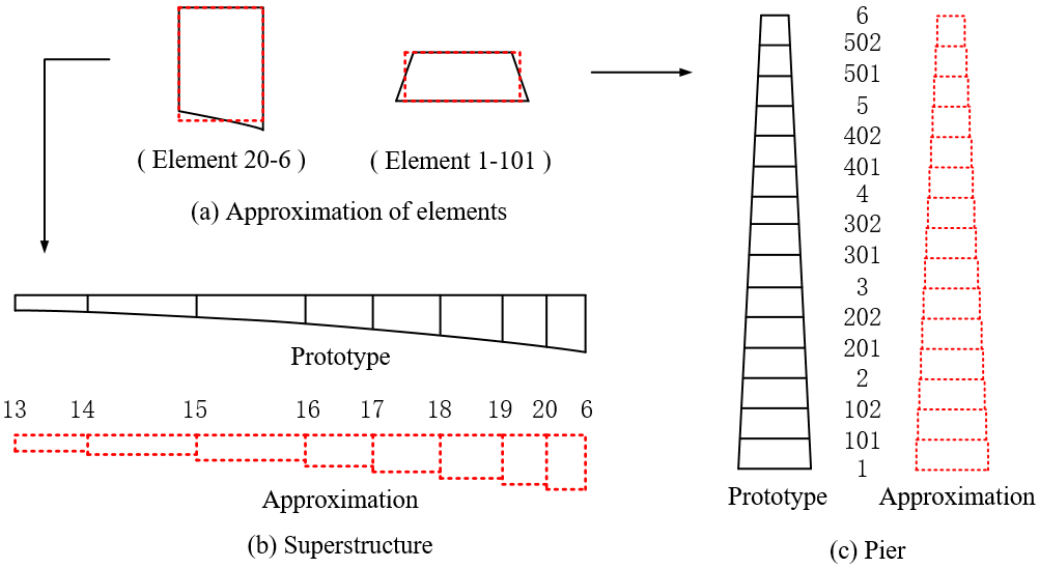

Fig. 5-4 Sketch map of the approximate model

In OpenSees FE model of the bridge, Concrete01 model and Steel02 model were selected to express the constitutive law of concrete and steel, respectively. The yield strength was set to be 340 MPa for the reinforced bars, and 240MPa for the hoops. The volumetric stirrup ratio was calculated as 0.21%. The elastic modulus is assumed to be 2 × 105MPa.

For concrete, the peak stress of cover concrete constitutive model (CCM) can be obtained by

converting the cubical compressive strength of concrete into prismatic compressive strength. The prismatic compressive stress used in China is closed to the cylinder compressive strength. As the strength of concrete used for the pier is C40, the standard value of concrete cubical compressive strength can be taken as,

$$f_{\mathrm{cu,k}} = 40\mathrm{MPa} \qquad (5\text{-}1)$$

According to the relationship of the standard value and the mean value of the cube compressive strength,

$$f_{\mathrm{cu,k}} = \mu^{s}_{\mathrm{f150}}\left(1-1.645\delta_{\mathrm{f150}}\right) \qquad (5\text{-}2)$$

The average compressive strength of concrete cubes can be obtained as $\mu^{s}_{\mathrm{f150}}=49.8\mathrm{MPa}$. δ_{f150} is the variation of concrete, 0.12 is for C40 concrete. Then according to equation (4-1), the mean value of prismatic compressive strength can be calculated,

$$\mu_{\mathrm{fc}} = 33.3\mathrm{MPa} \qquad (5\text{-}3)$$

Therefore, we can firstly determine the value of peak-strength parameter of cover CCM f_{cu} = 33.3MPa.

According to the method of determining the initial value of constitutive parameters in section 2.3.7, the other parameters of cover CCM can be determined as ε_{0u} = 0.002, ε_{uu} = 0.0038 and K = 0.85. Available from K, f_{uu} = 28.3MPa. Then, the parameters S_1 = 7.21, $S_2 = 3S_1$ = 21.6 and S_3 = 180 are determined according to the yield strength of the stirrup, f_{yh} = 240 MPa, and f_{cu}. Finally, based on the volumetric stirrup ratio, s = 0.21%, and the parameters of the core CCM can be determined as f_{cc} = 33.9MPa, ε_{0c} = 0.00209, f_{uc} = 28.7MPa, ε_{uc} = 0.00524. The detailed values of parameters CCM and steel model are listed in Table 5-1, where b is a factor related to the second stiffness of the reinforced bar.

Parameter	Concrete				Reinforced bar		
	f_c (MPa)	ε_0	f_u (MPa)	ε_u	f_{yh} (MPa)	E_s (MPa)	b
Cover	33.3	0.002	28.3	0.0038	340	2.0×10^5	0.01
Core	33.9	0.00209	28.7	0.00524			

Table5-1 Parameters for material constitutive models

As the main bridge pier were flexible with a height of 126.06m, the displacements at the pier top under the seismic loads may large. Therefore, in this paper, the geometrical nonlinearity of piers is considered by the co-rotation method provided by the OpenSees FE model.

Because of the FE model of the main bridge were two-dimensional model, the calculated natural frequency of the main bridge only included the longitudinal and vertical directions. The calculation results are shown in the third row of Table 5-2. The natural frequencies of the

Niulanjiang Bridge obtained from the environmental vibration method (field measurement) given in reference (Li Z., 2010) and (Li B., 2011) were used as a reference value, as shown in the second row of Table 5-2. It can be seen from the table that the calculated frequency given by the OpenSees FE model is close to the field measured data despite errors. So, we can believe the correctness of the OpenSees FE model of the main bridge.

Frequency （HZ）	1st order (Longitudinal direction)	1st order (Vertical direction)	2nd order (Vertical direction)	3rd order (Vertical direction)
Field data	0.50	1.18	1.90	2.38
Simulation	0.41	1.20	2.05	2.43

Table5-2 Frequency of Niulanjiang Bridge

5.3.2 Simplify the model

In order to reduce the time of hybrid simulation to improve the test efficiency, the element number of the refined FE model was reduced without greatly reducing the calculation precision. In this paper, the FE model whose element number was reduced is called a simplified model in this chapter. There are five elements of each pier and 7 elements of the super structure of the reduced FE model. Along the pier height, five integration points were set. The layout of the simplified model is shown in Fig. 5-5. Fig. 5-5 dotted line piers describes the changed dimension along the transverse direction. Considering that the section of pier bottom is the control section, in order to ensure that the seismic performance of the pier at the bottom of the finite element model is not weakened, the cross-section size of element 1-2 (element 7-8) was not the average width of Node 1 and Node 2, but the width at the bottom of pier. That is, the width of element 1-2 and element 1-7 is 10.7m.

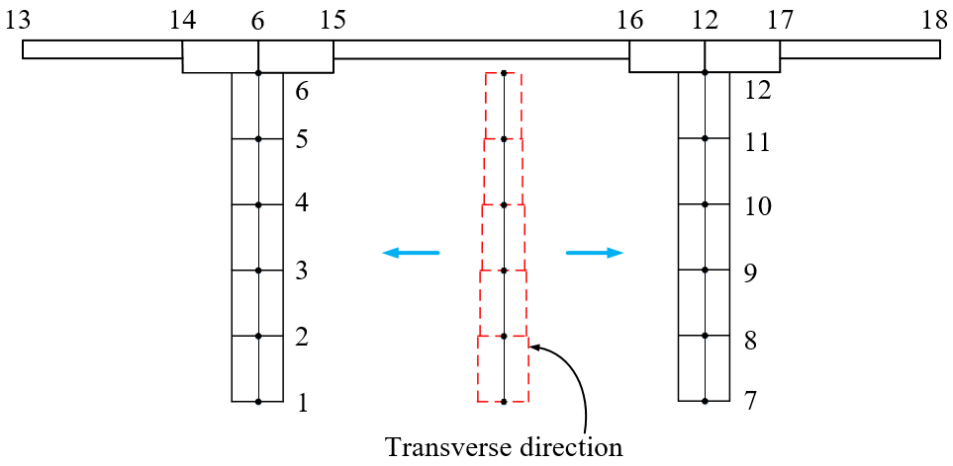

Fig. 5-5 Simplified model of the main bridge

The constitutive model for concrete and rebar used in the simplified model was the same as the refined model, and the parameter values were the same as well. Under the same seismic load (El-Centro NS, 1940), the dynamic analysis and the seismic response of the structure were carried out by using the refined model and the simplified model respectively. The displacement history of pier top of the two models under the earthquake with a peak accelerations of 0.22g and 0.62g are shown in Figure 5-6. It can be seen from the figure that under the two kinds of seismic intensity loads, the simplified model gives the displacement history was very close to that of the refined model. The analysis results show that the simplified model still has higher precision and can replace the refined model as the NS in the hybrid simulation.

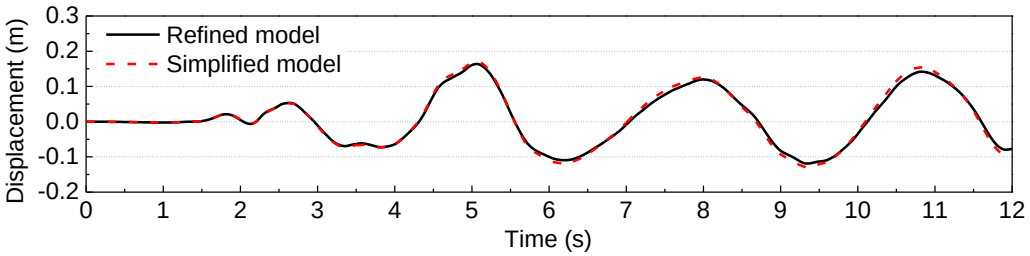

(a) PGA=220Gal

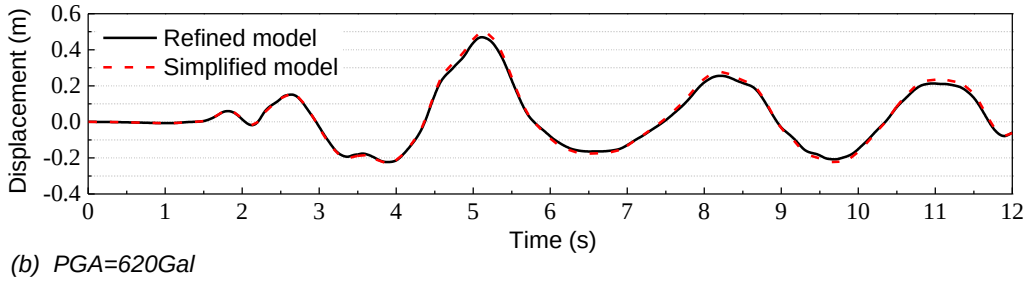

(b) PGA=620Gal

Fig.5-6 Time history of displacement for both the refined and simplified model-top of the pier

5.4 Test Layout

The hybrid test of the main bridge was carried out in the Harbin Institute of Technology Structure and Seismic Test Laboratory, and the PS was loaded with four-bar loading device. The four-bar loading device has mainly two support frames and one L-shaped load beam. The L-shaped load beam acts to connect the actuator with the test piece. In order to fix the pier specimen to the laboratory floor and connect with the L-shaped load beam at the same time, it is necessary to set concrete foundation and connecting beam respectively on the pier bottom and pier top. The height of the base and the beam were calculated to be 0.7 meters. According to the requirements of the loading device, the maximum height of the specimen (including the foundation and the beam) is 4.0 meters. Therefore, the maximum height of piers specimen itself is 2.6 meters. In order to compare with the results of other scholars, this paper chooses the same scaling ratio of

1:12 as the references (Sun Z., 2013; Jiang H., 2015; Li Z., 2010). At this scale ratio, the height of 2.6 m high pier corresponding to the original main pier was 31.2 m.

5.4.1 Test plan

The calculation model for the main bridge in the hybrid test is based on the simplified model in Section 5.3.2 but increases the length of the two piers (elements 1-2 and elements 7-8) along the pier height to 31.2 m and Experimental substructure fit, as shown in Figure 5-7. This calculation model has 18 nodes in total, with 17 units. The quality of the bridge superstructure and piers are all considered by the quality of the mass. The mass of each piers is concentrated at the top of the corresponding elements. The mass of the superstructure is divided into two parts which are respectively concentrated on the top nodes of the two piers. As shown in Figure 5-7, the computational model has 6 concentrated mass points, each of which takes into account 3 dynamic degrees of freedom, for a total of 18 dynamic degrees of freedom.

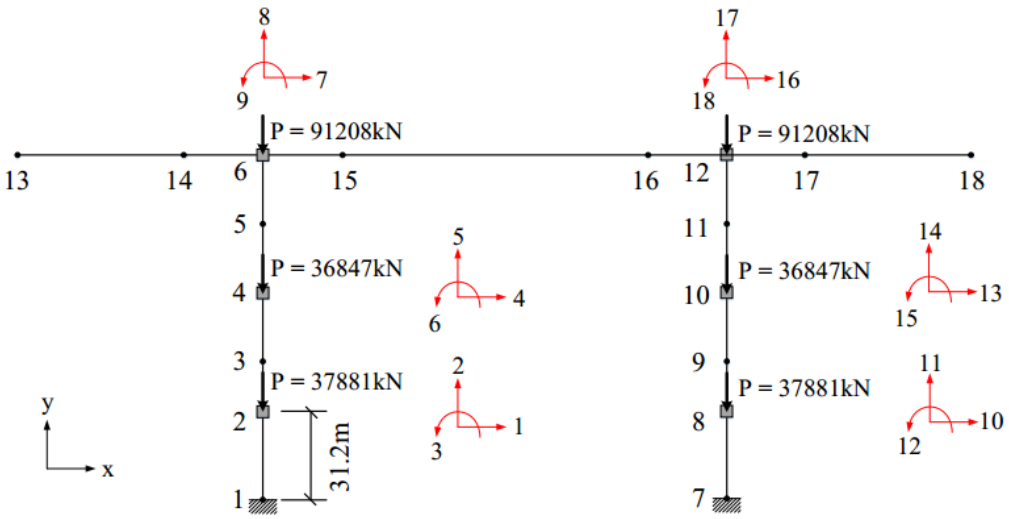

Fig. 5-7 Computing model of the main bridge

The weight of the superstructure and the piers are applied in the form of vertical external loads to the node where each mass point is, from the bottom to the top, 3788kN, 3684kN and 91208kN. Take the 1: 12 scale model of the lower left pier from the 31.2m section of the ground (the unit shown in Unit 1-2 in Figure 5-7) as the experimental sub-structure, the upper part of the left pier (part 2-6) and the right pier And the box girder using simplified model corresponding part of the full-size model as a numerical substructure of the hybrid test. According to the computational model, the equations of motion of the structure to be solved in the coordinator can be obtained as follows,

$$\begin{bmatrix} m_1 & & & & \\ & m_2 & & & \\ & & \ddots & & \\ & & & m_{17} & \\ & & & & m_{18} \end{bmatrix} \begin{bmatrix} \ddot{d}_1 \\ \ddot{d}_2 \\ \vdots \\ \ddot{d}_{17} \\ \ddot{d}_{18} \end{bmatrix} + \begin{bmatrix} c_1 & \cdots & c_{118} \\ \vdots & \ddots & \vdots \\ c_{18} & \cdots & c_{181} \end{bmatrix} \begin{bmatrix} \dot{d}_1 \\ \vdots \\ \dot{d}_{18} \end{bmatrix} + \begin{bmatrix} R_1 \\ \vdots \\ R_{18} \end{bmatrix} = \begin{bmatrix} m_1 a_g \\ G_1 \\ \vdots \\ G_3 \\ 0 \end{bmatrix} \quad (5\text{-}4)$$

For concise, its matrix is expressed as

$$\mathbf{M}\ddot{\mathbf{d}}(t) + \mathbf{C}\dot{\mathbf{d}}(t) + \mathbf{R}\left(\mathbf{d}(t)\right) = \mathbf{P}(t) \quad (5\text{-}5)$$

where **M** is mass matrix; m_i is the mass of the *i*-th degree of freedom; **d** is the displacement vector; d_i is the displacement of the *i*-th degree of freedom; **R** is the restoring force vector, which can be replaced by the product of structural stiffness **K** and displacement **d**, i.e. **R** = **K** · **d** (t), when the structure is linear; R_i is the restoring force of the *i*-th degree of freedom; **C** is damping matrix, and the classical Rayleigh damping is employed in this study, i.e. **C** = α **M** + β **K**; a_g is earthquake acceleration; *G* is gravity, where G_1 = 3788kN, G_2 = 3684kN, G_3 = 91208kN.

If we use **d**=0, $\dot{\mathbf{d}}$=0 and $\ddot{\mathbf{d}}$=0 as the initial values to solve Eq. (5-4), then *G* is considered a dynamic load and the structure will produce a vertical dynamic response under the action of *G*. However, in fact, gravity is a static load. The structural restoring force caused by gravity load in formula (5-4) should be counteracted by gravity. Therefore, the approach adopted in this paper is to obtain the displacement after gravity loading by the simplified structure-wide model and then use the displacement as the initial value to solve the dynamic equation. Mixed test concrete realization process:

1) Eighteen DOF dynamic differential equations as shown in Eq. (5-4) were established in the Hytest coordinator, and the vertical external loads and horizontal seismic loads were applied;
2) Set initial displacement in Hytest;
3) Before solving the equations of motion under horizontal seismic loads, the coordinator first sends the displacement initial values to the test substructure and numerical substructure, respectively;
4) Applying the displacement initial value to the corresponding degree of freedom of the numerical substructure to calculate the axial force;
5) The vertical actuator loads the experimental substructure step by step through displacement control until the received displacement command is obtained and the corresponding axial force is obtained.
6) return the obtained axial force of substructures to the coordinator to balance the vertical external load;
7) The coordinator solves the dynamic differential equations of the structure under the action of horizontal seismic loads and starts the hybrid load test of the structure.

In the hybrid simulation of high-pier reinforced concrete rigid frame bridge, the PS is a scaled model. Therefore, the similarity scale factors of the force and displacement exchanged between the PS and the coordinator needs to be derived from the Eq. (4-2) to (4-5) and show in Table 5-3. The NS is a full-scale model, so neither force nor displacement need to be converted. In Table

5-3, d_x and d_y denote the displacements of the piers of the original size in the x and y directions of the two nodes, respectively, and θ denotes the rotation angle. F_x and F_y denote the restoring forces of the top of the PS in the x and y directions, respectively, and M denotes bending moment; superscript c on behalf of the coordinator, p on behalf of the experimental substructure.

Target	Scaled factor	Generalized deformation			Generalized force		
		d_x	d_y	θ	F_x	F_y	M
Factor	1/12	1/12	1/12	1	$1/12^2$	$1/12^2$	$1/12^3$
Coordinator	-	d_x^c	d_y^c	θ^c	-	-	-
Received by the PS	-	$d_x^c/12$	$d_y^c/12$	θ^c	-	-	-
Measured force of PS	-	-	-	-	F_x^p	F_y^p	M^p
Received by Coordinator	-	-	-	-	$12^2F_x^p$	$12^2F_y^p$	12^3M^p

Table5-3 Ratio of similitude for physical substructure

5.4.2 Physical substructure (PS)

According to the loading equipment requirements in laboratory, both ends of the specimen need to be equipped with a base and a loading beam respectively to connect the specimen with the ground and the L-beam of loading device. The overall design of the specimen (the PS) after 1/12 scale of the prototype pier is shown in Fig. 5-8. As can be seen from the figure, the actual bridge piers 2600mm high, the first hollow section from the bottom up after the scale is complete, 2080mm high; the diaphragm thickness 70mm; the second hollow section due to the loading device is not high Complete, the height of 450mm. The basis of the specimen is the same as the loading beam, with dimensions of 2600mm, 1000mm and 700mm respectively. The specimen base is fixed to the ground by four ground anchors with a diameter of 100 mm. The load beam is connected to the four-bar L-beam by 12 high-strength bolts of 42 mm in diameter. Shown as the "along the bridge" for the direction of seismic load loading.

In the OpenSees model, the variable cross-section element is used to simulate the continuous variable cross-section piers of the original bridge. That is to say, the pier bottom pier 1-2 and the element 7-8 in Fig. 5-7 are equal cross-section elements. In this mixed experiment, the experimental substructure is used to replace the left pier unit 1-2. In order to make the experimental substructure and numerical substructure consistent and to simplify the machining process of the specimen, the substructure of the test was designed as an isosceles, that is, the lateral width of the specimen in Fig. 5-8 remained the same. The test substructure cross-sectional dimension is 1/12 of the scale according to the cross-sectional dimension of the numerical substructure unit 7-8. Fig. 5-2 (b) shows that the original cross-section chamfer size of the pier is 0.5m × 0.5m. According to 1:12 scale, scale model chamfer size smaller, only 4.2cm.

The wall thickness after the foot wall is only 7cm, smaller size. If the retaining chamfer will be difficult to sample processing, so the specimen further simplify the cross-section without chamfer hollow rectangular cross-section.

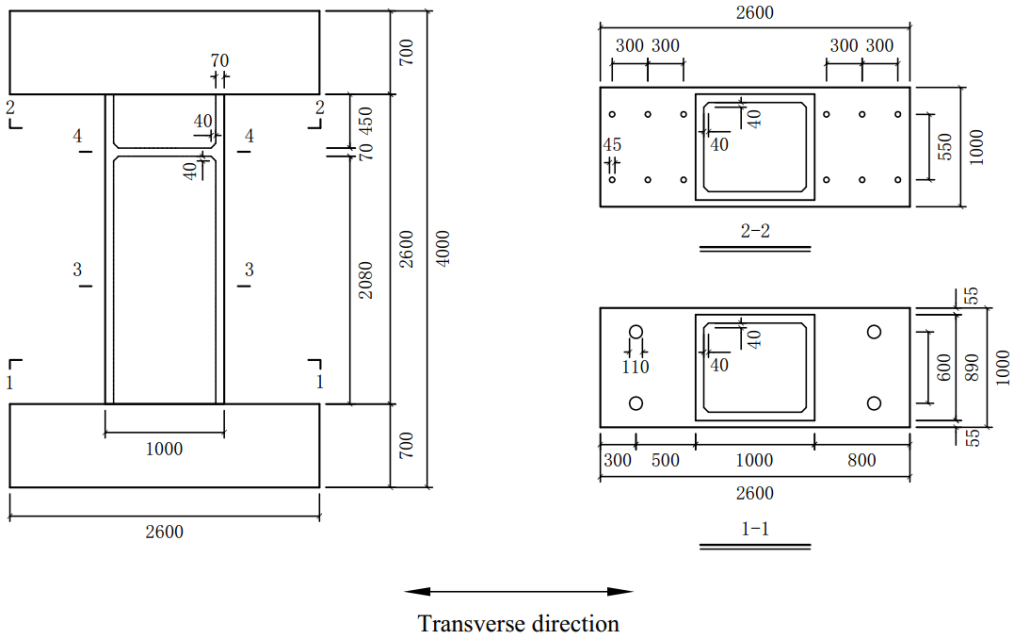

Fig. 5-8 Design of the specimen for physical substructure (Unit: mm)

In the prototype of the main pier, the reinforced bar is Grade II steel in the old code with a diameter of 28mm. According to 1/12 scale, the specimen longitudinal bar should be used Class II diameter 2.3mm steel. In order to ensure the consistency of the longitudinal rib strength grade, this paper replaces the HRB335 steel bar corresponding to the grade II steel in the new code. HRB335 grade steel bar minimum size of 6mm, cannot guarantee the bar size of the scale similarities. Therefore, under the condition of ensuring that the grade of rebar is similar to the prototype structure, this paper uses the same stirrup ratio to ensure that the scale size cannot meet the requirements. Because HRB335 grade 6mm rebar is round bar steel, it will result in insufficient adhesion with concrete. Therefore, HRB335 rebar with a diameter of 8mm is selected as the longitudinal reinforcement of the scale model. The standard cross section of the specimen after scaling and the cross section of the diaphragm are shown in Fig. 5-9. Fig. (a) is a standard cross-section of the specimen, corresponding to the 3-3 section in Fig. 5-8; Fig. (b) is a cross-sectional view of the diaphragm, corresponding to section 4-4 in Fig. 5-8.

In order to compare with the experimental results given in (Sun Z., 2013), we design the reinforcement ratio and volumetric ratio of test substructures to be the same as that of this reference, which is slightly higher than that of the bridge piers improve. Table 5-4 shows the comparison of the prototype pier structure, the numerical substructure and the experimental substructure in this paper and the design of the specimen in the reference (Sun Z., 2013), including the component size, reinforcement ratio and volumetric stirrup ratio.

After thin-walled hollow piles feet wall thickness of the specimen is thin, only 7cm, need to use a

smaller aggregate diameter and mobility of concrete pouring. The foundation and loading beams are made of standard concrete. Therefore, in the production process of the test piece, the foundation, the pier body and the loading beam need to be separately cast. In addition, due to the pier body contains the diaphragm, you need to pour two times. Therefore, after the steel banding is completed, the concrete pouring is divided into four stages: 1) pouring foundation; 2) pouring the lower pier of the diaphragm; 3) pouring the diaphragm and its upper pier; 4) pouring the loading beam. Concrete pouring time in the specimen for mid-December, Harbin outdoor temperature is not suitable for construction, so most of the commercial concrete has been discontinued. At that time, only two commercial concrete companies were still operating. They could provide C40 standard concrete for foundations and load beam sections, but neither provided concrete with smaller aggregate diameter and greater fluidity required for piers. Therefore, the paper is based on the use of commercial beams and loading of concrete, piers in the laboratory site mixing.

Before the concrete pouring, the concrete mixing tests were carried out according to the three mix design schemes respectively. Finally, according to the fluidity of concrete and the cube compressive strength of its standard test block, a compounding scheme is determined as shown in Table 5-5.

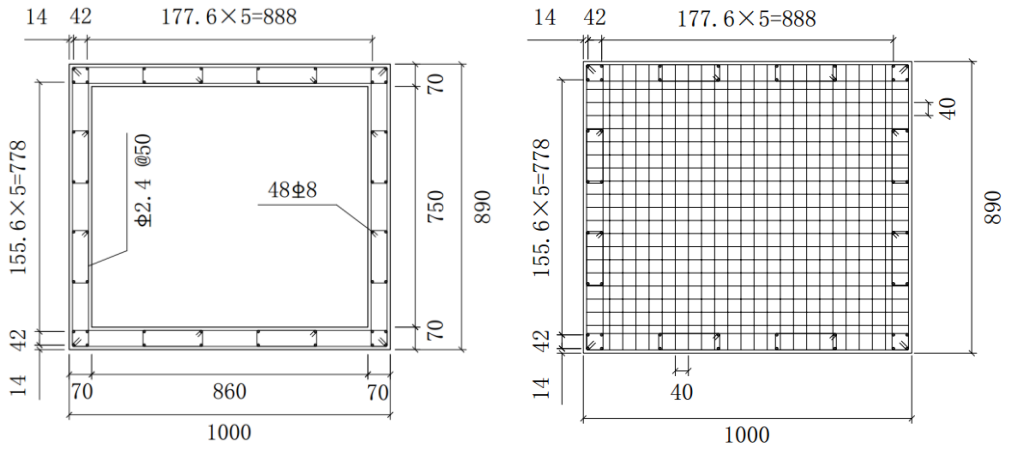

(a) Standard cross-section of the specimen *(b) Clapboard cross-section of the specimen*

Fig. 5-9 Cross sections of the specimen (Unit: mm)

Table5-5 Concrete mix of the pier specimen

Concrete mix	Cement	Water	Stone	Sand	water reducer
Mass（kg/m^3）	536.6	220	953.1	690.2	3.6
Proportion	1 : 0.41 : 1.78 : 1.29 : 0.0067				

During the construction of the test piece, the concrete is mixed and vibrated according to the specifications, and the concrete workability meets the requirements. In the pouring process of the test piece, there is no leakage of slurry and segregation phenomenon. After the formwork is

disassembled, the surface of the concrete is flat without any adverse phenomena such as honeycomb and pockmarks; the connection at the diaphragm is better.

The phased photograph of the specimen pouring process and the final cross-section photograph of the specimen and the specimen are shown in Fig. 5-10 and Fig. 5-11. Fig. 5-10 (a) is based on the diaphragm after the lower pier diaphragm demolition photos; Fig. 5-10 (b) part marked by the red rectangle is pier upper the diaphragm, where the template is not removed. Fig. 5-11(a) shows

(a) Base and the pier part below the clapboard

(b) Clapboard and the pier part above

Fig. 5-10 Foundation and the pier part under the diaphragm

(a) Complete specimen

(b) Standard cross-section

Fig. 5-11 The complete specimen of physical substructure and its standard cross-section

the whole picture after all the specimens have been demolished. The top of the specimen is the specimen loading beam required to connect with the four-link L-shaped loading beam. Fig. 5-11 (b) is the pier Standard thin-walled hollow rectangular cross-section, the figure is given below the diaphragm after pouring photos.

5.4.3 Loading and measurement programs

The PS is loaded with a steel-frame loading device, as shown in Fig. 5-12. Firstly, the PS is fixed on the ground of the laboratory by four anchors, and then the connecting beam of the specimen and the L-shaped load beam of the loading device were connected through 12 and anchor bolts. The loading device achieves the boundary conditions of the specimen through three actuators connected to the L-shaped loading beam. Actuator 1 (Horizontal Actuator): The left side is fixed on the reaction force wall, the right side is connected with the L beam, so as to realize the displacement of the horizontal displacement of the piers specimen. The actuator 2 and the actuator 3 (Two vertical actuators): the lower end of the steel frame is anchored to the ground of the test chamber to provide the supporting force for the vertical actuator; the upper end of the two vertical actuators is connected to the steel frame and the lower end is connected to the L-Beam connected to achieve vertical displacement of the freedom of the load (axial force); the same time, the two actuators to achieve the top of the specimen in the plane of the corner. During loading, the four links are not connected to the L-beam. Figure 5-13 shows the specimen loading during the test. Fig. (a) shows the loading view of the specimen, and Fig. (b) shows the elevational view on the right.

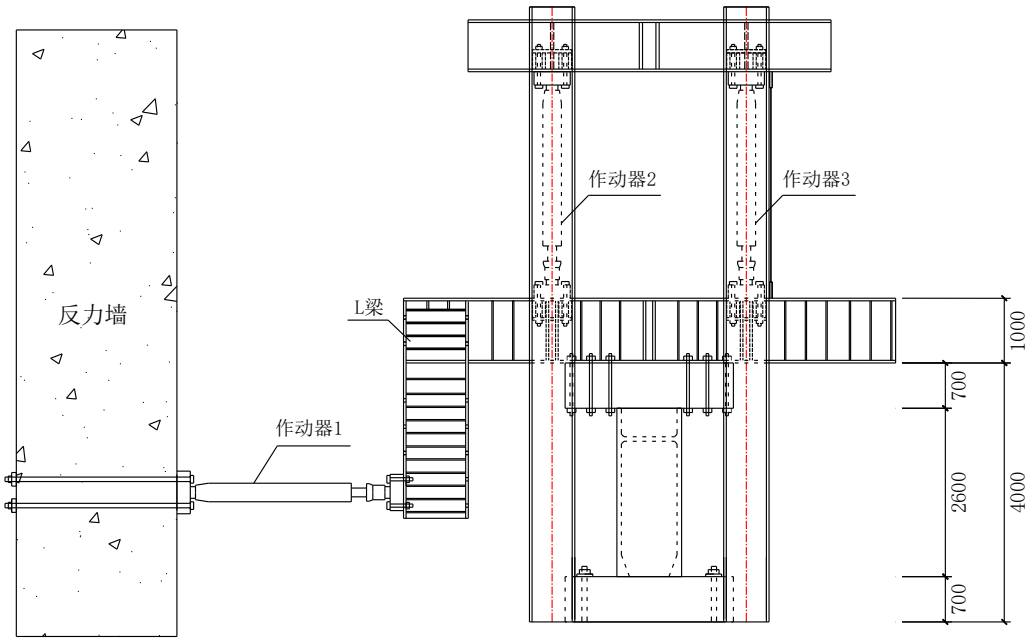

Fig. 5-12 Design for loading the pier specimen

In order to avoid the slippage between the specimen and the L-shaped loading beam during the loading process, two jacks are arranged on the two sides of the concrete loading beam at the top of the specimen to ensure the synchronization between the displacement of the specimen and the L-shaped loading beam. The specific layout of the jack shown in Figure 5-14.

The MTS test system was adopted for three actuators with a maximum output of 2000kN and a travel of 500cm. The controller is an MTS FlexTest60 controller and the control software is an MTS793-series software. Hytest Platform provides a module for data transfer with controllers, with the ability to transfer data directly with the controller. However, the displacement command calculated and issued by the Hytest coordinator is directly related to the degree of freedom. The horizontal and vertical degrees of freedom can be directly realized through the horizontal actuator and the vertical actuator. However, the realization of the degree of freedom of rotation requires Corner commands translate into displacement commands for both vertical actuators. In response to this problem, this article has written an interface program that can realize the shift command conversion function to link Hytest platform and MTS controller. Eq. (5-6) gives the displacement command conversion formula.

$$\begin{aligned} d_1 &= d_x \\ d_2 &= d_y + \theta \cdot l / 2 \\ d_3 &= d_y - \theta \cdot l / 2 \end{aligned} \qquad (5\text{-}6)$$

where d_x, d_y and θ represent the displacement commands of the three degrees of freedom sent by the coordinator to the MTS actuator control system; d_1, d_2 and d_3 respectively represent the displacement loading commands to be implemented by the three actuators; l represents two Vertical actuator distance between.

(a) Photo from the front view *(b) Photo from the side view*

Fig. 5-13 Photos for loading scheme of the pier specimen

Fig. 5-14 Layout of jack device at the top of the specimen

Through the pre-test load test analysis shows that the three actuators are used displacement outer ring control, loading time will greatly increase. The larger the displacement and the angle of rotation, the longer the outer loop control loads. In this paper, the outer ring displacement control is adopted for all three actuators when the local vibration is small. When the local vibration is large, the horizontal actuator still adopts the outer ring displacement control to ensure the accuracy of horizontal displacement loading. The two vertical actuators Open-loop displacement control is used to reduce load time. Load test analysis results show that the use of vertical actuator open-loop control load program can meet the requirements of test accuracy. Please refer to the reference (Wang Z., 2016) for the details and accuracy of the two loading methods.
Displacement meter layout shown in Fig.5-15. A horizontal displacement sensor (LVDT1) is arranged at the bottom of the specimen to observe whether there is a slip between the specimen

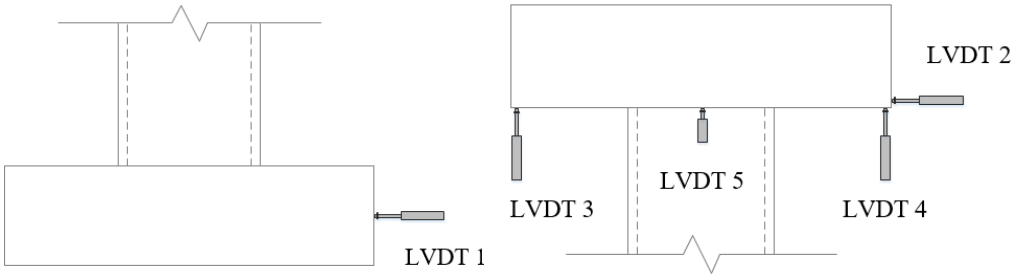

(a) Observation point at the foundation

(b) Observation points at the top of the specimen

Fig. 5-15 Arrangement of displacement meters

and the ground. A horizontal displacement sensor (LVDT2) is arranged in the loading beam at the top of the specimen for measuring horizontal displacement of the specimen. The combination of LVDT1 and LVDT2 is used for displacement outer-loop control. That is, the difference between the two displacement sensors is the actual displacement at the top of the specimen, and this displacement is used as the control target. A total of three vertical displacement sensors are

layout, where LVDT5 is arranged along of the centerline of specimen to observe the axial displacement which is the vertical displacement control target. LVDT3 and LVDT4 are used to control the rotation at the top of the specimen.

5.5 Model-updating hybrid simulation on tall-pier RC continuous rigid-frame bridge

In this section, the specimen shown in Section 5.4 is taken as the PS, and the simplified model presented in Section 5.3 is used as the NS for the hybrid simulation of the main bridge.

5.5.1 Test cases

There are two main cases of hybrid simulation of thin-walled high pier RC continuous rigid frame bridge, including: (I) standard hybrid simulation without parameter updating (SHS), and (II) hybrid simulation with updating the parameters of concrete constitutive model (CCM). For each case, hybrid simulations are implemented subjected to the earthquake with a PGA of 0.07g, 0.22g, 0.4g, 0.62g, 1.0g and 1.5g in turn. As there is only one specimen of the pier, the order of hybrid simulations carried out is SHS then UHS under 70gal seismic loads, SHS then UHS under 220gal, and so on. The specimen is finally destroyed in the case of 1.5g SHS, so the UHS of 1.5g case is not implemented. Table 5-6 shows the hybrid simulation numbers of the 11 cases that have been completed. The second number from 1 to 6 is for the PGA level. The third number, 1 refers to the SHS, whilst 2 the UHS. The seismic loads are as well the El-Centro (NS, 1940).

Cases	0.07g	0.22g	0.4g	0.62g	1.0g	1.5g
Standard Case (I)	C011	C021	C031	C041	C051	C061
Updating Case (II)	C012	C022	C032	C042	C052	--

Table5-6 Hybrid simulation cases of the main bridge

Same as the RC frame, the hybrid simulations of the bridge are carried out on the Hytest platform, and the flowchart is the same as shown in Fig. 4-8. Hytest solves the structural equations of motion. Matlab is responsible for the main program of parameter identification. OpenSees is for numerical modeling (including the NS and FE model of the PS). In the figure, the solid black line represents the SHS, the gray dotted line represents the identificaiton module, and the combination is that the UHS.

The CMs for the rebars and concrete in both the NS and the PS model are Steel02 model and Concrete01 model, respectively. And in Case I and Case II, values of the control parameters of the steel constitutive model (SCM) are the same and remain unchanged during the test, among which, the yield strength is obtained by the tensile tests. In case II, the initial values of the parameters for CCM are determined according to the approach provided in Section 2.3.7. And these initial values are used to the NS: i) for SHS, the values are used for the entire test without any change; ii) for UHS, they are only for the first-step calculation. The identified parameters are

then used for the computing of other steps.

5.5.2 Initial values of the concrete constitutive model

In order to determine the initial values of the parameters to be identified in case II (as well, the constant values of the parameters of material constitutive model in the NS in case I), the material tests of the reinforced bars, stirrups and concrete are carried out. Fig. 5-16 shows the tensile tests results of the reinforced bars and Fig. 5-17 shows the results of the stirrups. Refer to Table 5-7 for details about the steels and their properties. As a result, the yield strength of Steel 02 for rebars are 427 MPa in both the NS and the FE model of the PS.

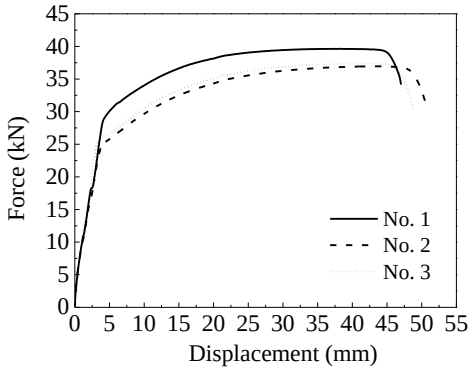

Fig. 5-16 Steel material experiment

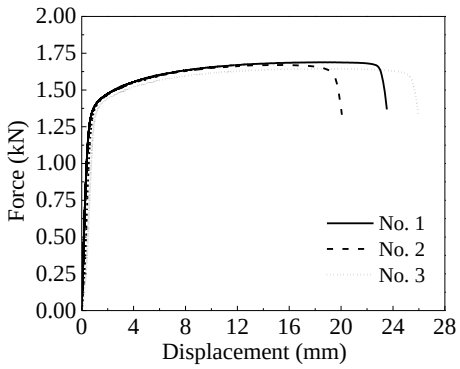

Fig. 5-17 Steel material experiment

The size of concrete specimens for the material test is 100mm × 100mm × 100mm, and the compressive strengths of the three concrete blocks at 28 days are shown in the second row of Table 5-8. The strengths then were converted into the compressive strength of 150mm × 150mm × 150mm block, as shown in the third row of Table 5-8. Unfortunately, the temperature for curing the specimen of the pier, i.e. the PS, is relatively low in the laboratory. Therefore, the actual compressive strength of the PS may be lower than the values obtained from the material tests. In order to provide a more accurate strength to reduce the error generated by the initial parameters, another compressive strength of concrete columns is measured by the rebound method. First, the average strength of the 150mm × 150mm × 150mm block is obtained, then the average value of the cylinder compressive strength.

Strength	Diameter (mm)	Mean of the maximum forces (N)	Mean of the yield strength (MPa)
Reinforced bar	8	37990	427
Stirrup	2.4	1668	313.4

Table5-7 Results of material tests of the rebars and stirrups

Length (mm)	1	2	3	4	5	6	7	8	9	Mean
100	53.0	59.3	54.2	55.0	54.2	56.2	56.6	54.6	58.9	55.8
150	50.4	56.3	51.5	52.2	51.5	53.4	53.7	51.9	56.0	53.0

Table 5-8 Compress strength of the concrete blocks

Three testing zones are divided of each side of the pier specimen for rebound method, and 16 testing points of each zone are selected. The measured strength by resiliometer of 192 testing points in total are shown in Table 5-9. Deleting the maximum and minimum values in each zone, the average value in each zone obtained is shown in Table 5-10. According to Table 5-10, the average value of all testing points can be calculated which is 40.8MPa and the standard deviation is 0.99MPa. According to the Eq. (7.0.3-3) of JGJ / T 23-2011, which is presented here by Eq. (5-7)

$$f_{\mathrm{cu,k}} = m_{f_{\mathrm{cu}}} - 1.645 S_{f_{\mathrm{cu}}} \qquad (5\text{-}7)$$

where, $m_{f\mathrm{cu}}$ is the mean of the measured values and $S_{f\mathrm{cu}}$ is their standard deviation. Then, the standard value of the compressive strength of the 150mm × 150mm × 150mm block coulde be calculated as 39.2MPa.

Zone	1	3	5	7	9	11	13	15
Points	2	4	6	8	10	12	14	16
Zone 1	~~42.8~~	39.0	39.3	42.7	40.8	41.7	39.2	40.0
	40.8	40.1	39.3	40.6	38.9	40.0	39.3	~~38.9~~
Zone 2	40.8	~~35.9~~	39.0	39.3	37.2	42.1	~~44.4~~	42.3
	40.8	41.0	38.3	41.1	41.0	39.3	38.3	37.4
Zone 3	44.2	42.3	40.6	41.0	39.5	40.0	~~44.3~~	41.0
	42.8	42.6	38.3	41.5	~~37.4~~	42.1	39.8	39.3
Zone 4	41.0	39.5	41.4	38.6	37.7	36.9	36.8	~~36.6~~
	39.9	40.0	41.0	42.3	39.8	41.6	40.6	~~43.4~~
Zone 5	~~42.7~~	38.8	39.2	41.0	38.4	37.8	38.1	38.5
	40.7	39.5	~~37.5~~	41.1	41.7	41.8	40.3	39.5
Zone 6	42.7	42.3	41.7	41.3	39.5	41.5	37.3	37.9
	40.1	~~43.7~~	42.6	~~37.7~~	40.5	38.4	39.4	39.6

Table 5-9 Concrete strength of each testing points by a resiliometer

Zone	1	3	5	7	9	11	13	15
Points	2	4	6	8	10	12	14	16
Zone 7	41.8	~~39.3~~	42.3	41.3	43.6	41.8	41.8	42.2
	41.5	39.4	43.8	~~45.4~~	41.7	43.3	43.8	41.4
Zone 8	43.7	42.4	41.0	40.5	40.1	41.4	~~44.7~~	44.3
	42.7	38.8	42.7	40.9	42.3	39.2	~~38.1~~	40.8
Zone 9	42.3	40.0	38.3	39.1	38.9	~~37.4~~	39.5	38.9
	39.1	42.5	40.6	39.3	41.0	39.2	37.6	~~42.7~~
Zone 10	44.3	44.1	~~40.1~~	42.6	44.5	40.5	40.4	44.1
	42.4	41.1	44.0	44.3	46.0	42.3	~~45.7~~	40.3
Zone 11	38.9	42.3	40.0	~~37.6~~	40.0	38.6	38.9	38.1
	~~45.7~~	40.9	40.8	40.9	40.8	42.7	39.2	40.6
Zone 12	41.0	~~38.4~~	39.2	42.3	42.7	39.5	40.8	44.0
	40.9	~~45.2~~	42.5	38.9	40.8	39.8	42.7	42.5

Continuous Table 5-9 Concrete strength of each testing points by a resiliometer

Zone	Mean	Zone	Mean	Zone	Mean	Zone	Mean
1	40.21	2	39.89	3	41.04	4	39.82
5	39.79	6	40.39	7	42.15	8	41.48
9	39.78	10	42.92	11	40.38	12	41.33

Table 5-10 Average value of concrete compressive strength of each testing zone

Then, according to Eq. (4-1), the mean of cylinder compressive strength can be obtained as 27.3MPa. Where, α = 0.76. Different types of compressive strengths of pier specimen is shown in Table 5-11. According to Table 5-7 and Table 5-11, it can be confirmed that the yield strength of stirrup is f_{yh} = 313.4MPa and the average value of the cylinder compressive strength is μ^{s}_{fc} = 27.3MPa.

After obtaining the cylinder compressive strength of concrete, f_{cu}, and the yield strength of stirrups, f_{yh}, the initial values of concrete constitutive parameters can be finally determined according to the approach given in Section 2.3, as shown in Table 5-12. As mentioned above, where f_{cu}, ε_{0u} and K are the three parameters to be identified, whilst the other parameters are remain to be unchanged. For brevity, the values of parameters shown in Table 5-12 are called the theoretical values in the following contents.

	Mean value of cubic compressive strength (μ^s_{f150})	Standard deviation (δ)	Standard value of cubic compressive strength ($f_{cu,k}$)	Mean value of cylinder compressive strength (μ^s_{fc})
Values (MPa)	40.8	0.99	39.2	27.3

Table5-11 Compress strength of the concrete from rebound method

Parameter	f_{cu} (MPa)	ε_{0u}	K_c	ε_{uu}	S_1	S_2	S_3
Initial values (Theoretical values)	27.3	0.002	0.8	0.0035	11.5	34.5	268.6
Status	Identified	Identified	Identified	Initial	Initial	Initial	Initial

Table 5-12 Initial values of concrete constitutive parameters

The special thin-walled hollow section weakened the shear capacity of components, making them become strong bending weak shear members. For flexural RC structures, beam-column elements with fiber section can simulate their seismic behavior and provide more reasonable analysis results. However, some studies have shown that fiber elements cannot give results with sufficient accuracy (Si et al., 2013). Considering that the large error caused by the FE model itself (hereinafter referred to as model error) may adversely affect the identification results, a SHS under 0.07g earthquake loads, the case C011 in Table 5-5, is carried out firstly. Then the parameters are offline identified after all the experimental data are collected. The identification results are shown in Fig. 5-18.

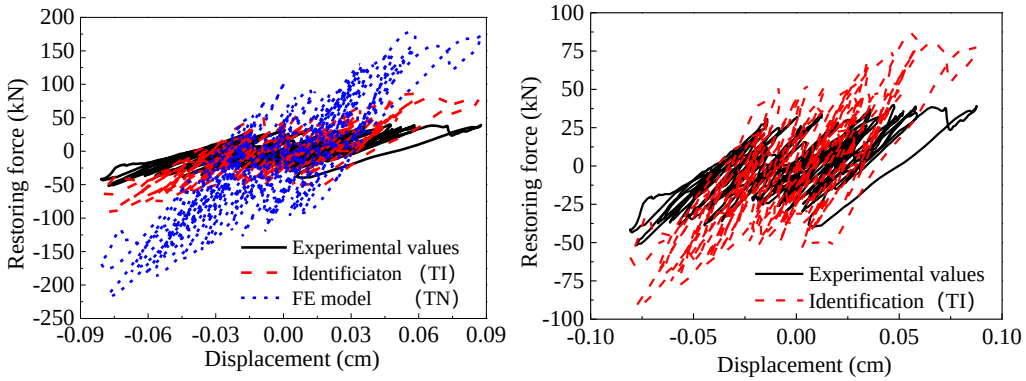

(a) Comparison of displacement-force curves between identification, finite element analysis and the experimental data

(b) Comparison between identification results and the experimental data – enlarged drawing

Fig. 5-18 Offline identification based on the experimental data of the PS in case C011 (Theoretical initial values of parameters)

In the legend ‘TI’ refers to the results that identified using the theoretical initial values given in Table 5-12. That is the results provided by the FE model using the identified parameters whose initial values are those theoretical ones. ‘TN’ presents the results that the FE model simulated using the theoretical initial values without any change in the entire process. As can be seen from Fig. 5-18 (a), the numerical simulation with the identified parameters is significant improved.

Fig. 5-18 (b) gives only the comparison of the force-displacement curve between identification results and the experimental data. From this enlarged drawing, it can be found that the two curves are not well matched. The errors of the identified stiffness and the maximum strength of the specimen between the two are still large. This is mainly caused by model errors generated from the fiber-sectional element which cannot enough take into account the shear effect, and is more suitable for the RC flexure-dominating members. However, the tall piers with thin-walled hollow section belong to the bending-shear scope, whose shear effects cannot be neglected.

To reducing model errors, seeking more accurate numerical models is the fundamental approach. However, this beyond the scope of this study. In this study, the adverse effect results from model errors is reduced by adjusting the initial values of parameters. From Fig. 5-18 (b), it can be seen that the stiffness and strength of the specimen are both larger than the measured ones. To reduce the stiffness and forces, a direct method is to reduce the value of peak strength in the concrete constitutive model. Fig. 5-19 shows the identification results after tuning the initial value of the most sensitive parameter f_{cu} with a value decreased from 27.3MPa to 12.7MPa. In this study, the tuned parameters are called the empirical values. So, in the legend, ‘EI’ refers to the identification results with the empirical initial values, i.e. f_{cu} = 12.7MPa. ‘TI’ still refers to the results that identified using the theoretical initial values. From Figure 5-19 (a), it can be seen that

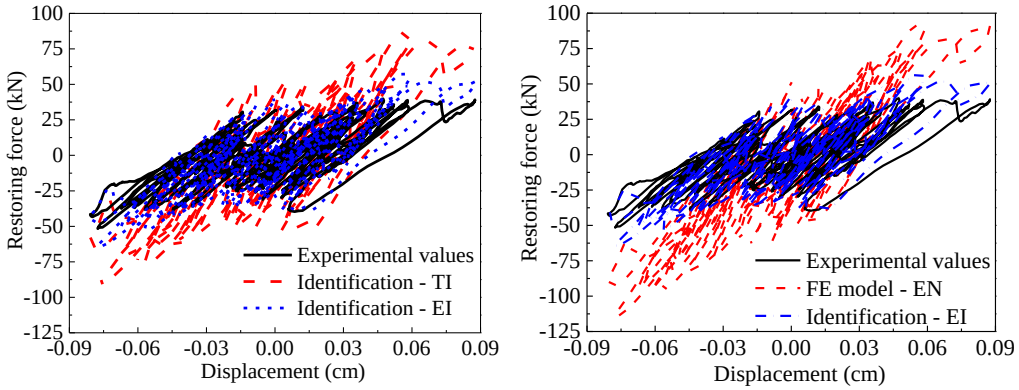

(a) Comparison of identification results using theoretical and empirical initial values of parameters

(b) Comparison of displacement-force curves between identification, finite element analysis and the experimental data

Fig. 5-19 Offline identification of the experimental data of the physical substructure in case C01 (Empirical initial values of parameters)

adjusting the initial value of f_{cu} can make up for the negative impact brought by model errors, making the results be significantly improved. Comparing the 'EN' curve with the 'TN' curve in Fig. 5-18(a), decreasing the initial value of parameter f_{cu} does indeed enhance the numerical analysis. However, comparing the 'EN' to the 'EI', it is found that the identification makes the numerical simulation more accurate.

In order to make the results more concise and understandable, a detailed explanation on the legends in Fig. 5-18 and Fig. 5-19 is presented here. Firstly, all the initial values of all parameters are determined based the method given in Section 2.3.7.

'T' means the theoretical initial values, among them, the values of the f_{cu} and the f_{yh} which is used for determine the values of the other six parameters except the f_{cu} are obtained from the material tests. 'E' refers to the empirical initial values, among them, the initial value of f_{cu} is decreased from 27.3MPa to 12.7MPa. 'N' and 'I' represent the two study cases: 'N' says the pure numerical simulation of the FE model without parameter identification; 'I' says the results provided by the FE model with the identified parameters. 'TN' and 'EN' denote the numerical results of the FE model using the T-values and E-values, respectively, without identification; 'TI' and 'EI' denote the numerical results of the FE model with the identified parameters using theoretical values (T-values) and empirical values (E-values) as the initial values for identification, respectively.

The following conclusions can be drawn from Figs. 5-18 and 5-19:

1. Comparing 'TI' with 'TN', and 'EI' with 'EN', we can see that the proposed identification method can improve the accuracy of the FE model regardless of whether the theoretical values or the empirical values of parameters are employed as the initial values;
2. Comparing 'EN' and 'TN', we can see that only by tuning the value of f_{cu} can compensate the errors generated by model errors and improve the accuracy of numerical simulation in some extent but still with a larger error.
3. Comparing 'TI' with 'EI', we can see that employing the E-values for identification can larger improve the accuracy than using the T-values. Decreasing the initial value of f_{cu} is an effective way to solve the problem existing large model errors.

Therefore, the parameter identification and model updating in all the following study cases are based on the empirical initial values.

5.5.3 Parameter Identification Results

In this chapter, all the cases on the thin-walled hollow section pier, including both the standard hybrid simulation (SHS) and the model-updating hybrid simulation (UHS), are implemented on the same specimen. The testing sequence is as follows: the SHS first then the USH under each PGA level with the PGA level from low to high.

Figs 5-20 to 5-24 show results of parameter identification and the comparison of the force-displacement relationships under the earthquake loads with PGA of 0.07g, 0.22g, 0.4g, 0.62g and 1.0g. Results at each PGA level include parameter identification results, comparison of force-displacement curves between the FE model with and without parameter identification, and the comparison of force-displacement curves between the SHS and UHS. In the legends, the 'Identification' refers to the results provided by the FE model using the identified parameters, the 'Initial values' says the results computed by the FE model using only the initial values without any change in the whole analysis process. The force-displacement relationship in the

comparison of SHS and UHS are the results at the boundary of the NS and the PS. As the comparison between the force-displacement curves provided by the FE model using the initial and identified parameters has been illustrated in Fig.5-19(b), it is not shown again in Fig. 5-20. As the same as that in the case of RC frame above presented, the parameter *K* related to the descending section of the constitutive equation stays unchanged under the earthquake loads with PGA of 0.07g, 0.22g, 0.4g, because that the *K* does not contribute to the restoring force. Hence the identification results of *K* are not presented in Figs. 5-20 to 5-22. It is worthy noted that the loading time of the UHS case with PGA equals to 0.4g is shorter than the other cases, because that the breakdown of the cooling system for actuators. However, the loading of the first peak of the acceleration of the ground motion is completed.

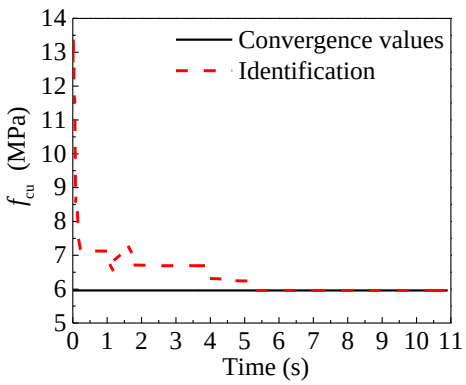

(a) Parameter f_{cu}

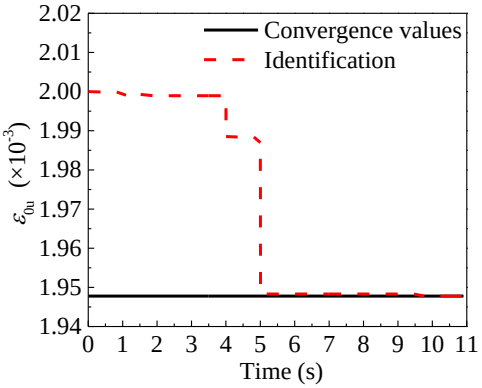

(b) Parameter ε_{0u}

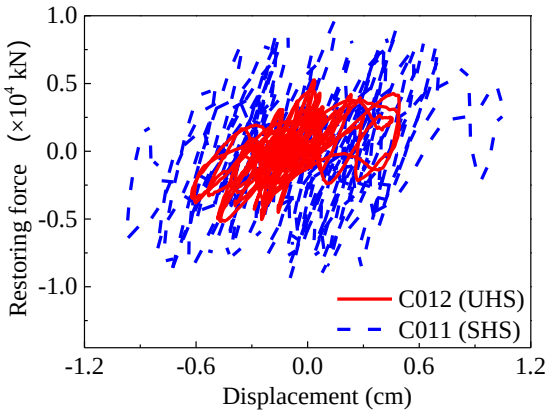

(c) Comparison of displacement-force relationship between SHS and UHS

Fig. 5-20 Identification results (PGA=0.07g)

The comparison of force-displacement relationship at the top of the specimen presented in Fig. 5-19(b), Fig. 5-21(c), Fig. 5-22(c), Fig. 5-23(d) and Fig. 5-24(d) show that the simulated results provided by FE model of the PS using the online identified parameters are in better agreement with the experimental results than those using the unchanged initial parameters. The accuracy of the PS model updated with the identified parameters is significantly improved. It can be seen

from the figures that at each PGA-level, the identification method can give a quite good estimation of the restoring forces. Compared with the cases of lower intensity, i.e. 0.07g and 0.22g, seismic loads, where the nonlinearity is weak, the identification method gives better estimation of the restoring forces in the cases with high-level seismic loads where the nonlinearity is stronger. This indicates that the hybrid simulation based on the updating of the parameters of concrete constitutive model (CCM) performs better in estimating the behavior with strong nonlinearity, and can be can be applied to evaluate the RC structures containing a large number of members that may undergo strong nonlinearity.

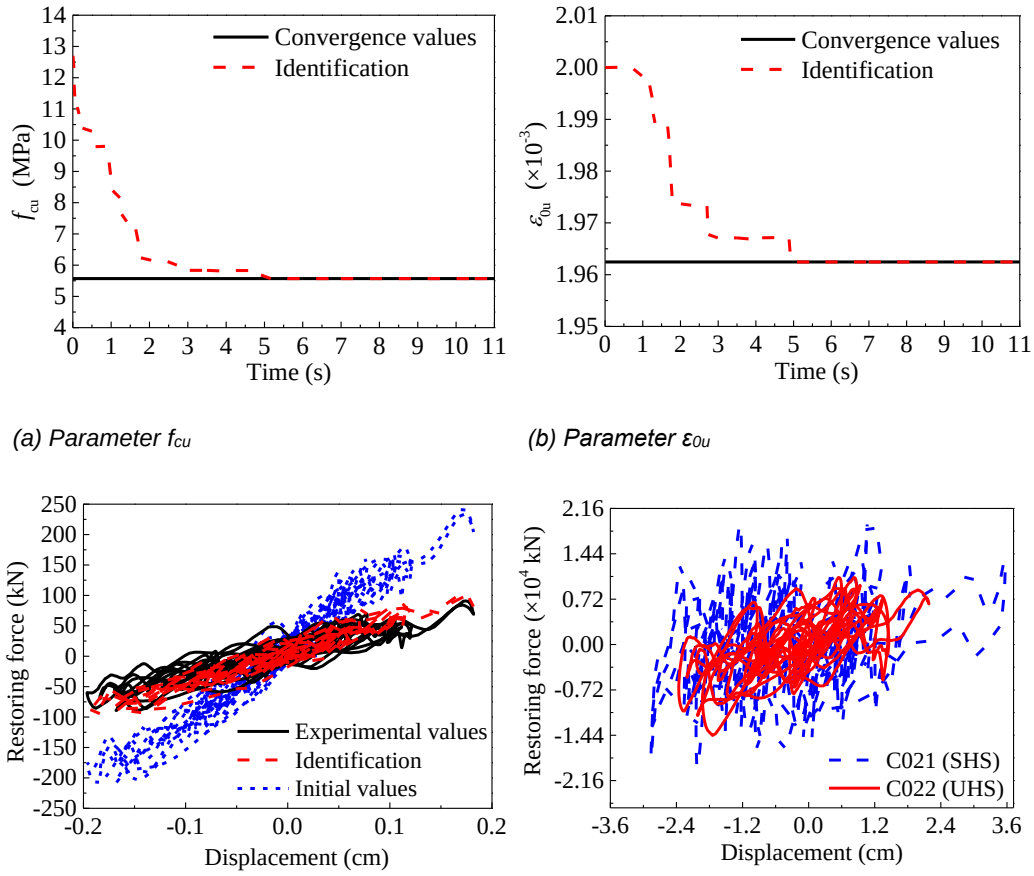

(a) Parameter f_{cu}

(b) Parameter ε_{0u}

(c) Displacement-force comparison of identification, FE analysis and experimental data

(d) Comparison of displacement-force relationship between SHS and UHS

Fig. 5-21 Identification results (PGA=0.22g)

From the figures shown the comparison of displacement-force relationship of the pier at the interface of the PS and the NS between the SHS and UHS, it is seen that there are large differences between the two. As the reliability of the proposed UHS are proved as above illustrated, we can conclude that the hybrid simulation with updating the parameters of the CCM is, to a large extent, provides a more accurate estimated results of the seismic behavior of the

bridge.

From the results of parameter identification of each PGA level, it is found that all the three parameters can converge to a steady value quickly and stably. Although the parameter *K* fluctuates during convergence when the earthquake load increases, the fluctuation is not large and the *K* can converge after the fluctuations. As the same with the cases of the RC frames in Chapter 4, for each parameter, the final convergence values in all the PGA levels are close to each other with a small deviation, as shown in Table 5-13

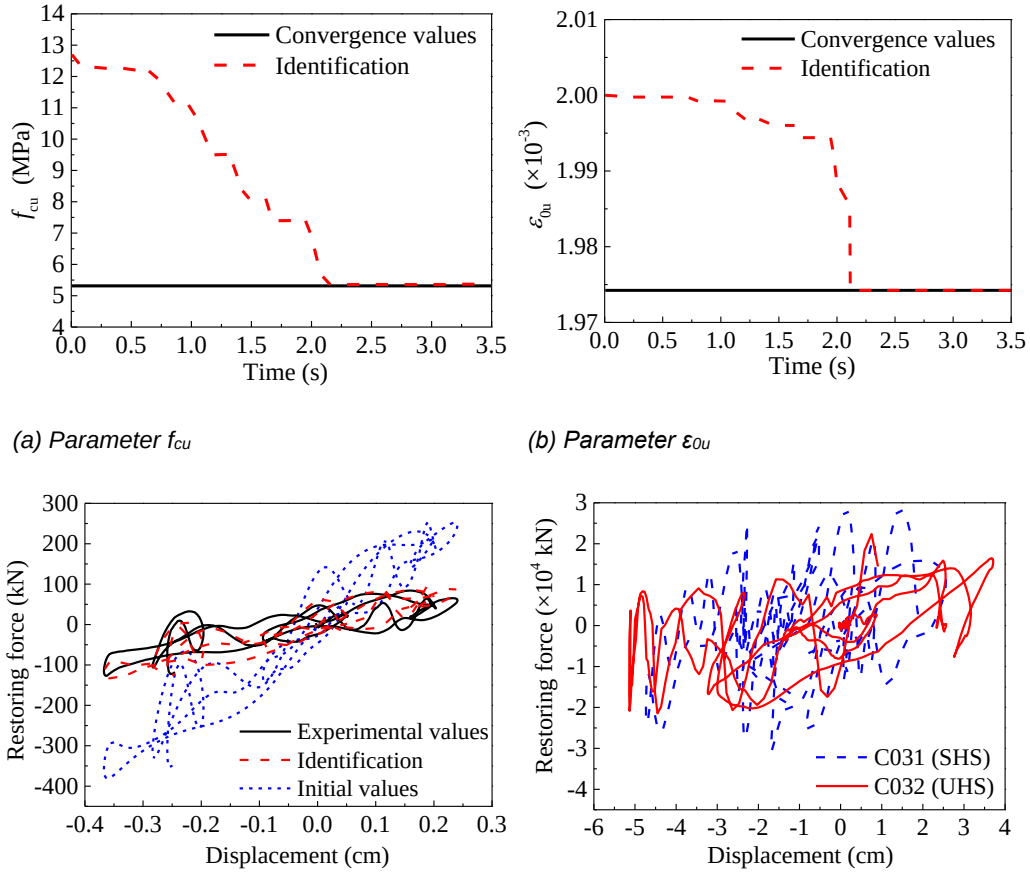

(a) Parameter f_{cu}

(b) Parameter ε_{0u}

(c)Displacement-force comparison of identification, FE analysis and experimental data

(d) Comparison of displacement-force relationship between SHS and UHS

Fig. 5-22 Identification results (PGA=0.4g)

The identification results can be mainly divided into two categories: i) lower PGA level, i.e. 0.07g, 0.22g and 0.4g, where the loads do not force the concrete enters into the deceasing branch of the constitutive law. In the three cases belonging to this category, the identified values are closed for each parameter; ii) higher PGA level, i.e. 0.62g and 1.0g, where the concrete is forced to undergo the decreasing branch and cracks and crushing appeared. The identified values are closed to each other of the two cases belonging to the second category. The statistical

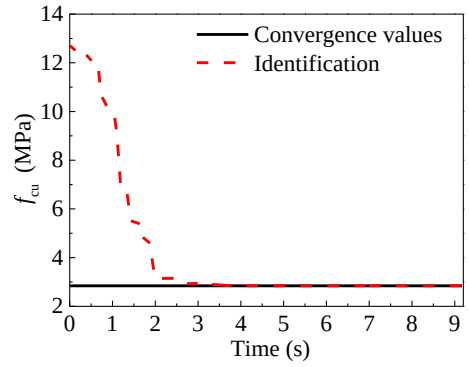

(a) Parameter f_{cu}

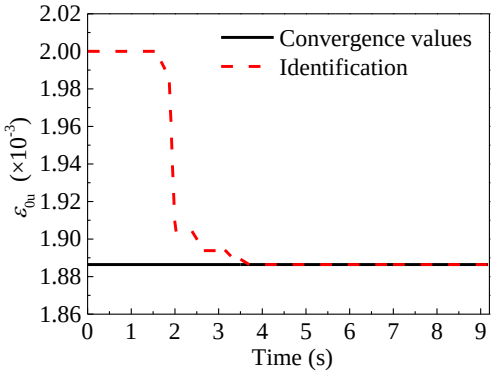

(b) Parameter ε_{0u}

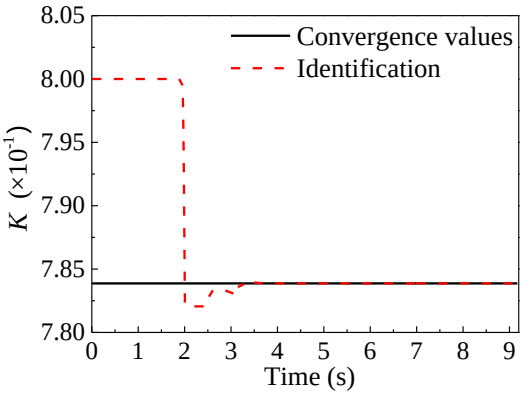

(c) Parameter K

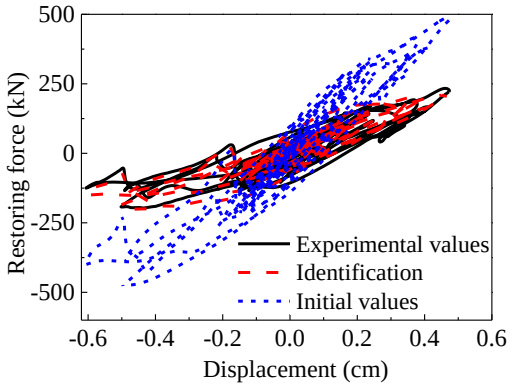

(c) Displacement-force comparison of identification, FE analysis and experimental data

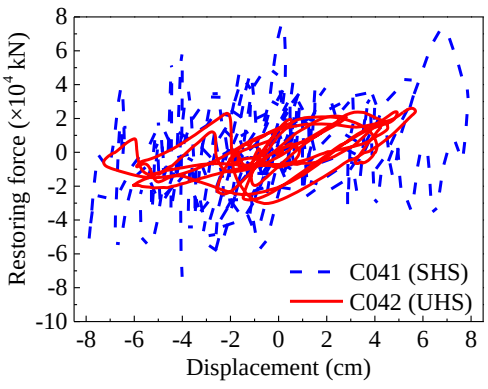

(d) Comparison of displacement-force relationship between SHS and UHS

Fig. 5-23 Identification results (PGA=0.62g)

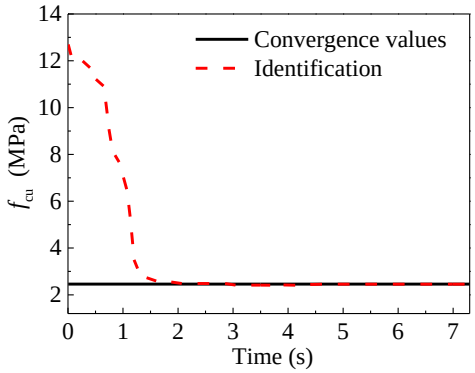

(a) Parameter f_{cu}

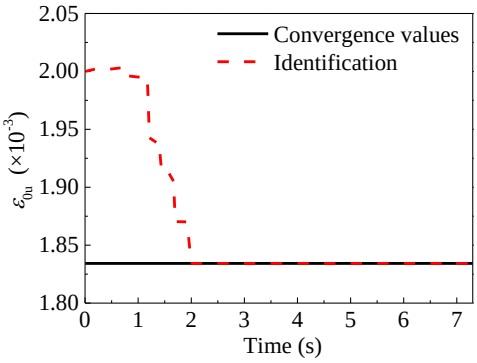

(b) Parameter ε_{0u}

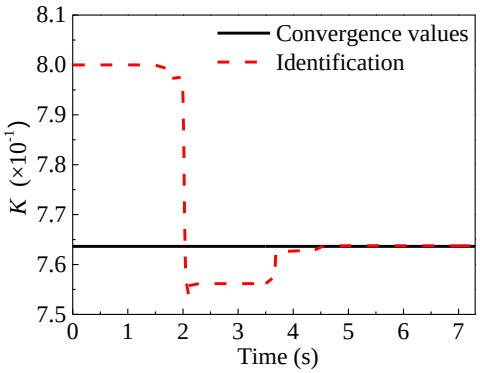

(c) Parameter K

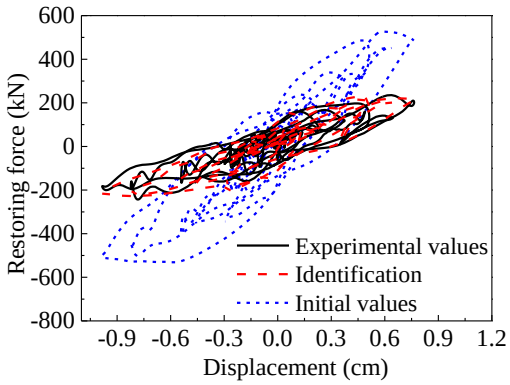

(c) Displacement-force comparison of identification, FE analysis and experimental data

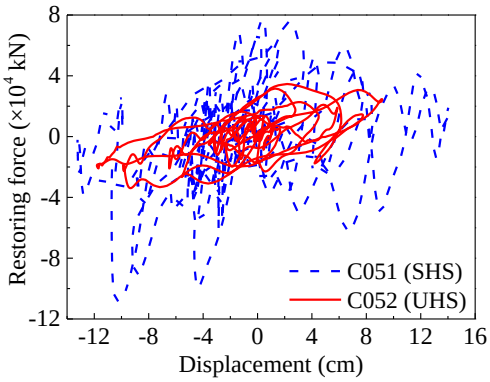

(d) Comparison of displacement-force relationship between SHS and UHS

Fig. 5-23 Identification results (PGA=1.0g)

representative values of each parameter are shown in Table 5-14. At the lower PGA level, the mean of the convergence value of the f_{cu} is 5.61MPa with a standard deviation of 0.267 which is much smaller than the statistical standard deviation of the compressive strength of concrete. The mean of the convergence value of the ε_{cu} is 0.00196 with a quite small standard deviation of 1×10^{-5}. At the higher PGA level, the mean of the final convergence value of the f_{cu} is 2.66MPa with a standard deviation of only 0.195. The mean of the convergence value of the ε_{0u} is 0.00186 with a very small standard deviation of 2.55×10^{-5}. The mean of the convergence value of the K are also very close, which are 0.78 and 0.76 respectively. This makes clear that the proposed identification method has high stability and good robustness to the measured noise.

It is worth noting that, in order to compensate the large model errors, the UKF forces the most sensitive parameter f_{cu} to converge to an unreasonable smaller value to meet the observed restoring forces. Because all the hybrid simulation cases are implemented on the same specimen, the damage is accumulated and gradually developed with the increasing of earthquake loads. This leads to a further larger model error, resulting in a further reduction of the convergence value of the f_{cu}.

Constitutive model	Case	f_{cu} (MPa)	ε_{0u}	K
Case without experiencing decreasing branch	C012 (0.07g)	5.96	0.00195	--
	C022 (0.22g)	5.57	0.00196	--
	C032 (0.4g)	5.31	0.00197	--
Case with experiencing decreasing branch	C042 (0.62g)	2.85	0.00188	0.78
	C052 (1.0g)	2.46	0.00183	0.76

Table 5-13 Converge value of concrete constitutive parameters

Typical value		f_{cu} (MPa)	ε_{0u}	K
Case without experiencing decreasing branch	Mean	5.61	0.00196	--
	Standard deviation	0.267	1.00×10^{-5}	--
Case with experiencing decreasing branch	Mean	2.66	0.00186	0.77
	Standard deviation	0.195	2.55×10^{-5}	0.01

Table 5-14 Representative values of the converge value of the parameters

5.5.4 Analysis of test results

In this section, the testing results are presented, including base sliding, axial forces of the

specimen, displacements at the top of the specimen, failure modes of the specimen, displacements at the pier top, displacements of the lumped mass, and effects by high-frequency on the dynamic responses of the bridge.

5.5.4.1 Testing results of the specimen

The specimen of the pier is displacement control using the outer-loop control method. Which is, the difference displacement between the top of the specimen and the foundation is the control target. When the difference between the control target, i.e. the realized displacement of the specimen, and the displacement command, i.e. the expected displacement, is within 0.1 mm, it is believed that the specimen has realize the displacement command. Using the out-loop control method, the displacement command can be also well realized even in the case that the displacement command is rather small. The comparison between the realized displacements and the expected ones is shown in Fig. 5-25. As can be seen that the realized displacements and the expected ones basically coincide, indicating that the specimen has achieved the commands. The maximum displacement command is less than 1mm, and the maximum deviation between the two is only 0.023mm, which demonstrate that the control of displacements can meet the requirements of the precision.

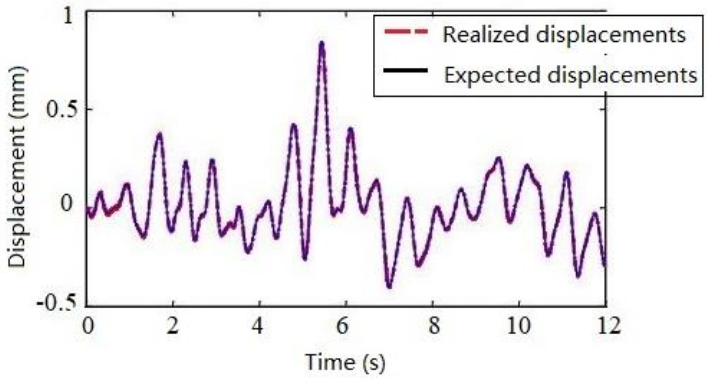

Fig. 5-25 Results of outer-loop control

Although the outer-loop control can ensure that the displacement command is well realized by the specimen, the loading and testing results can also be affected when the base sliding is too large. So, the LVDT1 shown in Fig. 5-15 is set to monitor the displacement of specimen foundation. Fig. 5-26 shows the results of the horizontal displacements of both the top and the base of specimen subjected to the earthquake of PGA of 0.07g and 0.62g. It is seen that the base slip is quite small with a maximum value less than 1mm.

The axial compression ratio of the bottom section of the pier is obtained according to the weight of the superstructures and the piers without considering the vehicle loading and the weight of the deck pavement. So, the axial compression ratio of the specimen is designed to be 0.25, from which the vertical constant load can be calculated as 1076kN. Removing the gravities of the L-type loading beam and the concrete beam on the top of the specimen, the force loading on the specimen by the two vertical actuators is 826 kN. Fig. 5-27 shows the time histories of the axial

force on the specimen under the PGA of 0.07g, 0.22g and 0.62g respectively. The solid curve is for the SHS, while the dashed curve is for the UHS.

It is found that the amplitude of the axial force of the specimen increases with the increase of the earthquake intensity in both the SHS and UHS cases. The axial compression ratio of the specimen changes from moment to moment under the earthquake loads, that is, the axial forces that the specimen subjected to changes from moment to moment. From the figure, it is seen that the loading scheme of various axial forces can be realized by the two vertical actuators.

An attentive reader can also find from Fig. 5-27 that the force fluctuation in the UHS case is larger than that in the SHS case before 1s. This is because the axial forces to the PS and the NS are achieved by applying to them the displacements which are pre-acquired from the numerical simulation of the whole bridge structure which subjects to the gravity. That is, a numerical simulation of the full-scale bridge with the initial values of the concrete constitutive parameters, which is under static gravity, is executed firstly. Then the displacements of each lumped mass are statically loaded to both the NS and the PS to simulate the gravity of the bridge before the hybrid simulation. Then, the axial forces can be measured and computed from the PS and the NS, respectively, to balance the gravity in the right of the motion equation of the bridge. By doing so, the values of concrete constitutive parameters employed in the full-scale FE model of the bridge where the pre-acquired displacements are obtained are the same as those employed in the NS of the SHS, but different with those in the NS of the UHS which the identified values are

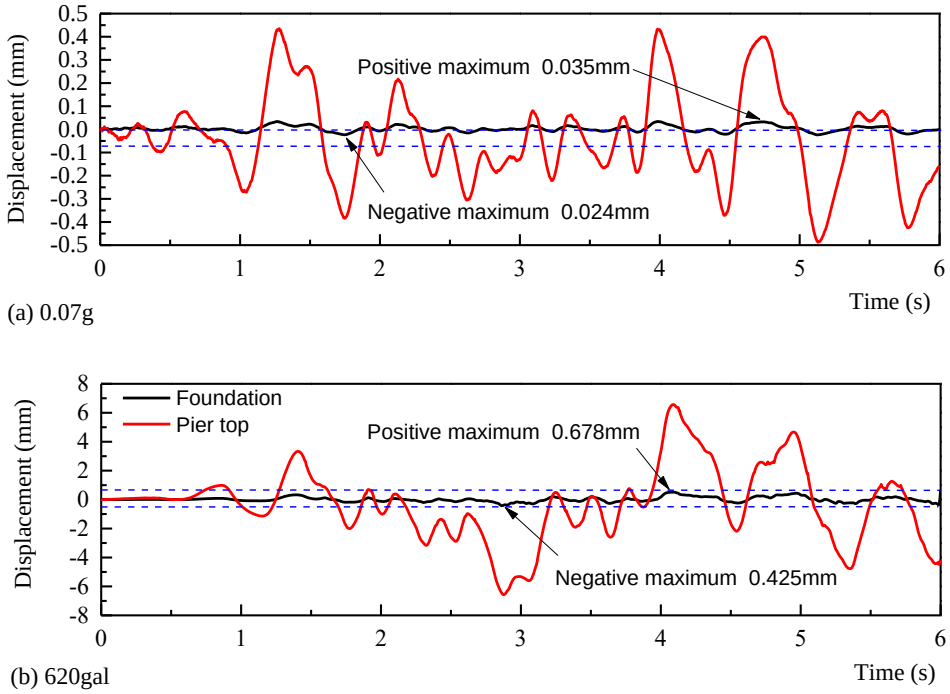

Fig. 5-26 Sliding displacement of foundation

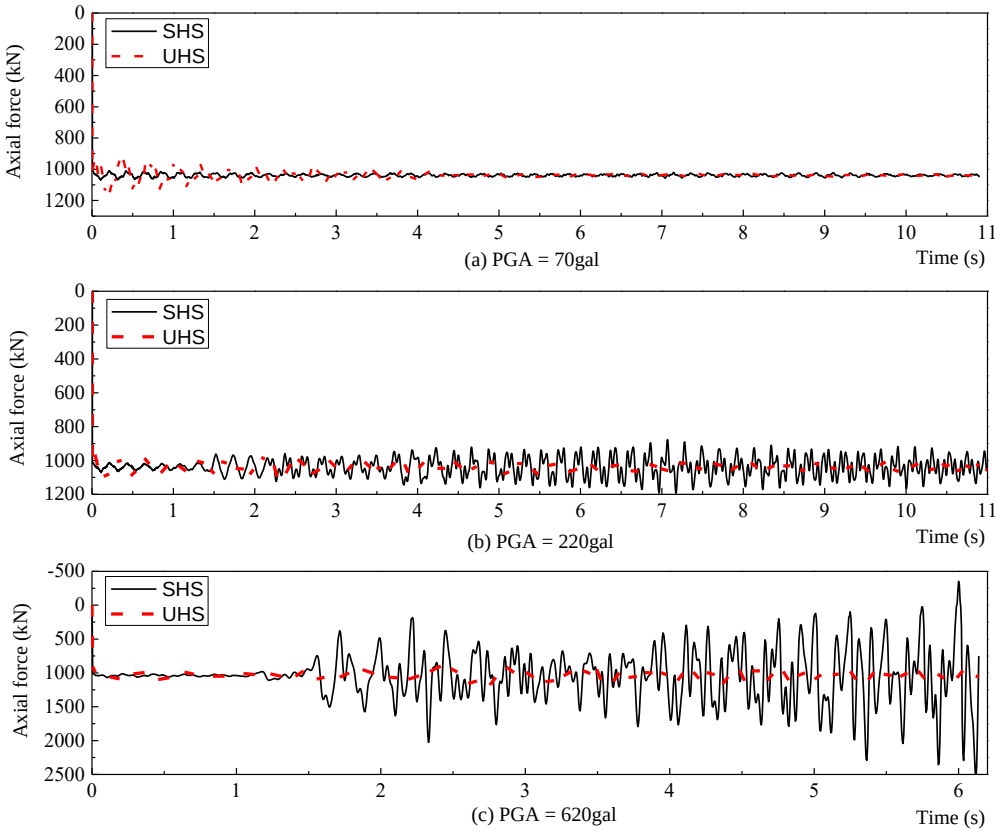

Fig. 5-27 Time histories of axial force

adopted. So, the computed axial force of the NS in the SHS are more close to the gravity in the right of the motion equation to eliminate the dynamic response by the gravity which should not be arouse. This is the reason for the fluctuation of gravity before 1s in the SHS is greater than that in the UHS.

From Figs. 5-27 (a), (b) and (c), it can be found that the influence caused by the high-frequency response of the bridge on axial forces is increased gradually with the increase of seismic intensity. The SHS overestimates the high-frequency effects and the UHS can provide a more accurate estimation on the seismic behavior of the large bridge structure.

5.5.4.2 Failure mode of the specimen

The specimen has a total of four sides. The side shown in Fig. 5-12 is referred to as the front side of the specimen, and the symmetrical side is the back side. The side where the actuator is equipped is called the left side, whilst the symmetrical side of the right side. The positive direction for the actuator loading is from the left to the right side.

The final destruction occurred at the first acceleration peak of the PGA level of 1.5g in the SHS case. The failure mode is bending-shear failure, and the development degree of bending cracks is similar to shear cracks. The fracture of the stirrup is the dominate reason for the final destruction of the specimen, this means that the shear damage accounted for a more important position. The main phenomena are that a wide diagonal crack exists in both the front and back

side of the specimen, as presented in Fig. 5-28; the fracture of the stirrups as shown in Fig. 5-29(c); the crushing and falling off of the concrete at the bottom of the specimen as well as around the diaphragm, which are shown in Fig. 5-29(a) and Fig. 5-29 (b).

Under the seismic load with a PGA of 0.07g and 0.22g, no cracks were observed. Under the PGA of 0.4g, there are slight bending cracks appears in the bottom of four sides of the specimen. As the load gradually increased to 1.0g, bending cracks on the left and right sides are gradually developed from the bottom to the top of the specimen, which are quite evenly distributed throughout the left and right sides. As the distribution of the bending cracks in the left side is similar with that in the right side, only the cracks in the right sides are shown in Fig. 5-30(a).

Under the earthquake load with a PGA of 0.62g, slight diagonal cracks occurrence in the bottom of the adjacent parts between the front/back side and the left/right. After the SHS under a PGA of 1.g earthquake load, a diagonal crack emerged from the bottom to the diaphragm with the width of 0.5mm, which is shown by the green solid line in Fig. 5-30(b). After the UHS under a PGA of 1.g earthquake load, a number of bending cracks appears as shown by the red dotted line in the Fig. 5-30(b), as well as some slight fine shear cracks appearing at the bottom of the specimen. After the 1.5g earthquake loads, the main diagonal crack becomes longer and wider, with a width of 3mm. Meanwhile, there is another diagonal crack parallel to the main one appearing with the width of 1mm.

The failure modes of the specimen in this study basically agrees with the results of the quasi-static tests provided by reference (Sun Z., 2013). In the literature, the quasi-static tests included the case with constant axial loads and the case with various axial loads. In the constant

(a) Crack distribution in front view

(b) Crack distribution in back view

Fig. 5-28 Failure mode of the specimen

(a) Crushing destruction at the bottom in the left elevation

(b) Crushing destruction at the diaphragm plate in the right elevation

(c) Tensile rupture of stirrup by tensile force

Fig. 5-29 Concrete crushing destruction of the specimen

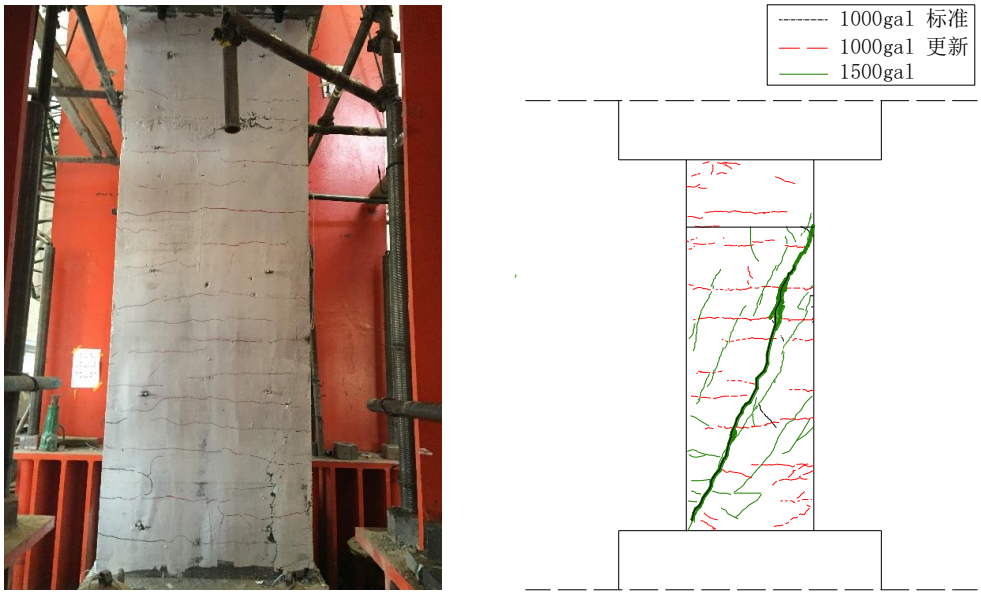

(a) Crack distribution in the right elevation

(b) Crack distribution in the front view

Fig. 5-30 Crack development of the specimen

axial-loading case, the failure of the specimen belongs to bending-shear modes, with the bending effects playing a leading role. While in the various axial-force case, the shear effect is dominating; and a wide diagonal crack is found as well. Comparing to the case with a constant axial force, the various axial force case is more close to the results provided by this study. However, there is still a difference that the angle of the shear crack and the horizontal line is less than that in this study. The various axial forces in the literature has a period with a compressive axial ratio from 0.1(left), to 0.2 (center), to 0.3(right). While, in this study the various axial forces

are random, which are generated by the earthquake loads.

Results show that the failure of a thin-walled hollow section pier is bending-shear mode, and the shear plays a leading role. Therefore, for such RC members, we need to pay more attention to the shear effects. In the numerical modeling, the influence of shear deformation must be considered. It can be seen that the diagonal crack finally extends to the diaphragm place, so whether the position of the diaphragm of the thin-walled hollow pier has any influence on the failure mode of the member deserves further study.

5.5.4.3 Seismic Response of the bridge

Because the superstructure of the bridge is not completely rigidly connected, the displacements of each degree of freedom in the left and right piers are not completely the same. However, the experimental results show that the two main piers has the same motion tendency and the displacements at the corresponding degrees of freedom of the two piers are relatively close. Therefore, only the left pier is taken as an example to analyze the dynamic response under earthquake load.

Fig. 5-31 shows the time history of pier top displacements under low-intensity earthquakes. Fig. 5-32 shows that under high-intensity earthquakes. Results show that the period of the dynamic response of the main bridge gradually increases with the increased intensity. It is seen from the figures that under the lower-level seismic loads, the maximum displacements obtained from the SHS are larger in both positive and negative directions than that obtained from the UHS. While, under the higher-level seismic loads, the maximum displacement obtained from the SHS in only the positive direction is larger than that obtained from the UHS; in the negative direction, the two are closed.

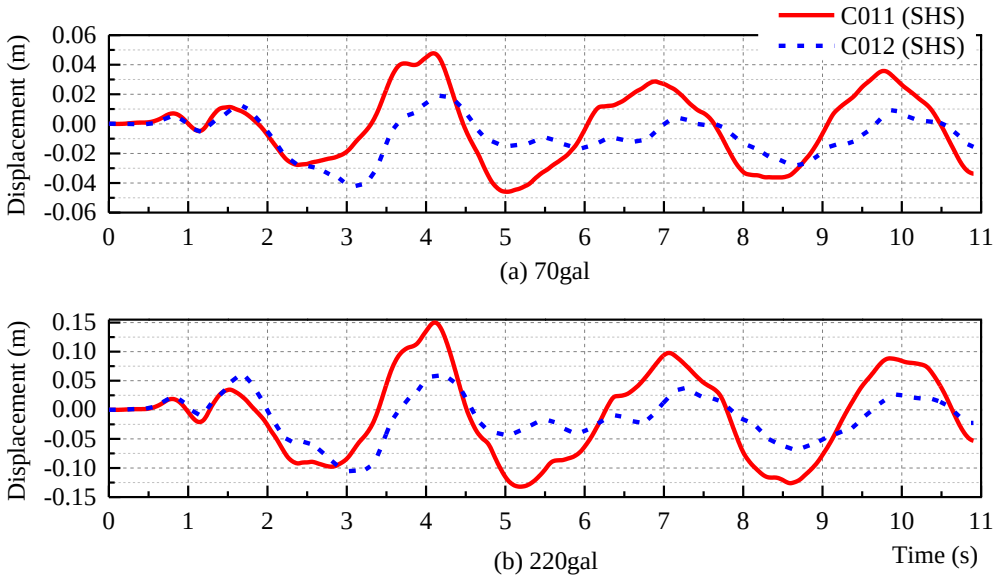

Fig. 5-31 Displacement histories at the top of the pier under earthquakes with low intensity

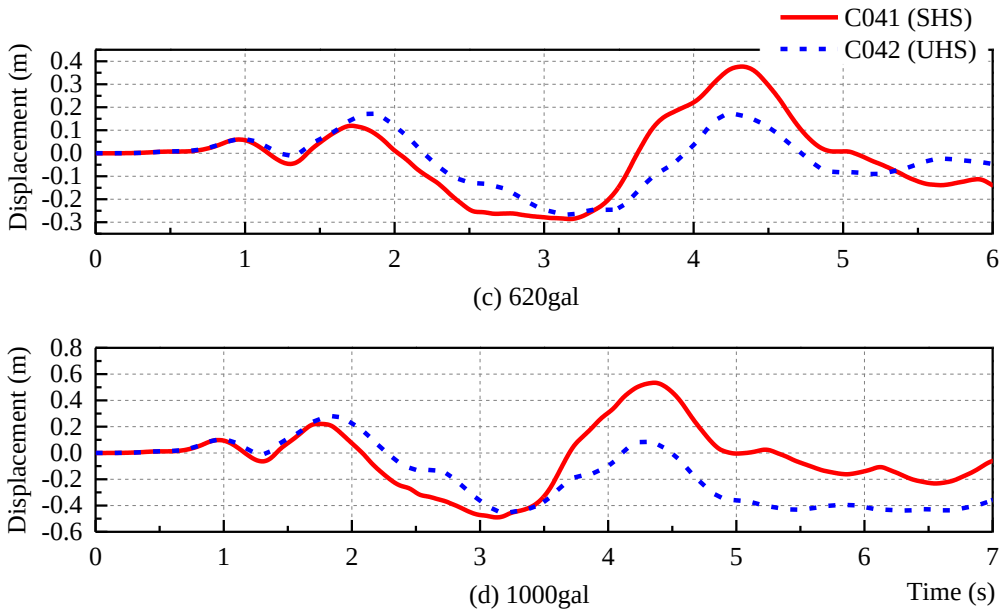

Fig. 5-32 Displacement histories at the top of the pier under earthquakes with low intensity

As we have proved the accuracy of the UHS, we can conclude that the SHS underestimate the seismic performance of the bridge when the maximum displacement is taken as the evaluation criterion. This will to a certain extent lead to the waste of the structural performance. Furthermore, the UHS can reflect the asymmetric stress state of the bridge subjected to the earthquake load, and provide a more accurate estimation of the seismic behavior of the bridge.

It is seen from both the Fig. 5-31 and Fig. 5-32 that in the early stage of the earthquake, the displacements of the pier top obtained by the SHS and UHS are relatively close, because the parameters have not reached the convergence. When the first acceleration peak (1.7s) is passing, the parameters converge rapidly, and then the displacement responses obtained by the two methods begin to differ. It should be noted that the first peak acceleration of the El-Centro seismic wave should be 2.14s. In order to shorten the testing time, this paper deleted the record of ground motions before 0.4s.

PGA level (g)	Displacement-UHS (cm)		Displacement-SHS (cm)	
	Positive	Negative	Positive	Negative
0.07	1.9	-4.2	4.8	-4.6
0.22	6.0	-10.5	15.0	-13.2
0.4	12.9	-17.4	24.6	-17.9
0.62	17.3	-26.7	37.7	-28.6
1.0	28.0	-45.4	53.4	-49.0

Table 5-15 Maximum value of horizontal displacement at pier top under each PGA level

The maximum displacements of the pier top at each PGA are listed in Table 5-15. It is found that the maximum positive displacement obtained from the SHS is about 2 times that from the UHS. At the PGA level of 1.0g, the maximum displacement of the pier top is 45.4cm, and the drift ratio is 0.36%. This indicates that, for the RC continuous rigid frame bridge with thin-walled hollow-section tall piers, shear failure has occurred at the bottom of the piers even when the drift ratio of the pier top is very small. Therefore, the drift ratio of pier top cannot be used as the only criterion to estimate the seismic performance of such bridges.

In order to analyze the influence of high-order frequency on dynamic response of such bridge, the horizontal displacements of the three lumped mass of the left pier are compared. The results show that the high-order mode of bridge is not excited when the seismic level is lower than 0.62g. As the seismic intensity increases, the higher modes of the bridge are excited, and the influence of the horizontal displacements of the two mass below on the displacements of the top mass appears. Fig. 5-33 and Fig. 5-34 show the displacement histories of the three mass of the left pier under the cases with a PGA of 0.62g and 1.0g, respectively. In the figures, the layout of Node 2 (about 1/4 pier height), Node 4 (about two-thirds pier height) and Node6 (pier top) please find in Fig. 5-7. For the SHS, it is seen Fig. 5-33 (a) and Fig. 5-34 (a) that the excitation by higher frequency emerged after 4s; the main vibration frequencies of Node 2 and Node 4 are basically the same, the vibration period is smaller than the top node; the direction of motion of Node 2 as well as Node 4 is different to that of Node 6.

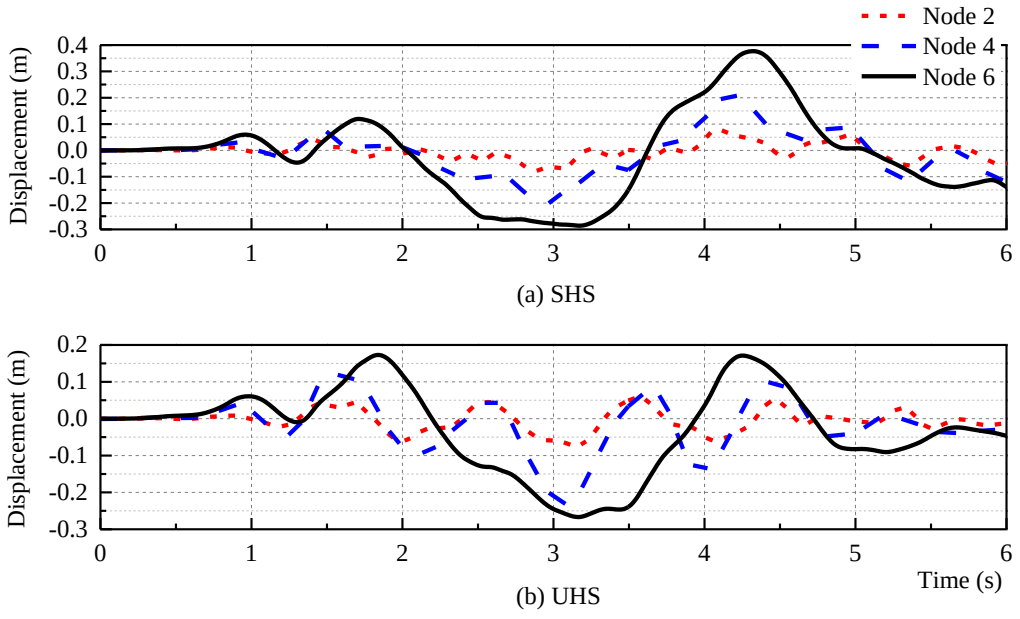

Fig. 5-33 Displacement of each horizontal DOF of the left pier (0.62g)

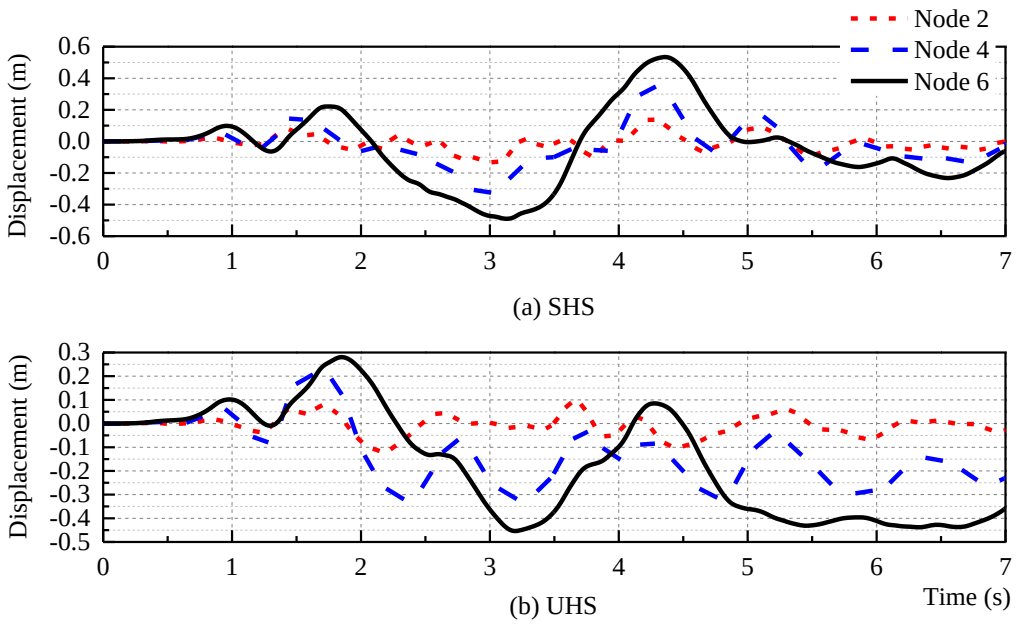

Fig. 5-34 Displacement of each horizontal DOF of the left pier (1.0g)

Comparing the results of the SHS and the UHS, it is found that the high-order responses are excited earlier in the UHS under the seismic level, and emerged from almost the first peak of the acceleration of the ground motion. From 2s to 4s, the top mass completes only one cycle, and during this time, three cycles has been finished of Node 2 and Node 4. For 0.62g case, the frequencies and directions of the movement of Node 2 and Node 4 are basically the same before 4s, while after 4s, Node 4 changes to be similar with Node 6. For 1.0g case, the inconsistent motion of each mass are more obvious.

To more intuitively understand the vibration of the main pier, a few illustration of modes of the pier are shown in Fig. 5-35 and Fig. 5-36. It can obviously see that the UHS can give a more accurate estimation of the higher frequency influence on dynamic responses of such tall pier bridge. It is also seen from the results provided by the UHS that the plastic hinge is not only developed at the bottom but also at the middle part of the pier. In the literature (Liang Z. and Li J., 2007) , the elastic-plastic beam-column element and fiber beam-column element are employed respectively to discuss the modeling high pier and the position that the plastic hinge emerged are investigated. The numerical result shown in this literature presents that the plastic hinge can produce in both the bottom and middle parts of the tall piers. This conclusion is just in accordance with the results provided by the UHS in this study.

By comparing the results under 0.62g case, the higher-frequency mode has not been too much excited in the SHS, while a rather obvious higher-order response appear in the USH and meanwhile the plastic hinges have developed and moved from the bottom to the middle part of the pier.

In brief, the SHS provides larger displacements at the pier top. In other words, if the maximum displacement at the pier top is adopted to be the criterion, the SHS will underestimated the seismic performance of such bridges. Furthermore, the SHS underestimated the effects caused

by higher-frequency on the dynamic response of the main bridge and the development of plastic hinges. With this respect, the SHS overestimate the actual seismic performance of such bridges. In conclusion, the proposed UHS can improve the accuracy of the NS, and hence the simulation of the whole bridge, and is superior to the SHS.

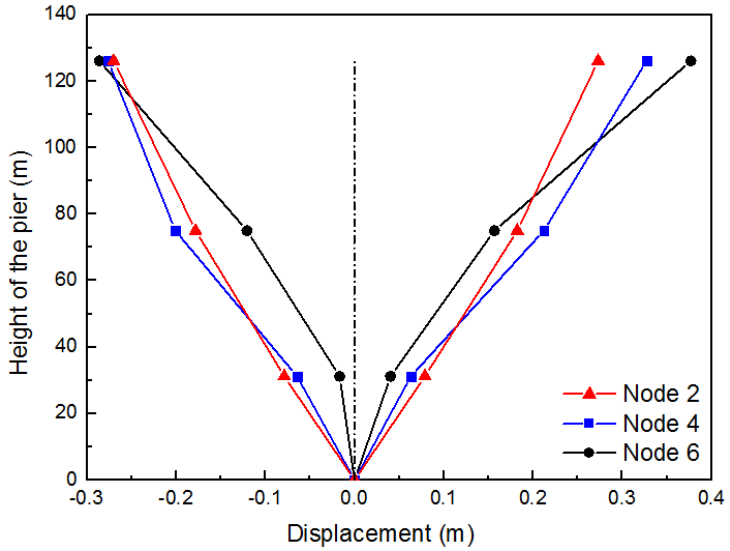

(a) SHS

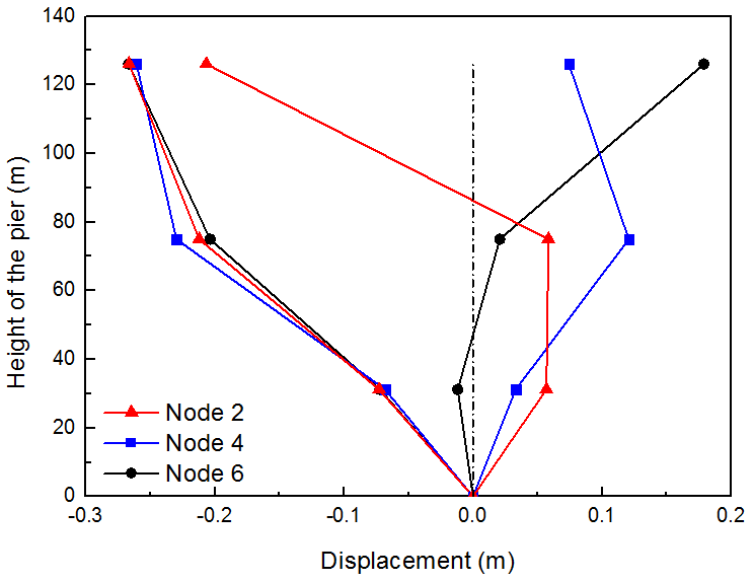

(b) UHS

Fig. 5-35 Sketch map of the vibration mode of the left pier (0.62g)

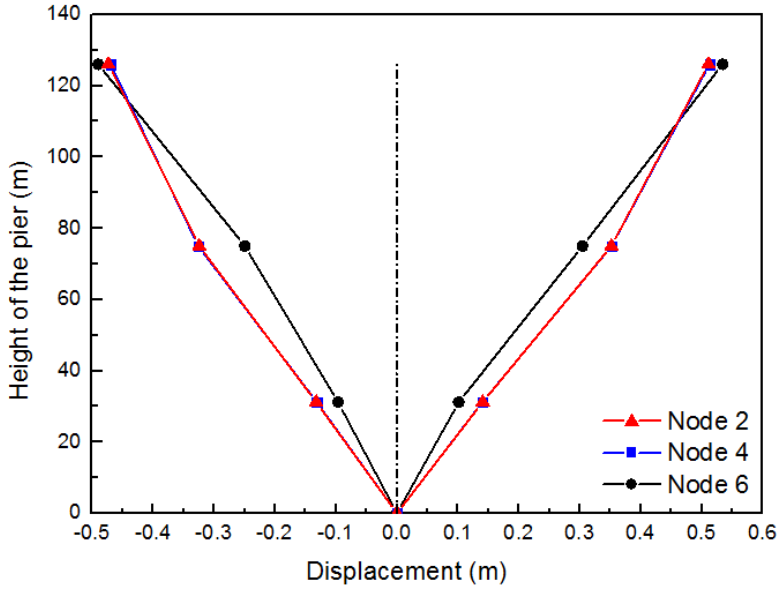

(a) SHS

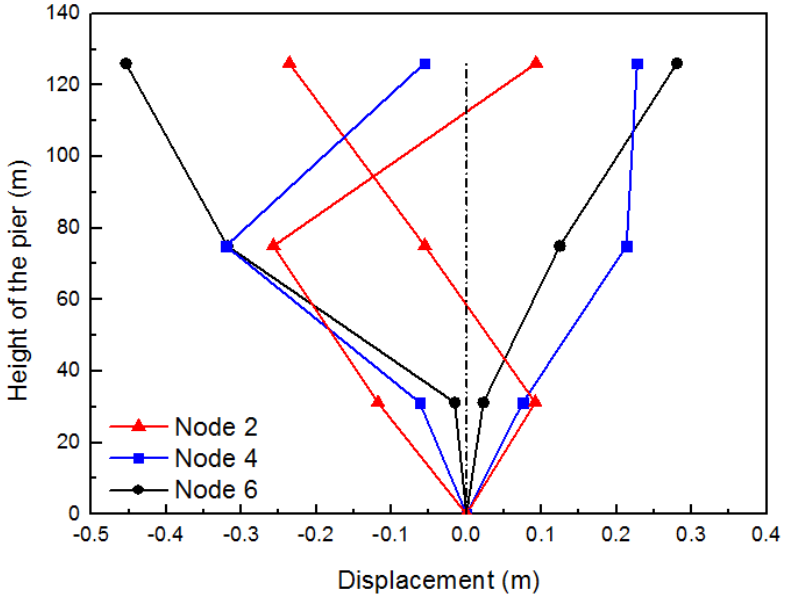

(b) UHS

Fig. 5-36 Sketch map of the vibration mode of the left pier (1000gal)

5.6 Summary

In this chapter, a RC rigid frame bridge is taken as the target structure for hybrid simulations. Both the standard hybrid simulations (SHSs) without model updating and model-updating hybrid

simulations (UHSs) are carried out under earthquake loads with different PGA levels. The 1:12 scaled specimen of a part of the left pier is taken as the PS and tested in the Laboratory, while the remaining is considered as the NS and simulated in OpenSees. The main conclusions are as follows:

1. The identification and updating of the concrete constitutive parameters can improve the accuracy of the NS and hence the reliability of the hybrid simulation. The convergence value of the parameters in five cases are close with quite small deviations. This further shows that OpenSees-embedded UKF can provide good estimation precision of the parameters and fast convergence rate.
2. The difference between the SHS and UHS results are larger than that for the case of RC frame presented in Chapter 4. The model updating is of great significance to hybrid simulation of large complex structures which contain more components that may undergo strong nonlinearity. The UHS method should be employed for estimating the structural seismic behavior, especially when only a few of the members can be experimentally considered and and the precision of hybrid simulation can be sharply reduced.
3. Large model errors can adverse effect the parameter identification. This study solved the problem by tuning the initial values of the concrete constitutive parameters. No matter whether large errors existing, parameter identification and updating can improve the accuracy of hybrid simulation of structures.
4. The failure of thin-walled hollow-section pier belongs to bending-shear failure mode, where shear effects is dominant with the stirrups being raptured. Higher-frequency contributes a lot to the dynamic responses of the RC rigid frame bridge with tall piers. Plastic hinges can develop at both the bottom and the middle part of the tall piers.

CONCLUSION

Hybrid simulation is one of the main testing methods to evaluate the seismic performance of structures. In order to reduce the errors of the modeling of the numerical substructure (NS) in the hybrid simulation to improve the overall accuracy of the hybrid simulation, a novel hybrid simulation with identifying and updating the parameters of concrete constitutive model is proposed. The key problem of model-updating hybrid simulation (UHS) is to identify the concrete constitutive parameters based on the restoring forces measured from the physical substructure (PS). Firstly, a unified constitutive model for both the unconfined and confined concrete is deduced firstly based on the existing concrete constitutive models, which can be more widely universal in model updating of hybrid simulation. Then an OpenSees-embedded UKF is proposed for identifying the parameters of concrete constitutive model and validated through both the numerical and experimental ways. Then this identification method is applied to a RC frame structure to achieve the UHS with updating the concrete constitutive parameters. Finally, this UHS method is employed for investigating the seismic behavior of a more complex RC rigid frame bridge with stronger nonlinearity. Conclusions are as follows:

1. The concept of the same constitutive models were clarified to illuminate the condition for model updating in hybrid simulation, by defining constitutive parameter and non-constitutive parameter. A unified model of unconfined and confined concrete was derived by analyzing the relationship of the parameters in both existing constitutive models of core and cover concrete and introducing the volumetric parameters as a non-constitutive parameter. The parameter sensitivity analysis of the constitutive parameters in the proposed unified constitutive model was carried out by using the finite element model of cantilever concrete column in OpenSees.
2. The accuracy of the UT transform based on the scaled symmetric sampling method of the UKF method is analyzed. Effects of the scalded coefficients of sampling on estimating the mean and variance is discussed, and the optimal values of the sampling coefficients are obtained for the case when the estimation of a Gaussian random variable reaches to the fourth-order precision of Taylor expansion. Aiming at the hybrid simulation, an OpenSees-embedded UKF is proposed to a more complicated nonlinear problem that the measurement equation is hardly to be analytical expressed. The characteristic of monotonic convergence of the UKF for single parameter identification of time-varying linear systems is proved by theoretical and numerical ways. The different sensitivities of concrete constitutive parameters leading to the different convergence rate causes the fluctuation during the convergence process.
3. A monotonic static test of a RC column is carried out to experimentally validate the identification method. Results shown that: i) The OpenSees-embedded UKF for identifying the concrete constitutive parameters has high robustness and reliability, and the convergence rate of parameter is fast. It can be applied to model-updating hybrid simulation; ii) the accuracy of the hybrid simulation with updating the concrete constitutive parameters is greatly improved compared with the standard hybrid simulation. The novel method can be further extended to large and complex structures; iii) the location, the order of crack occurrence and the damage intensity of the specimen are different for the the SHS and the UHS. Under low-level seismic load, the SHS overestimated the seismic performance of the RC frame.

However, underestimate the seismic performance under the high-level seismic loads, which may cause the waste of structural capacity.

4. Hybrid simulations of a RC rigid frame bridge are carried out to validate the UHS. Conclusions are as follows: i) the identification and updating of the concrete constitutive parameters can improve the accuracy of the NS and hence the reliability of the hybrid simulation. The convergence value of the parameters in five cases are close with quite small deviations. This further shows that OpenSees-embedded UKF can provide good estimation precision of the parameters and fast convergence rate; ii) the model updating is of great significance to hybrid simulation of large complex structures which contain more components that may undergo strong nonlinearity. The UHS method should be employed for estimating the structural seismic behavior, especially when only a few of the members can be experimentally considered and and the precision of hybrid simulation can be sharply reduced; iii) large model errors can adverse effect the parameter identification. This study solved the problem by tuning the initial values of the concrete constitutive parameters. No matter whether large errors existing, parameter identification and updating can improve the accuracy of hybrid simulation of structures; iv) the failure of thin-walled hollow-section pier belongs to bending-shear failure mode, where shear effects is dominant with the stirrups being raptured. Higher-frequency contributes a lot to the dynamic responses of the RC rigid frame bridge with tall piers. Plastic hinges can develop at both the bottom and the middle part of the tall piers.

This article has three main innovations:

1. Clarified the conditions of model updating for RC structures, and proposed a unified constitutive model of unconfined and confined concrete, making the model updating be more broadly applied to hybrid simulation.
2. A novel hybrid simulation with identifying and updating the concrete constitutive parameters was proposed, and the OpenSees-embedded UKF is proposed by developing the identification module in OpenSees.
3. The hybrid simulation with model updating was validated through a RC frame structure and applied to a large RC rigid frame bridge. The failure model and the high-order seismic responses were investigated of such bridge with thin-walled hollow-section tall piers.

However, some problems deserve further study:

1. The follow-up research should continue on other concrete constitutive models taking more factors into account, such as the one is more suitable for bending-shear RC members, the one considering the tensile behavior of concrete, and the one under multi-axial compressive forces.
2. The accuracy of unscented transform for variables with different distributions need to be further studied. Study should be focus on the model errors, and the positive influence of initial values of parameters to model errors.
3. Data transfer between the OpenSees and Matlab will reduce the computational efficiency. Adding a module in OpenSees to fulfill all the task of parameter identification and updating can be an effective way to improve the efficiency of the UHS.
4. Further investigate the influence roused by shear effects impacting on the seismic behavior of thin-walled hollow piers, the development of plastic hinges, and the failure model and the collapse form of the bridge with such piers.

BIBLIOGRAPHY

Abbiati G., et al., (2015), *Hybrid Simulation of a Multi-Span RC Viaduct with Plain Bars and Sliding Bearings*, Earthquake Engineering & Structural Dynamics, 44, 13, 2221-2240

Agbabian M. S., et al., (1991), S*ystem Identification Approach to Detection of Structural Changes*, Journal of Engineering Mechanics, 117, 370-390

Astroza R., Ebrahimian H., Conte J. P., (2015), *Material Parameter Identification in Distributed Plasticity FE Models of Frame-Type Structures Using Nonlinear Stochastic Filtering*, Journal of Engineering Mechanics, 141, 5, 1-17

Bonnet P. A., et al., (2010), R*eal-Time Hybrid Experiments with Newmark Integration, Mcsmd Outer-Loop Control and Multi-Tasking Strategies*, Earthquake Engineering & Structural Dynamics, 36, 1, 119-141

Bosco M., et al., (2016), *Improvement of the Model Proposed by Menegotto and Pinto for Steel*, Engineering Structures, 124, 442-456

Bouc R., (1967), *Forced Vibration of Mechanical Systems with Hysteresis*, Proc Con，Nonlinear Oscillation，Prague，Czechoslovakia

Caravani P. and Thomson W. T., (1974), *Identification of Damping Coefficients in Multidimensional Linear Systems*, Journal of Applied Mechanics, 41, 2, 379-382

Carrion J. and Spencer B., (2008), *Real-Time Hybrid Testing Using Model-Based Delay Compensation,* Smart Structures Systems, 4, 6, 809-828

Chatzi E. N. and Smyth A. W., (2009), *The Unscented Kalman Filter and Particle Filter Methods for Nonlinear Structural System Identification with Non-Collocated Heterogeneous Sensing*, Structural Control & Health Monitoring, 16(1), 99-123

Chatzi E. N., Smyth A. W., Masri S. F., (2010), *Experimental Applicationof On-Line Parametric Identification for Nonlinear Hysteretic Systems with Model Uncertainty*, Structural Safety, 32, 5, 326-337

Chen C., (2007), *Development and Numerical Simulation of Hybrid Effective Force Testing Method*, Lehigh University, Bethlehem, USAClough R. W., (1966), *Effect of Stiffness Degradation on Earthquake Ductility Requirements*, University of California，California. USA

Chen H P, Bicanic N. (2000), *Assessment of Damage in Continuum Structures based on Incomplete Modal Information*, Computers & Structures, 74, 5, 559-570

Chung J. and Hulbert G.M., (1993), *A Time Integration Algorithm for Structural Dynamics with Improved Numerical Dissipation: the Generalized-α Method*, Journal of Applied Mechanics, 60, 2, 371-375

Combescure D. and Pegon P., (1997), *α-Operator Splitting Time Integration Technique for Pseudodynamic Testing Error Propagation Analysis*, Soil Dynamics and Earthquake Engineering, 16, 7-8, 427-443

Crisfield M. A., Shi J., (2010), *A Co-rotational Element/Time-integration Strategy for Non-linear Dynamics*, International Journal for Numerical Methods in Engineering, 37, 11, 1897-1913

Darby A. P., Williams M. S., (2002), Blakeborough A., *Stability and Delay Compensation for Real-Time Substructure Testing*, Journal of Engineering Mechanics, 128, 12, 1276-1284

Deng L., (2010), *Numerical Stability Analysis of Substructure Testing*, Harbin Institute of

Technology, Harbin, China, (Doctoral thesis, in Chinese)
Dermizakis S N，Mahin S A. (1985), *Development Of Substructuring Techniques for On-line Computer Controlled Seismic Performance Testing*, Earthquake Engineering Research Center, University of California, Report No. UCB/EERC-85/04, California, USA
Doob J. L., (1953), *Stochastic Processes*, Wiley, New York, USA
Drury D., et al., (2002), *Advances in Numerical Experimental Substructuring Techniques Using MCS Control*, 12 European Conference in Earthquake Engineering, 1-10
Du X., Chen M., Han Q., (2011), Experimental Evaluation of Seismic Performance of Reinforced Concrete Hollow Bridge Columns, Journal of Vibration and Shock, 30, 11, 254-259 (in Chinese)
Du W., (2013), Seismic Performance Analysis of RC Beam-column Joints and Frames based on Bouc-Wen Model, Harbin Institute of Technology, Harbin, China, 44-51 (Master's thesis, in Chinese)
Elanwar H.H. and Elnashai A. S., (2014), *On-line Model Updating in Hybrid Simulation Tests*, Journal of Earthquake Engineering, 18, 3, 350-363
Eleni N., et al., (2009), The unscented Kalman Filter and Particle Filter Methods for Nonlinear Structural System Identification with Non-collocated Heterogeneous Sensing, Structural Control and Health Monitoring, 16, 99-123
Fan Y., (2010), *Development of Networked Structural Laboratories*, Hunan University, Changsha, China, 1-76, (Doctoral thesis, in Chinese)
Fan Y., et al., (2011), Study on Remote Collaborative Pseudo-dynamic Tests of Multi-story frames, China Civil Engineering Journal, 44, 2, 28-35 (in Chinese)
Friswell M. I., Mottershead J. E., (1995), *Finite Element Model Updating in Structural Dynamics*, Kluwer Academic Publishers, Alphen aan den Rijn, Netherlands
Friswell M. I., Mottershead J. E., Ahmadian H., (2001), *Finite-element Model Updating Using Experimental Test Data: Parametrization and Regularization*, Philosophical Transactions of the Royal Society of London. Series A：Mathematical，Physical and Engineering Sciences，London, U.K., 169-186
Gallardo-Zafra R. and Kawashima K., (2009), *Analysis Of Carbon Fiber Sheet-Retrofitted RC Bridge Columns under Lateral Cyclic Loading*, Journal of Earthquake Engineering, 13, 129-154
Gao X. (2012), *Development of a Robust Framework for Real-Time Hybrid Simulation: From Dynamical System, Motion Control to Experimental Error Verification*, Purdue University, USA, (Doctoral thesis, in Chinese)
Ghanem R., (1995), *Structural-System Identification. I: Theory*, Journal of Engineering Mechanics, 121, 2, 255-264
Guo Y., Zeng D., Xiao Y., (2009), Development of a Remotely Collaborative Pseudo-dynamic Testing Platform for Bridge Structures, Journal of Hunan University (Natural Sciences), 36, 9, 1-6 (in Chinese)
Hakuno M.，Shidawara M.，Hara T., (1969), *Dynamic Destructive Test of a Cantilever Beam，Controlled by An Analog-computer*, Transaction of the Japan Society of Civil Engineer, 171, 1,1-9
Han Q. et al., (2013), *Experimental Study of Hollow Rectangular Bridge Column Performance under Vertical and Cyclically Bilateral Loads*, Earthquake Engineering and Engineering Vibration, 12, 3, 433-445

Hashemi M. J., Masroor A., Mosqueda G., (2014), *Implementation of Online Model Updating in Hybrid Simulation*, Earthquake Engineering & Structural Dynamics, 43, 3, 395-412
Hilber H. M., Hughes T. J. R., Taylor R. L., (1977), *Improved Numerical Dissipation for Time Integration Algorithms in Structural Dynamics*., Earthquake Engineering & Structural Dynamics, 5, 3, 283-292
Hognestad E., (1951), *Study of Combined Bending and Axial Load in Reinforced Concrete Members*, University of Illinois at Urbana Champaign, USA, 128
Horiuchi T., et al., (1999), *Real-Time Hybrid Experimental System with Actuator Delay Compensation and Its Application to a Piping System with Energy Absorber*, Earthquake Engineering & Structural Dynamics, 28, 10, 1121-1141
Hoshiya M. and Saito E., (1984), *Structural Identification by Extended Kalman Filter*, Journal of Engineering Mechanics, 110, 12, 1757-1770
Hughes T. J. R., (1977), *A Note on the Stability of Newmark's Algorithm in Nonlinear Structural Dynamics*, International Journal for Numerical Methods in Engineering, 11, 2, 383-386
Hughes T. J. R., Caughey T. K., Liu W. K., (1978), *Finite-element Methods for Nonlinear Elastodynamics which Conserve Energy*, Journal of Applied Mechanics, 45, 2, 366-370
Ibarra L. F., Medina R. A., (2005), Krawinkler H., *Hysteretic Models that Incorporate Strength and Stiffness Deterioration*, Earthquake Engineering & Structural Dynamics, 34, 12, 1489-1511
Jiang H., (2015), Study on Seismic Damage Mechanism of Thin-walled Hollow Square Bridge Piers, Institute of Engineering Mechanics, China Earthquake Administration, Harbin, China, 25-27
Julier S. J., (2002), *The Scaled Unscented Transformation*, American Control Conference，IEEE, 6, 4555-4559
Julier S. J., (2003), *The Spherical Simplex Unscented Transformation*, 3, 2430-2434
Julier S. J. and Uhlmann J. K., (1996), *A General Method for Approximating Nonlinear Transformations of Probability Distributions*, Technical report，Robotics Research Group，Department of Engineering Science，University of Oxford, Oxford, UK
Julier S. J. and Uhlmann J. K., (2002), *Reduced Sigma Point Filters for the Propagation of Means and Covariances through Nonlinear Transformations*, American Control Conference, IEEE, 2, 887-892
Julier S. J., Uhlmann J. K., Durrant-Whyte H. F., (1995), *A New Approach for Filtering Nonlinear Systems*, American Control Conference (IEEE), 3, 1628-1632
Jung R. Y., (2005), *Development of Real-Time Hybrid Test System*, University of Colorado at Boulder, Boulder, USA, (Doctoral thesis)
Kalman R., (1960), *A New Approach to Linear Filtering and Prediction Theory*. Transactions ASME. J. Basic Eng, 82, D, 35-46
Kent D. C. and Park R., (1971), *Flexural Members with Confined Concrete*, Journal of the Structural Division, 97, 1969-1990
Kim H. K., (2011) *Development and Implementation of Advanced Control Methods for Hybrid Simulation*, University of California, Berkeley, Berkeley, USA, 1-34, (Doctoral thesis)
Kwon O. S., et al., (2005), *A Framework for Multi-Site Distributed Simulation and Application to Complex Structural Systems*, Journal of Earthquake Engineering, 9, 5, 741-753
Kwon O. S. and Kammula V., (2013), *Model Updating Method For Substructure*

Pseudo-Dynamic Hybrid Simulation, Earthquake Engineering & Structural Dynamics, 42, 13, 1971-1984

Li H. Mao C. X., Ou J., (2013), *Identification of Hysteretic Dynamic Systems by Using Hybrid Extended Kalman Filter and Wavelet Multiresolution Analysis with Limited Observation*, Journal of Engineering Mechanics, 139, 5, 547-558

Li J., Ren D., Yang W., (2007), Experimental Study on 2-D Constitutive Relationship for Concrete, China Civil Engineering Journal, 40, 4, 6-12 (in Chinese)

Liang Z., and Li J., (2007), Investigation on Rational Analytical Model of Tall Bridge Pier, Earthquake Engineering and Engineering Vibration, 27, 2, 91-98 (in Chinese)

Loh C. and Tou I., (2010), *A System Identification Approach to the Detection of Changes in Both Linear and Non-Linear Structural Parameters*, Earthquake Engineering & Structural Dynamics, 24, 1, 85-97

Lu J. and Huang S., (1998), Statistical Analysis of Limit Tensile Strain of Full-graded Concrete Samples, Journal of HeHai University (Natural Sciences), 26, 1, 99-102 (in Chinese)

Lu X., (2015), Elasto-plastic Analysis of Buildings against Earthquake, China Building Industry Press, 21-26 (in Chineses)

Mander J. B., (1983), *Seismic Design of Bridge Piers*, University of Canterbury, Christchurch，New Zealand, 47-94 (Doctoral thesis)

Mander J. B.，Priestley M. J.，Park R., (1988), *Theoretical Stress-Strain Model for Confined Concrete*, Journal of structural engineering, 114, 8, 1804-1826

Mariani S. and Ghisi A., (2007), *Unscented Kalman Filtering for Nonlinear Structural Dynamics*, Nonlinear Dynamics, 49, 1-3, 131-150

Megalooikonomou K. G., Monti G., Santini S., (2012), *Constitutive Model for Fiber-Reinforced Polymer-and Tie-Confined Concrete*, ACI Structural Journal, 109, 4, 569-578

Mei Z., et al., (2018), *Hybrid Simulation of Structural Systems with online Updating of Concrete Constitutive Law Parameters by Unscented Kalman Filter*, Structural Control & Health Monitoring, 25, 2, e2069

Menegotto M., (1973), *Method of Analysis for Cyclically Loaded R. C. Plane Frames Including Changes in Geometry and Non-Elastic Behavior of Elements under Combined Normal Force and Bending*, Proc. IABSE Symposium on Resistance and Ultimate Deformability of Structures Acted on by Well Defined Repeated Loads, 15-22

Mosqueda G., et al., (2008), *Hybrid Seismic Response Simulation on a Geographically Distributed Bridge Model*, Journal of Structural Engineering, 134, 4, 535-543

Nakano Y. and Yang W. J., (2005), *Substructure Online Test by Using Real-Time Hysteresis Modeling with a Neural Network*, Proceedings of the First International Conference on Advances in Experimental Structural Engineering, 38, 267-274

Nakashima M., (1985), *Part 1: Relationship between Integration Time Interval and Response Stability in Pseudo Dynamic Testing*, Journal of Structural and Construction Engineering, 353, 29-36

Nakashima M., (1985), *Part 2: Relationship between Integration Time Interval and Accuracy of Displacement, Velocity, and Acceleration Responses in Pseudo Dynamic Testing (Stability and Accuracy Behavior of Pseudo Dynamic Response)*, Journal of Structural and Construction Engineering, 358, 35-42

Newmark N. M., (1959), *A Method of Computation for Structural Dynamics*, Proc Asce, 85, 1, 67-94

Ning X., (2013), Research on H-Infinity Control for Real-Time Hybrid Simulation, Harbin Institute of Technology, Harbin, China, 52-72 (Master's thesis, in Chinese)

Ozcebe G. and Saatcioglu M., (1989), *Hysteretic Shear Model for Reinforced Concrete Members*, Journal of Structural Engineering, 115, 1, 132-148

Pan P., Nakashima M., Tomofuji H., (2010), *Online Test Using Displacement–Force Mixed Control*, Earthquake Engineering & Structural Dynamics, 34, 8, 869-888

Pan P., et al., (2010), *Development of Peer-To-Peer (P2P) Internet Online Hybrid Test System*, Earthquake Engineering & Structural Dynamics, 35, 7, 867-890

Pan T. *Energy Consistent Integration Method and Its Applications to Hybrid testing*, Harbin Institute of Technology, Harbin, China, 1-16, (Doctoral thesis, in Chinese)

Papavasileiou G. S. and Megalooikonomou K. G., (2015), *Numerical Simulation o FRP-Confined Circular Bridge Piers Using Opensees*, International Conference Opensees Days, Second International Conference, Salemo, Italy

Park Y.J. and Young J., IDARC: *Inelastic Damage Analysis of Reinforced Concrete： Frame-Shear-Wall Structures*, NCEER

Pauschke J., George E., Brown Jr., (2003), *Network for Earthquake Engineering Simulation*, Proceeding on NEES Consortium Annual Meeting, May, edited by Structures Congress, USA, 21-22

Penizen J. (1962), Dynamic Response of Elasto-plastic Frames, Journal of Structural Division, 88, ST7, 1322-1340

Phillips B. M. and Spencer B. F., (2013), *Model-Based Multiactuator Control for Real-Time Hybrid Simulation*, Journal of Engineering Mechanics, 139, 2, 219-228

Phillips B. and Spencer B., (2013), *Model-Based Feedforward-Feedback Actuator Control for Real-Time Hybrid Simulation*, Journal of Structural Engineering, 139, 7, 1205-1214

Pinto A. V., (2013), *Cyclic Tests on Large-Scale Models of Existing Bridge Piers with Rectangular Hollow Cross-Section*, Earthquake Engineering and Structural Dynamics, 32, 13, 1995-2012

Pinto A. V., et al., (2004), *Pseudo-Dynamic Testing of Bridges Using Non-Linear Substructuring*, Earthquake Engineering & Structural Dynamics, 33, 1125-1146

Qiu F.，Qian J.，Chen Z., (2000), *Seismic Test Methodology for Structures*, China Science Publishing，Beijing, China. (in Chinese)

Ramberg W. and Osgood Ws R., (1943), *Description of Stress-Strain Curves by Three Parameters*, Technical Report Archive & Image Library, 902

Sakai J. and Kawashima K., (2003), *Modification of The Giuffre, Menegotto and Pinto Model for Unloading and Reloading Pathswith Small Strain Variations*, Doboku Gakkai Ronbunshu, 738, 159-169

Schellenberg A., Mahin S. A., Fenves G. L., (2006), *Application of An Experimental Software Framework for International Hybrid Simulation*, International Conference on Earthquake Engineering，Taipei，Taiwan

Scott B. D.，Park R.，Priestley M. J., (1982), *Stress-Strain Behavior of Concrete by Overlapping Hoops at Low and High Strain Rates*, ACI Journal Proceedings, 79, 1, 13-27

Shao X., Mueller A., Mohammed B. A., (2015), *Real-Time Hybrid Simulation with Online Model*

Updating：Methodology and Implementation, Journal of Engineering Mechanics, 142, 2, 04015074

Sheikh S. A. and Uzumeri S. M., (1983), *Analytical Model for Concrete Confinement in Tied Columns*, Journal of Structural Engineering, 109, 12, 2952-2954

Shen T., (2013), Research on Seismic Performance of Continuous Concrete Rigid Frame Bridge with Long Spans and High Piers under Strong Earthquake, Northeast Forestry University, Harbin, China, 20-27

Shinozuka M. and Ghanem R., (1991), *Structural System Identification. II：Experimental Verification*, Journal of Engineering Mechanics, 121, 2, 265-273

Si B., Sun Z., Wang D., (2013), Hysteretic Analysis Model Considering Shear Deformation for RC Thin-walled hollow bridge Pier, Journal of Dalian University of Technology, 53, 6, 864-870 (in Chinese)

Sim'O J. C. and Tarnow N., (1992), *The Discrete Energy-momentum Method*, Zeitschrift Für Angewandte Mathematik Und Physik, 43, 757-792

Sinha B. P., Gerstle K. H., Tulin L. G., (1964), *Stress-Strain Relations for Concrete under Cyclic Loading*, ACI Structural Journal Proceedings, 61, 2, 195-212

Sivaselvan M. V., et al., (2010), *Dynamic Force Control with Hydraulic Actuators Using Added Compliance and Displacement Compensation*, Earthquake Engineering & Structural Dynamics, 37, 15, 1785-1800

Soliman MTM. And Yu CW., (1967), *The Flexural Stress-Strain Relationship of Concrete Confined by Rectangular Transverse Reinforcement*, Magazine of Concrete Research, 19, 61, 253-262

Song W. and Dyke S., (2013), *Real-Time Dynamic Model Updating Of A Hysteretic Structural System*, Journal of Structural Engineering, 140, 3, 04013082

Spencer B. F., et al., (2004), *NEESgid：A Distributed Collaboratory for Advanced Earthquake Engineering Experiment and Simulation*[C]. Proceedings of 13th World Conference on Earthquake Engineering, August, Vancouver, Canada

Sugiura K., Nagata N., Suzuka Y., et al., (1998), *Internet Related Structural Testing*, Proceedings of the Eighth KKNN Seminar on Civil Engineering, Singapore, 219-224

Sun Z., (2012), Research on the Seismic Deformation Capacity of RC Bridge Columns, Institute of Engineering Mechanics, China Earthquake Administration, Harbin, China, 81-89 (Doctoral thesis, in Chinese)

Sun Z., (2013), Comparative Study on Shear Strength of RC Thin-walled Hollow Bridge Piers under Seismic Effect, China Civil Engineering Journal, 46, 12, 81-89 (in Chinese)

Sun Z., et al., (2012), Analysis on Ductile Deformability of Hollow Reinforced Concrete Bridge Piers, Journal of the China Railway Society, 34, 1, 91-96 (in Chinese)

Tada M. and Pan P., (2007), *A Modified Operator Splitting (OS) Method for Collaborative Structural Analysis (CSA)*, International Journal for Numerical Methods in Engineering, 72, 4, 379-396

Takahashi Y. and Fenves G. L., (2006), *Software Framework for Distributed Experimental -Computational Simulation of Structural Systems*, Earthquake engineering & structural dynamics, 35, 3, 267-291

Takahashi Y. and Iemura H., (2000), *Inelastic Seismic Performance of RC Tall Piers with Hollow*

Section, Proceedings of the 12th World Conference on Earthquake Engineering, New Zealand, 1353

Takanashi K., Udagawa K., Seki M., et al., (1975), *Nonlinear Earthquake Response A Structures by a Computer-actuator On-line System (Part 1 Details of the System)*, Bulletin of Earthquake Resistant Structure Research Center, 8, 1-17

Takashi Y., Kazutoshi N., Eiichi W., et al., (2005), *International Collaborative Pseudo Dynamic Testing Method for Continuous Elevated Bridges by Using Internet*, Advances in Experimental Structural Engineering, 18, 1, 371-376

Takeda T., (1970), *Reinforced Concrete Response to Simulated Earthquakes*, Journal of the Structural Division Proceedings of the American Society of Civil Engineers, 96, 2557-2573

Takizawa H. and Aoyama H., (2010), *Biaxial Effects in Modelling Earthquake Response of R/C Structures*, Earthquake Engineering & Structural Dynamics, 4, 6, 523-552

Tan X. and Wu B., (2012), Pseudo-dynamic Testing with Control Technique Combining Displacement Outer Loop and Force Inner Loop, Journal of Vibration and Shock, 31, 14, 16-21 (in Chinese)

Taniguchi H., et al., (1980), *Non-Linear Earthquake Response Analysis of Structures by a Computer-Actuator On-Line System (Part IV: Response Analysis of One Bay-One Story Frames with High Strength Bolted Connections)*, Transactions of the Architectural Institute of Japan, 291, 33-41

Tao D., (2013), Data-driven-based and Model-based Approaches for Structural Seismic Damage Detection, Harbin Institute of Technology, Harbin, China, 115-142 (Doctoral thesis, in Chinese)

Tasbihgoo F. Caffrey J. P. Masri S. F., (2007), *Development of Data-Based Model-Free Representation of Non-Conservative Dissipative Systems*, International Journal of Non-Linear Mechanics, 42, 1, 99-117

Taucer F. F., Spacone E., Filippou F. C., (1991), *A Fiber Beam-Column Element for Seismic Response Analysis of Reinforced Concrete Structures*, Earthquake Engineering Research Center (EERC), University of California, Report No. UCB/EERC-97/17, California, USA, 3-21

Van Der Merwe R, and Wan E. A., (2001), *The Square-Root Unscented Kalman Filter for State and Parameter-Estimation*, Acoustics, Speech, and Signal Processing, IEEE, 6, 3461-3464

Wagg D. J. and Stoten D. P., (2010), *Substructuring of Dynamical Systems via the Adaptive Minimal Control Synthesis Algorithm*, Earthquake Engineering & Structural Dynamics, 30, 6, 865-877

Wallace M. I., et al., (2010), *Stability Analysis of Real-Time Dynamic Substructuring Using Delay Differential Equations*, Earthquake Engineering & Structural Dynamics, 34, 15, 1817-1832

Wan E. A. and Van Der Merwe R., (2000), *The Unscented Kalman Filter for Nonlinear Estimation*, Adaptive Systems for Signal Processing, Communication, and Control Symposium, IEEE, 153-158

Wang T., (2014), Hybrid Testing Method for Civil Structures based on Model Updating, Harbin Institute of Technology, Harbin, China (Doctoral thesis, in Chinese)

Wang T. and Wu B., (2013), *Real-Time Hybrid Testing with Constrained Unscented Kalman Filter*, 5th International Conference on Advances in Experimental Structural Engineering, Taiwan

Wang T., Wu B., Zhang J., (2011), Adaptive Pseudo-Dynamic Substructure Testing based on Least Square Method, Structural Engineers, 27, s1, 57-62

Wang T., Zhang J., Wu B., (2013), Adaptive Substructure Testing Method with Unscented Kalman Filter, Journal of Vibration Engineering, 26, 3, 328-334

Wang X., (2007), Sliding Mode Control of Real-Time Substructure Testing, Engineering Mechanics, 24, 6, 174-179 (in Chinese)

Wang Z., (2012), Control and Time Integration Algorithms for Real-Time Hybrid Simulation, Harbin Institute of Technology, Harbin, China, 44-59 (Doctoral thesis, in Chinese)

Wang Z., (2016), Outer Loop Control Methods for the Hybrid Test Software Hytest, Harbin Institute of Technology, Harbin, China, 52-72 (Master's thesis, in Chinese)

Wang Z. and Wu B., (2009), A Real-Time Approach to Delay Estimation based on the Least-Square Algorithm, Journal of Vibration Engineering, 22, 6, 625-631

Wen Y. K., (1976), *Method for Random Vibration of Hysteretic System*, Journal of the Engineering Mechanics Division, 102, 2, 249-263

Wood W. L., Bossak M., Zienkiewicz O. C., (1980), *An Alpha Modification of Newmark's Method*, International Journal for Numerical Methods in Engineering, 15, 10, 1562-1566

Wu B., et al., (2005), *Stability and Accuracy Analysis of The Central Difference Method for Real-time Substructure Testing,* Earthquake engineering & structural dynamics, 34, 7, 705-718

Wu B., et al., (2006), *Operator-splitting Method for Real-time Substructure Testing*, Earthquake Engineering & Structural Dynamics, 35, 3, 293-314

Wu B., et al., (2016), *Hybrid Simulation of Steel Frame Structures with Sectional Model Updating*, Earthquake Engineering & Structural Dynamics, 45, 8, 1251-1269

Wu B., et al., (2016), *Energy Consistent Integration Method and Its Applications to Hybrid testing*, 25th National Conference on Structural Engineering，August, Baotou, China

Wu B. and Wang T., (2014), *Model Updating with Constrained Unscented Kalman Filter for Hybrid Testing*, Smart Structures and Systems, 14, 6, 1105-1129

Wu B., Wang Z., Bursi O.S., (2013), *Actuator Dynamics Compensation Based on Upper Bound Delay for Real-Time Hybrid Simulation*, Earthquake Engineering and Structural Dynamics, 42, 12, 1749-1765

Wu M. and Smyth A., (2007), Application of the Unscented Kalman Filter for Real-time Nonlinear Structural System Identification, Structural Control and Health Monitoring, 14, 7, 971-990

Wu M. and Smyth A., (2008), *Real-Time Parameter Estimation for Degrading and Pinching Hysteretic Models*, International Journal of Non-Linear Mechanics, 43, 9, 822-833

Yang G., et al., (2017), *Hytest: Platform for Structural Hybrid Simulations with Finite Element Model Updating*, Advances in Engineering Software, 112, 200-210Yang J. N., Huang H., Lin S., (2006), *Sequential Non-Linear Least-Square Estimation for Damage Identification of Structures*, International Journal of Non-Linear Mechanics, 41, 1, 124-140

Yang J., (2014), Development of MTS Communication Module and Distributed Hybrid Test Function for Hytest Testing Platform-Hytest, Harbin Institute of Technology, Harbin, China, (Master's thesis, in Chinese)

Yang J. N. and Lin S., (2004), *On-Line Identification of Non-Linear Hysteretic Structures Using an Adaptive Tracking Technique*, International Journal of Non-Linear Mechanics, 39, 9, 1481-1491

Yang J. N., et al., (2006), *An Adaptive Extended Kalman Filter for Structural Damage Identification*, Structural Control & Health Monitoring, 13, 4, 849–867

Yang W. J. and Nakano Y., (2005), *Substructure Online Test by Using Real-Time Hysteresis Modeling with a Neural Network*, Advances in Experimental Structural Engineering, 38, 267-274

Yang Y. S., et al., (2009), *Preliminary Study on Online Updating Hybrid Simulation*, NCREE, National Center for Research on Earthquake Engineering, Technical Report 09-001, Taiwan

Yang Y. S., et al., (2007), ISEE: *Internet-based Simulations for Earthquake Engineering Part I: Database Approach*, Earthquake Engineering and Structural Dynamics, 36, 15, 2291-2306

Yang Y. S., et al., (2012), *An Online Optimization Method for Bridge Dynamic Hybrid Simulations*, Simulation Modelling Practice and Theory, 28, 42-54

Yassin MHM., (1994), *Nonlinear Analysis of Prestressed Concrete Structures Under Monotonic and Cycling Loads*, University of California, Berkeley, USA

Yu Y. and Lv X., (1998), 3-D Constitutive Relationship of Confined Concrete, Journal of Tongji University, 26, 6, 622-626 (in Chinese)

Yun C. B. and Shinozuka M., (1980), *Identification of Nonlinear Structural Dynamic Systems*, Mechanics Based Design of Structures & Machines, 8, 2, 187-203

Yun C. B., Kim W. J., Ang A. H. S., (1989), D*amage Assessment of Bridge Structures by System Identification*, Structural Safety and Reliability, 2179-2186

Zeng C., (2014), Multi-axial Dynamic Structural Testing System and Its Control Strategies, Journal of Vibration and Shock, 33, 2, 1-6

Zhang J., (2010), *Adaptive Substructure Pseudo-dynamic Testing Method*, Harbin Institute of Technology, Harbin, China, (Master's thesis, in Chinese)

Zhang J., Wu B., Wang T., (2011), *Adaptive Substructure Testing Method based on Least Square*, International Conference on Electric Technology and Civil Engineering (IEEE), 1907-1910

Zhang H, et al., (2010), *Parameter Identification of Inelastic Structures under Dynamic Loads*, Earthquake Engineering & Structural Dynamics, 31, 5, 1113-1130

Zhao J., et al., (2003), *Considerations for the Development of Real-Time Dynamic Testing Using Servo-Hydraulic Actuation*, Earthquake Engineering & Structural Dynamics, 32, 11, 1773-1794

Zhou H., (2012), Control Methods of Single-Degree-of-Freedom Real-Time Hybrid Testing, Harbin Institute of Technology, Harbin, China, 27-54 (Doctoral thesis, in Chinese)